SURFACE LAYER DYNAMICS AND A STUDY OF FINESTRUCTURE IN KNIGHT INLET, BRITISH COLUMBIA

Augustine van der Baaren

B. Sc. (Mathematics) Acadia University

A THESIS SUBMITTED IN PARTIAL FULFILLMENT OF

THE REQUIREMENTS FOR THE DEGREE OF

MASTER OF SCIENCE

in

THE FACULTY OF GRADUATE STUDIES

DEPARTMENT OF OCEANOGRAPHY

We accept this thesis as conforming

to the required standard

THE UNIVERSITY OF BRITISH COLUMBIA

March 1988

In presenting this thesis in partial fulfilment of the requirements for an advanced degree at the University of British Columbia, I agree that the Library shall make it freely available for reference and study. I further agree that permission for extensive copying of this thesis for scholarly purposes may be granted by the head of my department or by his or her representatives. It is understood that copying or publication of this thesis for financial gain shall not be allowed without my written permission.

Department of Oceanography

The University of British Columbia
Vancouver, Canada

Date 29-04-88

Abstract

In the first part of this thesis I investigated the surface layer dynamics of Knight Inlet to see which of the governing forces: inertial accelerations, pressure gradient, or stress, dominated the momentum balance for a steady two-layer flow. I estimated the inertial terms and pressure term in the momentum equation, which had been integrated over the surface layer, from conductivity, temperature, and depth data measured in Knight Inlet in the springs of 1986 and 1987. I solved for the coefficient of interfacial friction, k, so that an estimate of the interfacial stress, $\tau_i = \rho k \Delta u^2$, could be made.

I obtained the idea of the Knight Inlet analysis from an earlier attempt I had made at resolving the balance of forces in the Fraser River plume. I found an estimate of the friction coefficient at the interface for the plume; $k = 1.55 \times 10^{-4}$, which was much smaller than an assumed value used by Cordes, *et al.* (1980).

The results of the Knight Inlet study showed that within the inlet (inside the sill), the pressure gradient and the stress dominated the balance for high runoff conditions. Estimates of the coefficient of friction were on the order of 10^{-2} and 10^{-3}. The depth of the interface appeared to be constant inland of the sill.

The second part of this thesis was a qualitative study of finestructure in Knight Inlet. I processed the CTD data measured in 1986 and 1987 to find the first differences of temperature and salinity. I used the profiles of ΔT and ΔS to describe features present in the upper and lower water. Later, data that had been measured with a special microprofiler at the same time as the 1987 CTD data were sampled, were compared to the CTD data. For this comparison, I studied profiles of $\frac{dT}{dz}$ (calculated as a centered first difference), and the log of the variance of $\frac{dT}{dt}$.

Results of this study were that the upper water ($< 30\,m$) appeared more highly active than the deeper water ($> 30\,m$), especially at the head of the inlet, at the sill, and in the region of the interface. The deeper water contained fluctuations of temperature and salinity that were

concentrated in patches which were several meters thick. For the year, 1987, the microprofiler revealed the existence of temperature variations that were more significant than I had originally judged from the profiles of ΔT and ΔS. Values of the variance of the temperature gradient, $\frac{dT}{dt}$ in some areas of the deeper water were almost as large as values in the upper water.

Contents

List of Tables

List of Figures

Acknowledgements

I thank God that it's over!

I gratefully acknowledge the financial support of the Natural Sciences and Engineering Research Council of Canada, the Bank of van der Baaren, Dr. G. S. Pond, and all the other taxpayers of Canada.

I am infinitely grateful for the endless encouragement, helpful advice, moral and academic support given to me by my supervisor, Dr. G. S. Pond. I would also like to thank my committee members, Dr. D. Farmer and Dr. P. H. LeBlond for their comments and insight, which helped to improve the quality of my paper.

I will fondly remember the friendship and moral support of my folks, Carol, Jinro, Karyn, office 1329 (?), the Weavers, the Aussies, Garto LaGarto and others of 2719 Alma St., C. B., los chicanos (y chicanas y Rodolfo), the softball teams (Zoo and Ocgy), the Ocgy swim team, officina de turismo de Mexico (?), the beergarden, Heather and the rest of the gang back home, BCTel, Warren Lee's Used Car Parts, the crew of the CSS Vector, the techies, Vivian (I owe her innumerable cookies from Duke's), Howly, T. B. (really...the car was great), and anyone else I forgot to mention....oh, yeah, the gang back home!!!!–I already mentioned them!?!? Oh, well...

I would like to recognize the full support of Wonderbra.

Chapter 1

Introduction to Surface Layer Dynamics Problem

1.1 General

A fjord is a deep estuary which has been formed by glacial carving. There is usually a subsurface sill at the entrance, or mouth, which is often composed of glacial moraine material; there may be inner sills, as well.

Fresh water discharges into the fjord from rivers generally found at the head of the inlet. This river water is found at the surface and flows seaward becoming more saline as it nears the mouth. The increase in density occurs as a consequence of entrainment of salt water from below into the surface layer. The salt water enters the system at depth as an inflowing layer originating at the mouth of the inlet, and it is the inflow of salt water which maintains the salt balance in the system.

Environmental concerns with disposal of industrial waste and biological interest in nutrient cycling and transport of organisms necessitate a better understanding of the details of fjord circulation.

1.2 Objectives

The movement of water in a fjord, as was described in the previous section, follows the

classic idea of estuarine circulation. It is a much simplified and idealized description, but the main premise of an outflowing layer and an inflowing layer is widely accepted.

This study attempts to examine the importance of the forces which combine to drive the surface layer flow in a fjord and to discover which of these forces dominates in the dynamical balance for a steady state.

The distribution of fluid properties measured in the field and equations describing the dynamics of the fjord provided the means to find estimates of the relevant forces.

Two problems are presented: a brief study on the dynamics of the Fraser River plume, and the main study on the balance of forces in Knight Inlet's surface layer.

1.2.1 Motivation

Fraser River plume

Research on entrainment in the Fraser River (British Columbia) plume by R. E. Cordes, *et al.* (1980) motivated the attempt to study the dynamic balance within an estuarine environment. They had observed a downstream deceleration of the plume and they stated that entrainment provided one means for decelerating the plume. One of the assumptions made by them was that the downstream deceleration, not caused by entrainment, was equal to the sum of wind stress effects, pressure gradient, and the interfacial Reynolds stress between the brackish plume water and the water below. They derived an estimate of the sea surface slope (ignoring the wind stress, which was shown to be small) on the further assumption that their derived pressure gradient acceleration was a result of only the sea surface slope. A value for the coefficient of friction, which is contained in the expression for the Reynolds stress in terms of the surface layer velocity squared, had to be assumed.

An estimate of the friction coefficient can be made by using CTD (conductivity, temperature, and depth) data, which were measured in the Strait of Georgia, to determine dynamic heights from the density structure (and, consequently, a sea surface slope from a least squares fit of these values), and by using the value for the deceleration calculated by Cordes, *et al.* It

was interesting to see how close the estimate of the friction coefficient was to the value which was used by Cordes, *et al.*

Unfortunately, the significant lack of "good" data prevented me from carrying on further investigation of the dynamics in the Fraser River plume area, but the availability of CTD data for Knight Inlet suggested to me that a similar study of circulation dynamics could be conducted in a fjord. This idea was further enhanced by the existence of a short study of the dynamics of the surface layer in Knight Inlet by Wetton (1981). The idea of extending the Fraser River study into a study of the dynamical balance of forces in Knight Inlet's surface layer seemed a viable topic of research for part of my thesis, and, although he used wind stress rather than interfacial stress, Wetton's general methods of analysis of his CTD data seemed applicable to my problem.

Wetton's Knight Inlet study

Wetton's work involved an examination of the terms in a steady state version of the momentum balance for a two-layer fjord with a motionless bottom layer. The assumed motionless lower layer is contradictory to the classical interpretation of fjord/estuarine circulation. Also, in his examination, he utilized wind data to give an estimate of wind stress on the surface layer, but he ignored the effects of an interfacial stress.

He used dynamic heights to estimate the slope of the sea surface in his study of Knight Inlet surface layer dynamics. This quantity is very difficult to measure directly and Wetton's approach based on observed densities seemed entirely feasible.

I thought that the dynamics of Knight Inlet's surface layer could be better investigated by refining Wetton's approach and by repeating the exercise of finding the friction coefficient, as in the Fraser River plume study, to give an estimate of interfacial stress. The friction coefficient will be a useful parameter to know for the development of numerical models of fjords in the future.

1.3 Knight Inlet: general

Knight Inlet is a deep ($\approx 550\,m$ at its deepest) fjord situated on the west coast of mainland British Columbia as seen in Figure 1.1. It is long, close to $100\,km$ from the head to the mouth, and has an average width of $2.5\,km$. The sill is relatively shallow ($\approx 60\,m$) and is found about $75\,km$ from the head. The first half of its length from the mouth is relatively straight, but the second half contains several bends.

The high volume of fresh water is provided by the Klinaklini and Franklin rivers. The runoff can be as large as $800 - 900\,m^3s^{-1}$ during spring snowmelt. The average yearly discharge is $400\,m^3s^{-1}$. The two-layer density structure is applicable for most of the year because of this high fresh water discharge.

Webb (1985) gives a very good, concise description of the physical oceanography of Knight Inlet in the introduction to his doctoral dissertation.

The physical processes of Knight Inlet have been much studied and documented in the past. Knight Inlet has also been used many times as an example of a typical deep, stratified inlet in many models of fjord circulation (eg. Freeland and Farmer, 1980; Farmer and Freeland, 1983; Long, 1975; Wetton, 1981; Webb, 1985; Pickard and Rodgers, 1959; and Farmer and Smith, 1980; Pearson and Winter, 1978).

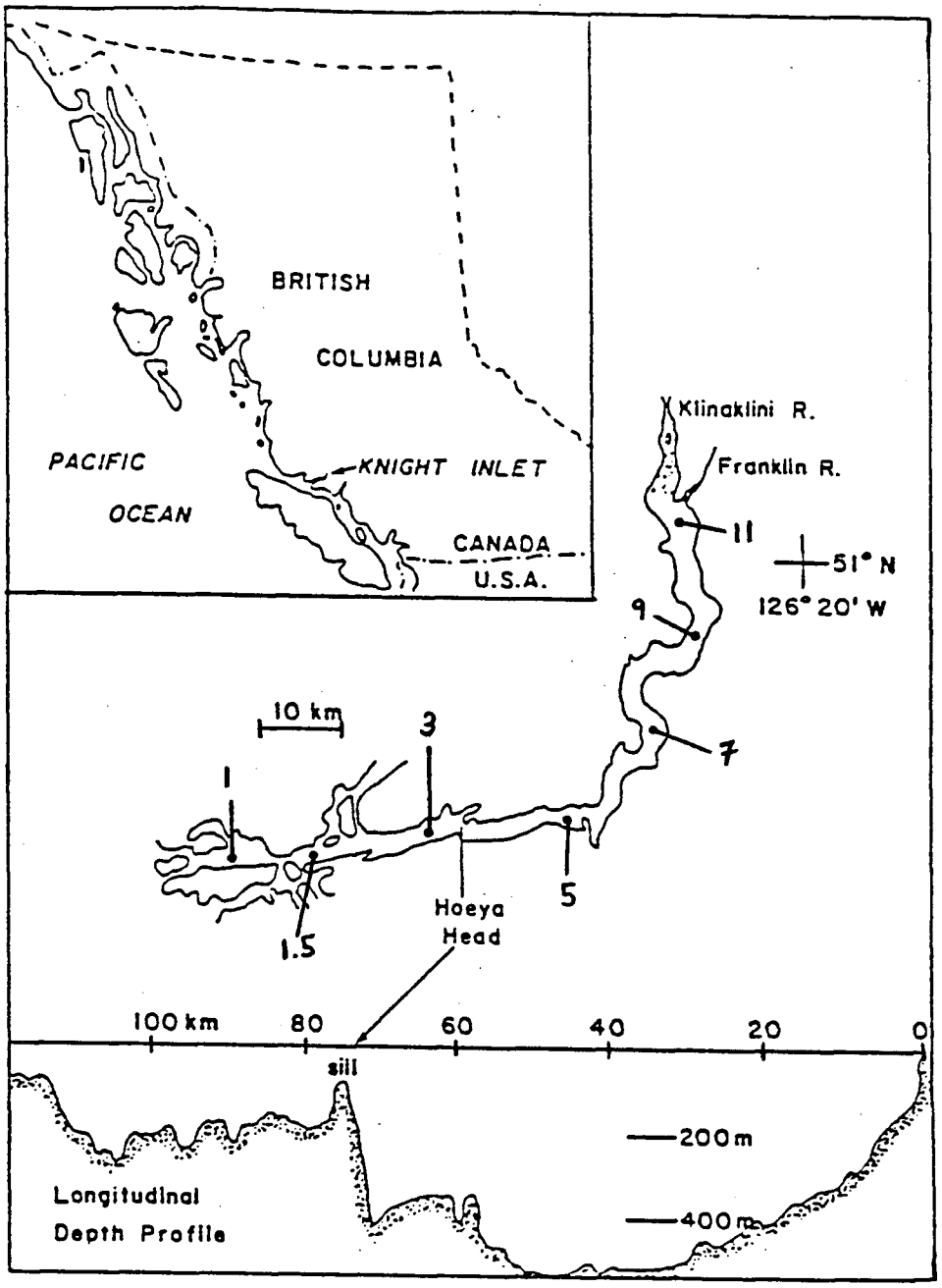

Figure 1.1: Map of Knight Inlet with longitudinal cross-section. The inset is of the British Columbia coast showing the location of Knight Inlet. The location of the CTD stations in Knight Inlet are denoted with a •. The lowest station number, station 1, is located near the mouth and station 11 is at the head (adapted from Farmer and Smith, 1980).

Chapter 2

Theory for Surface Layer Dynamics Problem

2.1 Momentum

The simple model that I used in this study consisted of two layers as shown in Figure 2.1. The depth averaged surface flow is labelled $u_1(x)$, and the depth averaged return flow is $u_2(x)$. The depth of the interface is $h(x)$, and $h_2(x)$ is the thickness of the inflowing layer. The density of the surface layer is represented by σ_1, which is defined as $\rho_1 - 1000\ kg\,m^{-3}$ where ρ_1 is the actual density of the surface layer. Similarly, the density of the inflowing layer is represented by σ_2. The positive x direction is towards the mouth and the z direction is positive upwards.

When researchers describe fjord dynamics, one possible representation is directly derived from the Navier Stokes equations. These equations represent the flow as the sum of the mean flow, a tidal component, and a fluctuating part (Farmer and Freeland, 1983). A condition of incompressibility is invoked, temporal averages are taken (usually over a tidal cycle (Dyer, 1973)), and assumptions, such as no correlation between fluctuations and tidal flow are made so that the Navier Stokes equations are reduced to a more workable form. Turbulent stresses, or Reynolds stresses, are much larger than molecular stresses so that the molecular stresses can be ignored. Generally, a steady state is also assumed. At this point, theories tend to differ depending on what further assumptions are made to arrive at a momentum balance

In my case, as well as all the previously mentioned assumptions, I assumed that there was

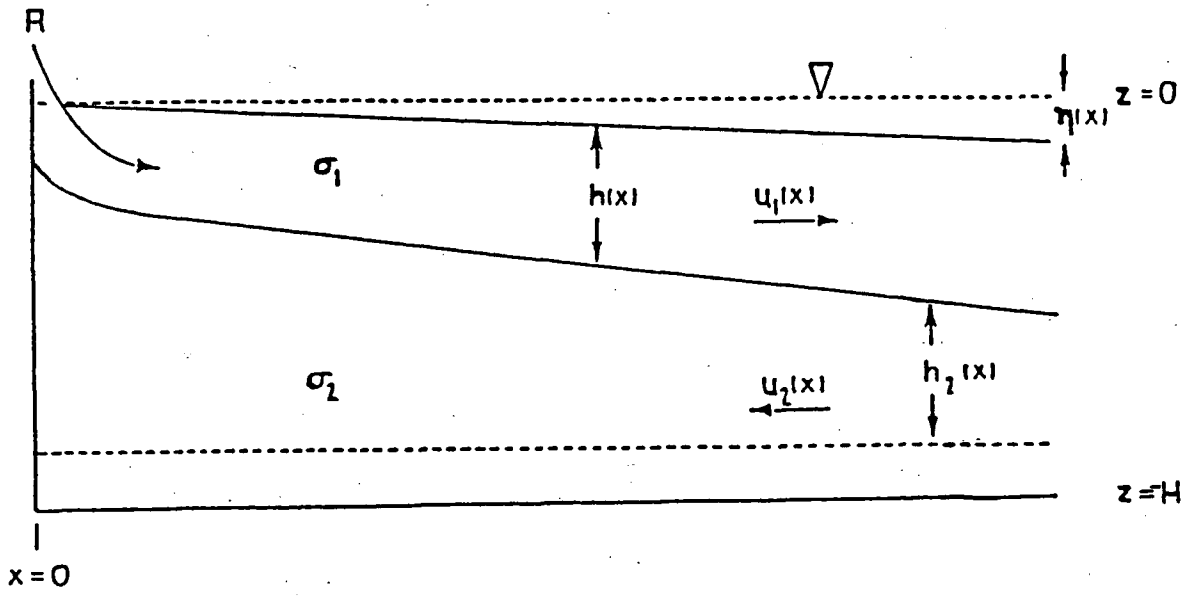

Figure 2.1: Two-layer model of fjord circulation, adapted from Freeland and Farmer (1980).

no flow or variation in the y direction (across the fjord). Wetton (1981) showed in his appendix that tidal processes are probably only important near the sill for a deep fjord such as Knight Inlet. Therefore, I ignored their influence. Rotational effects, as well, were not considered by me since Knight Inlet is so narrow. The horizontal momentum equation (for along channel flow) that I used is

$$u\frac{\partial u}{\partial x} + w\frac{\partial u}{\partial z} = -\frac{1}{\rho}\frac{\partial p}{\partial x} - \frac{\partial}{\partial z}(\overline{u'w'}) \tag{2.1}$$

The terms on the leftside represent the inertial terms. The rightside consists of the pressure gradient acceleration and the Reynold's stress due to fluctuating velocities. It should be noted that in the derivation of equation 2.1, the term $\frac{\partial}{\partial x}(\overline{u'u'})$ was assumed negligible. This assumption is usually made by researchers when modelling fjords, but Farmer and Freeland (1983) state that this assumption is not strictly correct due to horizontally mixed water sporadically entering the system. It may be that $\frac{\partial}{\partial z}(\overline{u'u'})$, associated with tidal currents, is not negligible, but it could not be investigated with the data that I used in this study.

In taking a two-layer approach, equation 2.1 had to be integrated across each layer. I did this integration term by term. While integrating over the surface layer, the limits of integration were $-h$ and η. However, $\eta << h$, and so, in most cases, the upper limit could be taken to be $z = 0$. For example, $\int_{-h}^{\eta} u^2 dz = \int_{-h}^{0} u^2 dz + \int_{0}^{\eta} u^2 dz$, and with $\eta << h$, the second term could be neglected. While integrating pressure terms, η had to be retained because $g\frac{\partial \eta}{\partial x}$ is the pressure gradient at the surface. Henceforth, where appropriate, integration will be from $-h$ to 0 rather than from $-h$ to η.

2.1.1 The inertial terms

Integration of the first inertial term over the surface layer results in

$$\begin{aligned}
\int_{-h}^{0} u\frac{\partial u}{\partial x}\,dz &= \frac{1}{2}\int_{-h}^{0}\frac{\partial u^2}{\partial x}\,dz \\
&= \frac{1}{2}\frac{\partial}{\partial x}\int_{-h}^{0} u^2\,dz - u_{-h}^2\frac{d(-h)}{dx} \\
&= \frac{1}{2}\frac{\partial}{\partial x}\int_{-h}^{0} u^2\,dz.
\end{aligned}$$

since $u_{-h} = 0$. The integral is simpler to evaluate by moving the origin to $z = -h$. The surface which, was formerly at $z = 0$, was moved to $z = h$:

$$\frac{1}{2}\frac{\partial}{\partial x}\int_0^h u^2\,dz. \tag{2.2}$$

Since no direct measurements of currents were made during the experiment, the profile of the surface layer flow was unknown and had to be assumed. Three cases will be discussed: a uniform velocity; a linear relationship; and a quadratic relationship.

If the velocity, u, is assumed to be uniform in the surface layer then $u = u_1$. The volume transport over that layer will be equal to $u_1 h$ for a layer of depth, h. This situation is not likely to be true in a fjord. For a flow reversal to exist, the surface layer velocity will have to decrease to zero at some point. The velocity, then, will definitely depend on the depth. The linear profile and the parabolic profile both seemed to be reasonable assumptions.

Assuming a linear velocity profile

Let $u = c\frac{z}{h}u_1$ be the linear relationship between u and z where c is some constant to be solved for. Since u_2 is the average over the upper layer, $u_1 h = \int_0^h c\frac{z}{h}u_1\,dz$. Solving this integral gives $c = 2$ so that $u = 2\frac{z}{h}u_1$. At $z = 0, u = 0$ and at the surface, $u = 2u_1$. After substituting this definition of u, equation 2.2 becomes

$$\frac{1}{2}\frac{\partial}{\partial x}\int_0^h u^2\,dz = \frac{2}{3}\frac{\partial}{\partial x}(u_1^2 h).$$

Integration of the second inertial term, $w\frac{\partial u}{\partial z}$, results in

$$\int_0^h w\frac{\partial u}{\partial z}\,dz = \int_0^h w\frac{\partial}{\partial z}(2u_1\frac{z}{h})\,dz = \int_0^h w(2\frac{u_1}{h})\,dz. \tag{2.3}$$

The entrainment velocity, w, was found from the continuity equation, $\frac{\partial w}{\partial z} = -\frac{\partial u}{\partial x}$, which had been integrated over depth, from $z = h$ to level z.

$$\int_h^z \frac{\partial w}{\partial z'}dz' = w(z) = -\int_h^z \frac{\partial u}{\partial x}dz' = \int_z^h \frac{\partial u}{\partial x}dz' = \frac{\partial}{\partial x}\int_z^h u dz' + u_{-h}\frac{dh}{dx}. \tag{2.4}$$

The term, $u_{-h}\frac{dh}{dx}$, vanishes since the velocity at the interface is zero. This result made sense, since $\frac{\partial u}{\partial x} > 0$ and $dz > 0$, $w > 0$, which meant that the entrainment velocity was directed upward. For $u = 2u_1\frac{z}{h}$:

$$w = 2\frac{\partial}{\partial x}\int_z^h u_1\frac{z'}{h}dz' = \frac{\partial}{\partial x}(u_1 h - \frac{z^2 u_1}{h}) \tag{2.5}$$

For $z = 0$ (the entire layer), $w = \frac{\partial}{\partial x}u_1 h$, and, for $z = z$, w is the change in the x direction of the total transport minus the transport to level z. With this substitution for w, $\int_0^h w\frac{\partial u}{\partial z}\,dz$ in equation 2.3 becomes

$$\frac{4}{3}\frac{\partial}{\partial x}(u_1^2 h). \tag{2.6}$$

Assuming a parabolic profile

Let $u = c(\frac{z}{h})^2 u_1$. With the use of the previous method, $u = 3(\frac{z}{h})^2 u_1$. This changed equation 2.2 as follows:

$$\frac{1}{2}\frac{\partial}{\partial x}\int_0^h u^2 dz = \frac{9}{10}\frac{\partial}{\partial x}(u_1^2 h). \tag{2.7}$$

The entrainment velocity becomes:

$$w = \frac{\partial}{\partial x}\int_z^h u dz' = 3\frac{\partial}{\partial x}\int_z^h \frac{z^2 u_1}{h^2}\,dz = \frac{\partial}{\partial x}(u_1 h - \frac{z^3 u_1}{h^2}). \tag{2.8}$$

Now, $\int_0^h w\frac{\partial u}{\partial z}\,dz$ in equation 2.3 becomes

$$\frac{9}{5}\frac{\partial}{\partial x}(u_1^2 h). \tag{2.9}$$

The second inertial term is the momentum that is required to accelerate the entrained fluid from $u = 0$ at the interface to the velocity appropriate to the level it reaches. If the surface layer velocity were uniform, w at $z = 0$ (interface) would be $\frac{\partial}{\partial x}(u_1 h)$. In this case, the fluid would need to be accelerated by u_1.

The inertial terms sum to be $\frac{3}{2}\frac{\partial}{\partial x}(u_1^2 h)$ for $u = u_1$. For the linear profile they sum to be $2\frac{\partial}{\partial x}(u_1^2 h)$, and for the parabolic profile, they sum to be $\frac{27}{10}\frac{\partial}{\partial x}(u_1^2 h)$ for $u = u_1$. The inertial terms change by 80% from constant u to one which is parabolic.

There is not much historical data for Knight Inlet that would help in making the decision between the two profiles. Pickard and Rodgers (1959) have figures representing current measurements made in Knight Inlet. A parabolic curve would seem to suit these figures more than a line; therefore, I assumed a parabolic profile for the velocity in this analysis.

Knudsen's relations

Knudsen's relations for conservation of volume and salt flux provided estimates for u_1 and u_2. The conservation of volume, stated simply, says that what goes in, must come out, ie. $R + Vol_{in} = Vol_{out}$ where R is the amount of river discharge. The relation was rewritten as

$$R + u_2 h_2 B = u_1 h B \tag{2.10}$$

to comply with Figure 2.1. B is the width of the inlet, and is assumed constant for Knight Inlet. I took both u_1 and u_2 to be positive numbers.

The conservation of salt is similar, ie. $Salt_{in} \times Vol_{in} = Salt_{out} \times Vol_{out}$.

$$S_1 u_1 h B = S_2 u_2 h_2 B$$

where $S_1 \propto (\rho_1 - \rho_0)$ is the salt content of the top layer and $S_2 \propto (\rho_2 - \rho_0)$ is the salt content of the lower layer. In this analysis, it is written as the following conservation of buoyancy equation:

$$u_1(\rho_1 - \rho_0)h = u_2(\rho_2 - \rho_0)h_2 \tag{2.11}$$

The density was used instead of the salinity since density and salinity profiles are nearly the same. The value of ρ_0 is $1000\, kg\, m^{-3}$, the density of fresh water. These last two equations are similar to ones used by Freeland and Farmer (1980).

2.1.2 Pressure gradient

The hydrostatic pressure of a water column, extending from the surface to a certain depth, is equal to the total weight of the fluid above that depth, per unit area, while the fluid is

at rest (hence, "static") (Defant, 1961). This is called the sea pressure when dealing with the ocean. The total pressure includes the atmospheric pressure. For simplicity, sea pressure will be referred to as just pressure unless stated otherwise. Changes in the vertical sense are described by:

$$dp = -g\rho dz. \tag{2.12}$$

The minus sign is present because z increases upward.

The pressure at any level, z, can be found by integrating the previous equation (equation 2.12) from the surface, $z = \eta$, to z:

$$p = -\int_{\eta}^{z} g\rho(z)\, dz + p_a \tag{2.13}$$

where the density, ρ, varies with depth, and p_a is the atmospheric pressure which is assumed to be constant.

The horizontal pressure gradient, or *pressure force/unit volume* in the x direction, is

$$\frac{\partial p}{\partial x} = \frac{\partial}{\partial x}\int_{z}^{\eta} \rho g\, dz = \int_{z}^{\eta} \frac{\partial \rho}{\partial x} g\, dz + g\rho_\eta \frac{\partial \eta}{\partial x} \tag{2.14}$$

where ρ_η is the density at the surface, and $\frac{\partial \eta}{\partial x}$ is the sea surface slope. This gradient can be calculated by determining the pressure at level z from observed densities, and then by finding the slope (using a least squares fit) along the inlet (Wetton, 1981). Since CTD casts are done from the sea surface, which is slanted along the inlet, the gradient that is calculated from the density distribution will be off by the amount that the sea surface slants (ie. the sea surface slope).

Where the density is uniform the first term on the far right of equation 2.14 is zero. The pressure gradient is then entirely due to the sea surface slope. The resulting flow is called barotropic flow. Baroclinic flow is caused by density variations in a non-homogeneous fluid. The integrated effects of the horizontal density variations will increase with depth and compensate for the surface slope effect. For $z \approx \eta$, the first term in equation 2.14 must be small; therefore, outflow (downstream flow) will occur. If the effect from the density variations becomes greater than that of the surface slope, then a flow reversal will occur. It is not correct to presume that

the pressure gradient will be dominated by the sea surface slope at depth unless the effects of the density variations are shown to be negligible.

Geopotential and dynamic heights

Dynamic heights were used by Wetton (1981) to find $\frac{\partial p}{\partial x}$. This approach seemed to be simple and straightforward so I followed suit. The dynamic height, D, between two levels, a and b, is defined such that $D\ dyn\,m\ =\ 0.1(\Phi_b\ -\ \Phi_a)\,J\,kg^{-1}$ and where $1\,dyn\,m$ is called a dynamic meter and is equal to $10\,J\,kg^{-1}\,(=\,m^2s^{-2})$. The non-standard unit of D is convenient since D is numerically almost equal to the difference between levels a and b in meters.

$\Phi_b\ -\ \Phi_a$ is the difference in geopotential (gravitational potential) between two levels, a and b, and can be found by integrating the change in geopotential of a mass, $d\Phi\ =\ g\,dz$:

$$\Phi_b\ -\ \Phi_a\ =\ \int_a^b d\Phi\ =\ \int_a^b g\,dz\ =\ -\int_{p_a}^{p_b} \alpha\,dp. \tag{2.15}$$

p_a and p_b are the pressures at levels a and b. $\alpha = \frac{1}{\rho}$ is the specific volume and is defined as the sum of $\alpha_{35,0,p}$ and δ, the specific volume anomaly, where

$$-\int_{p_a}^{p_b} \alpha\,dp\ =\ -\int_{p_a}^{p_b} \alpha_{35,0,p}\,dp\ -\ \int_{p_a}^{p_b} \delta\,dp. \tag{2.16}$$

The first integral on the rightside of equation 2.16 is called the standard geopotential distance between surfaces of equal pressure known as isobaric surfaces, p_a and p_b. It represents the contribution of water at uniform salinity, $35\,ppt$, uniform temperature, $0°C$, and some pressure, p. The second integral in equation 2.16 is called the geopotential anomaly and gives the amount of deviation from the standard.

D between two levels is calculated from the density field:

$$10D\ =\ -\int_{p_a}^{p_b} \alpha dp\ (m^2s^{-2}) \tag{2.17}$$

When calculating the dynamic height, D, the specific volume anomaly can be approximated (for waters less than $1000\,m$ deep) by

$$\Delta_{S,T}\ =\ (\frac{1000}{1000+\sigma_t}\ -\ 0.97266)\frac{1}{1000}\,m^3kg^{-1}$$

(Pond and Pickard, 1983). σ_t is a convenient way of expressing density: $\sigma_t = (\rho(S,T,0) - 1000)\, kg\, m^{-3}$. The other components of the specific volume anomaly are deemed negligible compared to $\Delta_{S,T}$ so that it is sufficient to use only the integral containing $\Delta_{S,T}$ (ie. $\delta \approx \Delta_{S,T}$).

In my computations, I calculated $\int_{p_{100}}^{p_z} \Delta_{S,T}\, dp$ using a simple trapezoid rule. I used intervals of $0.5\, m$ for the integration and then I summed the values I obtained for the overall interval, $100\, m$ to $z\, m$ where z is the depth of the isobaric surface. The units that resulted from this integration were $m^2 s^{-2}$. When I divided these dynamic height values by 10, the result was in units of dynamic meters and these units for D were used for the dynamic heights which were in turn used to find the isobaric slopes. The slopes were later multiplied by 10 to give $g \int \frac{\partial \zeta}{\partial x}$ in $m^2 s^{-2}$.

I assigned the pressures values of $-10z\, Pa$ (z is the depth), rather than computing the integral, $p = -\int \rho g dz$. It is explained in Pond and Pickard (1983) that the error involved is $\approx 1.5\%$.

Since the pressure field is found from the observed densities as well, the pressure gradient can be determined with the use of dynamic heights. The relationship between the pressure gradient at a specific level and the gradient of calculated dynamic heights is shown in the next section. This explanation was taken from Dyer (1973).

Pressure gradient

The first term of equation 2.14 can be rewritten

$$\int_z^\eta \frac{\partial \rho}{\partial x} g\, dz \simeq - < \rho > \frac{\partial}{\partial x} \int_{p_\eta}^{p_z} \alpha\, dp = - < \rho > 10 \frac{\partial D}{\partial x}\ (m^2 s^{-2}) \qquad (2.18)$$

where $< \rho >$ is the depth averaged density between η and z, and p_η is the pressure at the sea surface (atmospheric pressure) (Dyer, 1973).

The second term, $g\rho_\eta \frac{\partial \eta}{\partial x}$, as was mentioned previously, can be thought of as an integration constant of the integral, $\frac{\partial}{\partial x} \int_z^\eta \rho g\, dz$. It is a difficult quantity to measure directly, but can be found by assuming that there is a depth, $z = LNM$, where $\frac{\partial p}{\partial x} = 0$ (there is no movement).

Then

$$g\rho_\eta \frac{\partial \eta}{\partial x} = -g \int_z^\eta \frac{\partial \rho}{\partial x}\, dz = <\rho> \frac{\partial}{\partial x} \int_{p_\eta}^{p_{LNM}} \alpha\, dp \tag{2.19}$$

so that now

$$\frac{1}{\rho}\frac{\partial p}{\partial x} = -\frac{\partial}{\partial x}\int_{p_\eta}^{p_z} \alpha\, dp + \frac{\partial}{\partial x}\int_{p_\eta}^{p_{LNM}} \alpha\, dp \ (m\, s^{-2}). \tag{2.20}$$

The two integrals on the right can be recognized as the integrals used to determine D.

Isobaric slopes

Wetton found it convenient to express the pressure gradients in terms of the slopes of isobaric surfaces. This approach also seemed reasonable so I did likewise. The relationship between the slopes of isobaric surfaces and pressure gradients is explained in the following paragraphs.

The line where an isobaric surface cuts a plane is called an isobar and the pressure is the same along this line. The more closely spaced that the isobars are along the plane, the stronger the pressure gradient is. If an isobaric surface of pressure, p, intersects a geopotential surface (on which the geopotential is the same everywhere), then the slope of the isobaric surface with respect to the geopotential surface has x component, $\frac{\partial z}{\partial x}$. The associated force is $g(\frac{\partial z}{\partial x})_p$ (von Arx, 1962). The hydrostatic approximation gives the relation between the isobaric slope and the pressure gradient: $-\frac{1}{\rho}\frac{\partial p}{\partial x} = g\frac{\partial z}{\partial x}$. The isobaric slope is more commonly written as $\frac{\partial \zeta}{\partial x}$. The minus sign is due to the fact that the force of the pressure gradient is directed from high pressure to low pressure.

In the end, there is a relationship between the isobaric slopes and D:

$$\frac{1}{\rho}\frac{\partial p}{\partial x} = \frac{\partial D}{\partial x} + constant = -g\frac{\partial \zeta}{\partial x} \tag{2.21}$$

In keeping with the idea of integration over the surface layer, the gradients should be integrated:

$$\int_{-h}^{\eta} \frac{1}{\rho}\frac{\partial p}{\partial x}\, dz = -\int_{-h}^{\eta} g\frac{\partial \zeta}{\partial x}\, dz \ (m^2 s^{-2}). \tag{2.22}$$

A least squares fit through the dynamic heights, calculated at each station between the "level of no motion" (where the pressure gradient is zero), and the level of any isobaric surface, will provide estimates of the slopes of these surfaces needed for the integration.

2.1.3 Reynold's stress

The stress term can be written as

$$-\frac{\partial}{\partial z}(\overline{u'w'}) = -\frac{1}{\rho}\frac{\partial \tau_{xz}}{\partial z} \tag{2.23}$$

where τ_{xz} is the x component of the net momentum flux across the boundaries caused by the fluctuating velocity w' (Dyer,1973). If the rightside of equation 2.23 is integrated through the top layer then the stress becomes

$$\frac{1}{\rho}(\tau_w - \tau_i)$$

where τ_w is the mean wind stress at the surface and τ_i is the mean interfacial stress.

If the wind is not strong, the mean wind effect can be set to 0. Hence, the stress term is reduced to

$$-\frac{1}{\rho}\tau_i$$

This can be estimated by $-k\Delta u^2$ by letting $\tau_i = \rho k \Delta u^2$. The coefficient, k is the coefficient of friction and Δu is the difference between the surface layer velocity and the velocity of the inflowing layer. If the second layer were stationary, then the stress would be a constant times the surface layer velocity squared, but since it is assumed that there exists an inflow at depth, the contribution of this velocity to the shear must be considered as well.

It is known that the wind may influence surface flow markedly in Knight Inlet. If it is blowing up-inlet, the normal flow can even be reversed (Pickard and Rodgers, 1959). Therefore, it is not always justified to ignore the importance of the wind. If it is included in the analysis, an estimate of the wind stress can be made by using $\tau_w \approx \rho_a C_D u_w^2$ where ρ_a is the density of air ($\approx 1.2\, kg\, m^{-3}$), C_D is the drag coefficient ($\approx 1.2 \times 10^{-3}$) and u_w is the wind speed. The values of ρ_a and C_D are taken from Cordes, *et al.* (1980) and Wetton (1981), respectively.

The subsequent data analysis concerns itself with finding estimates for k. Generally, for a fjord, $2.0 \times 10^{-3} \leq k \leq 5.0 \times 10^{-3}$ (Dyer, 1973). It should be noted that Dyer's coefficient, k, was the frictional coefficient for the bed shear stress at the bottom. He does not mention where these bounds came from, but I suspect that they were estimated indirectly.

Chapter 3

Analysis and Results of Surface Layer Dynamics Problem

3.1 The Fraser River plume

My work on the Fraser River plume led into my work on Knight Inlet so I will briefly present the simple analysis of my Georgia Strait CTD data and the results that I obtained.

Research on entrainment in the Fraser River plume by R. E. Cordes, *et al.* (1980) resulted in an estimate being made of the sea surface slope. Their area of study encompassed that part of the Strait of Georgia extending from Sand Heads (near Vancouver) to Vancouver Island. Their estimate for $\frac{\partial \eta}{\partial x}$ was $7.0 \times 10^{-5}\, mm^{-1} = 0.07\, mkm^{-1}$. To determine this gradient, they set the portion of the observed downstream deceleration not due to entrainment equal to the sum of the acceleration due to the pressure gradient and the acceleration due to the interfacial friction:

$$u\frac{\partial u}{\partial x} = -\frac{1}{\rho}\frac{\partial p}{\partial x} - \frac{1}{\rho}\frac{\tau_i}{h} \tag{3.1}$$

where $h = 3\, m$, and $\tau_i = \rho k u^2$. They assumed the coefficient of friction, k, to have the value of 0.001.

On 16 July 1986, CTD data were collected across the Strait of Georgia from Sand Heads to Active Pass (Figure 3.1). These data were processed by me in an attempt to find the sea surface slope and a value for k.

I calculated dynamic heights for each of the seven stations using a level of no motion at

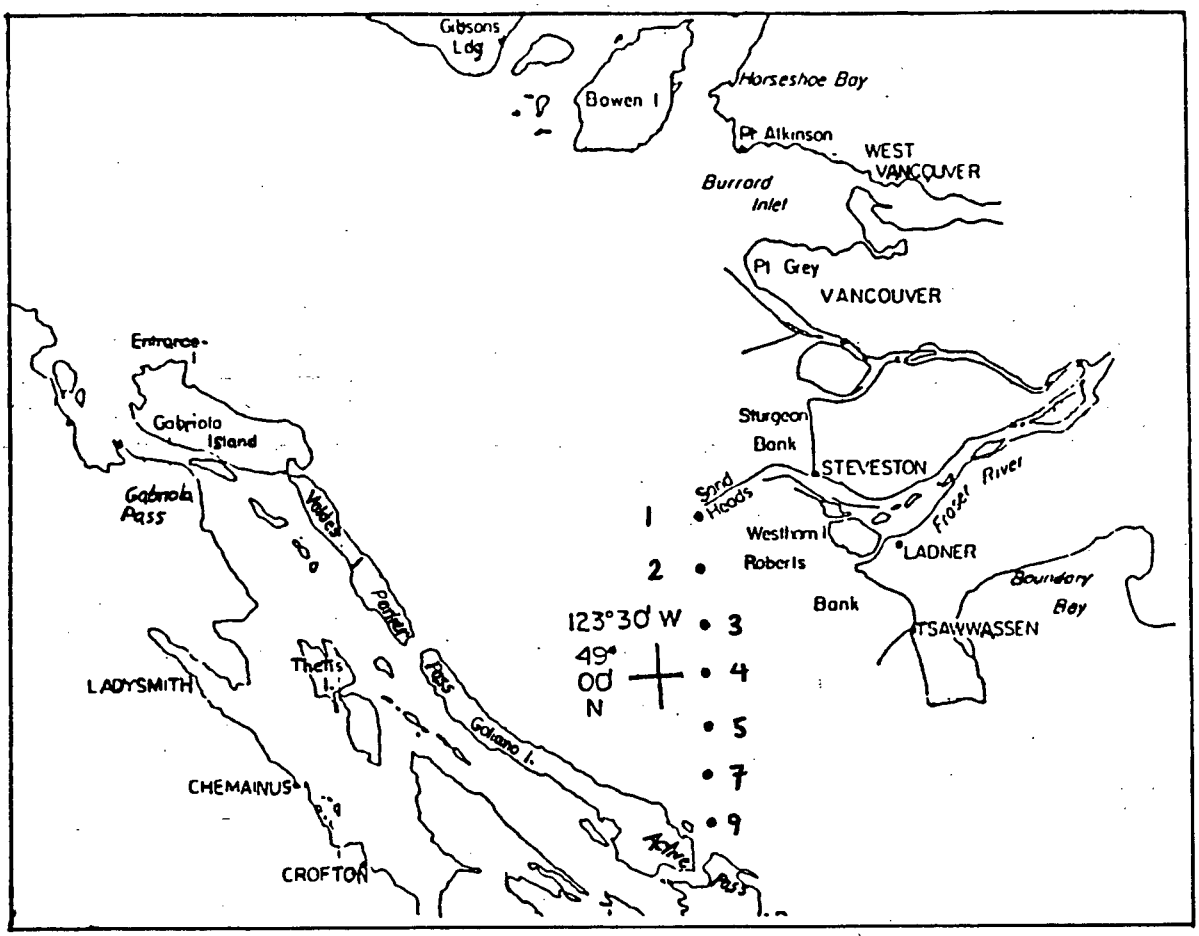

Figure 3.1: Map showing location of Georgia Strait CTD stations which are denoted with a •. Station 1 is located by Sands Head and station 7 is near Active Pass (adapted from Thomson, 1981).

Station	Distance from station 1 (km)	Dynamic height (dyn m)
1	0.0	0.532
2	4.3	0.509
3	7.9	0.487
4	11.8	0.493
5	15.5	0.516
6	19.2	0.511
7	22.7	0.543

Table 3.1: Georgia Strait dynamic heights

$100\,m$ (Figure 3.2). At station 1 the maximum depth measured was $45\,m$. I assumed that between stations 1 and 2, the density structure was fairly uniform from $45\,m$ to $100\,m$. The deeper values of σ_t at station 2 were used for the calculation of the density anomalies for station 1 from $45\,m$ to $100\,m$ and these anomalies were summed with those that were calculated for $1\,m$ to $45\,m$ at station 1 to give the dynamic height at that station. Table 3.1 lists the dynamic heights of all 7 stations relative to $100\,m$.

I used a linear regression of the dynamic heights at the first three stations to find the sea surface slope (Figure 3.3). Measurements were made at seven stations, but stations $4-7$ would have had the sea surface slanting in a direction which did not seem consistent with "plume behavior" (Figure 3.2). This anomalous situation might have been partially due to the fact that the CTD transect was from Sands Head to Active Pass and it might not have provided sufficient coverage of the plume. Also, the transect was performed near the start of a flood tide and the flooding water could have changed the density make-up enough to change the sea surface slope; both wind and tide would have had an effect on the surface flow of the plume. Unfortunately, I did not have wind or tide data. These last four stations were omitted from the slope calculation, which left only three data points to work with.

For the first three stations $\frac{\partial \eta}{\partial x} = -5.6 \times 10^{-6}\, mm^{-1}$. If it is assumed that the pressure gradient is due to the sea surface slope alone, as Cordes, *et al.* assumed, then $\frac{1}{\rho}\frac{\partial p}{\partial x} = g\frac{\partial \eta}{\partial x} \approx -5.6 \times 10^{-5}\, ms^{-2}$. This value is ten times smaller than that estimated by Cordes, *et al.* When this value is combined with the deceleration that they found ($= -6 \times 10^{-5}\, ms^{-2}$), a value of

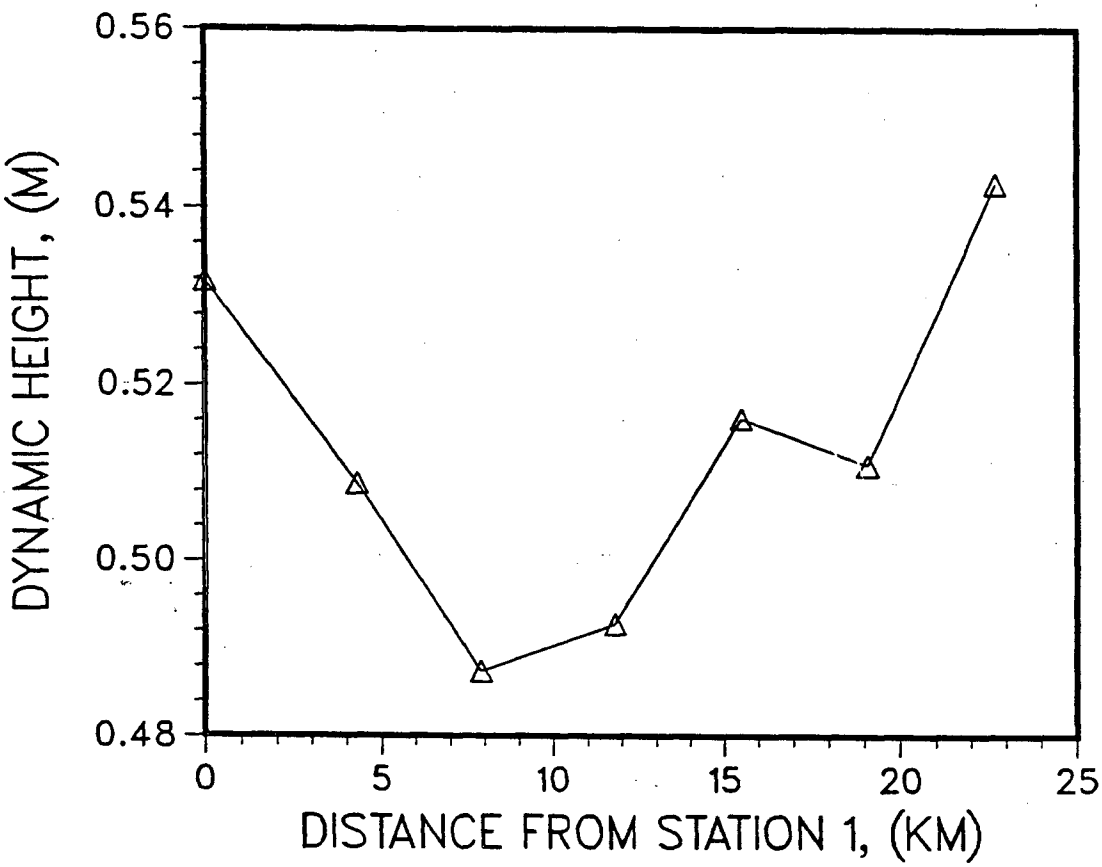

Figure 3.2: Dynamic heights of 1986 Georgia Strait CTD stations.

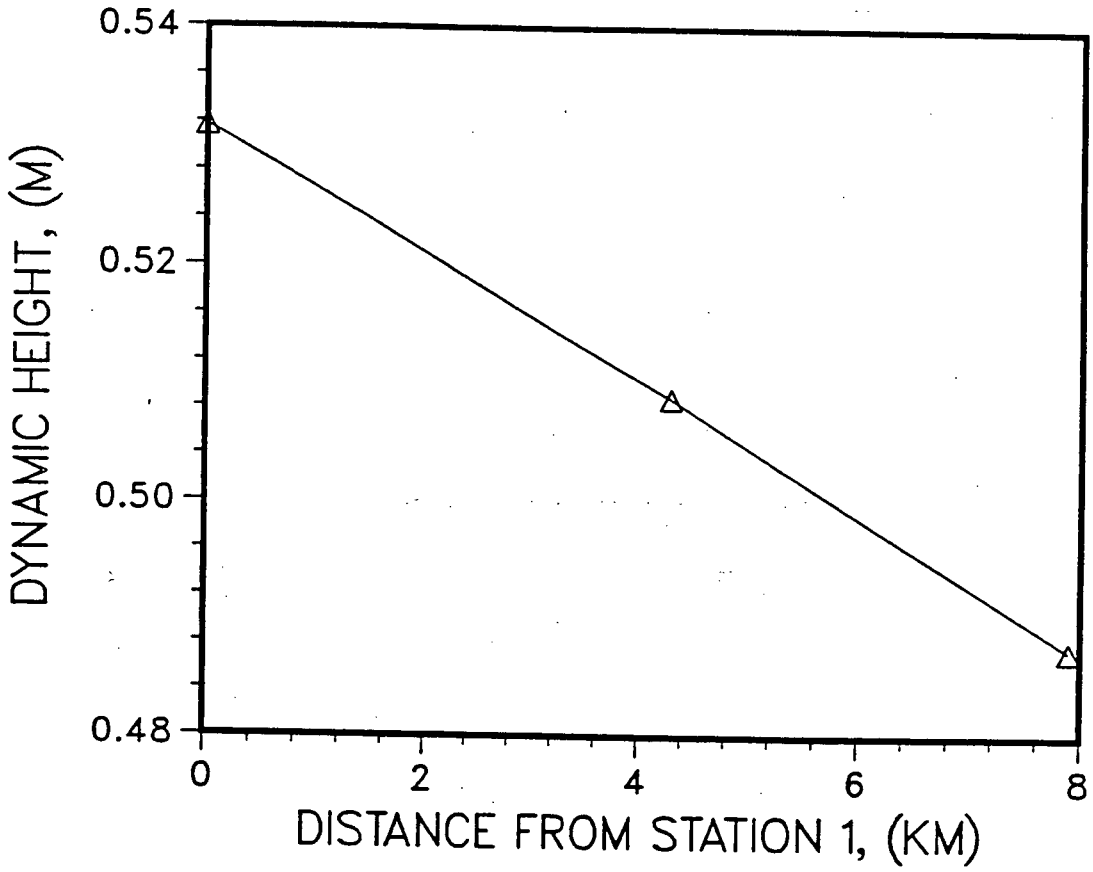

Figure 3.3: Sea surface slope of stations 1 to 3 in Georgia Strait.

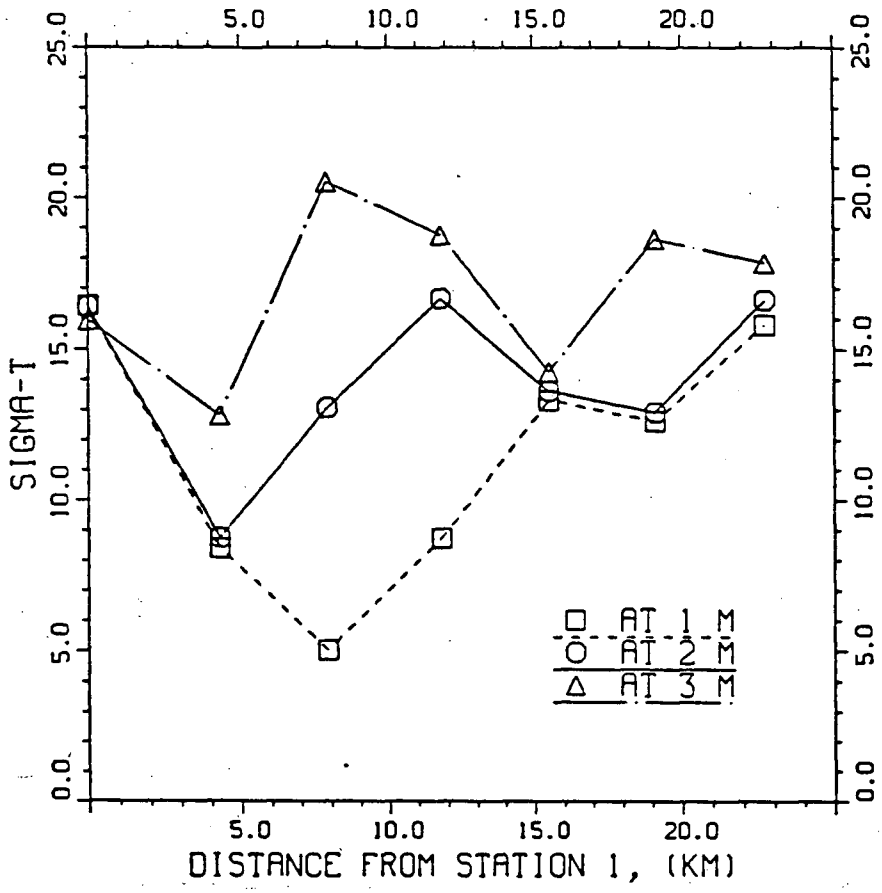

Figure 3.4: Densities (σ_t) across Georgia Strait at 1, 2, and 3 m depths for July 1986 data.

$-1.16 \times 10^{-4}\, ms^{-2}$ results for the Reynolds stress term. With $h = 3\,m$ and $u = 1.5\,ms^{-1}$, k was found to equal 1.55×10^{-4}. This k is about six times smaller than the assumed k used by Cordes, *et al.* These estimates for the pressure gradient and interfacial stress are important results since they show that the three terms (pressure, stress, and deceleration) are all of comparable value.

They assumed that the pressure gradient was due only to the sea surface slope, but, in theory, the density of water in the plume increases as it moves away from the river and the variation in density may also contribute to the pressure gradient. Figure 3.4 shows that σ_t does not increase for the first three stations, and that the surface density actually decreases from station 1 to station 3. Any effect that the density variations might have on the pressure gradient will be included if slopes of isobaric surfaces are calculated for the surface layer. For

the first three stations, then, I integrated the isobaric slopes for the top $3\,m$ to find a value for the net pressure gradient; the integrated value was $-1.2 \times 10^{-4}\,m^2 s^{-2}$. I divided this value by $h = 3$ to obtain $\frac{1}{\rho}\frac{\partial p}{\partial x} = -4.0 \times 10^{-5}\,ms^{-2}$, which is like an average pressure gradient for the top $3\,m$. The magnitude of the average pressure gradient is less than $|g\frac{\partial \eta}{\partial x}| = 5.6 \times 10^{-5}\,ms^{-2}$ so that the interfacial stress, in the case where density variations are considered, will be smaller.

The data set that was collected for the Fraser River plume study was not particularly well suited for a complete analysis of the balance of forces, since only three stations were used in the estimation of a pressure gradient and direct estimates of the deceleration could not by made. However, there was available to me recently gathered CTD data for inlets on the southern British Columbia coast, and so I decided to try and study the dynamics in Knight Inlet.

3.2 Knight Inlet

I estimated the inertial terms and the pressure term in the integrated momentum equation, and, with these values, I solved for the coefficient of friction. In order to do this, I first had to estimate several parameters.

Six vertical CTD casts were performed in Knight Inlet during the night of 31 May 1986 and the morning of 1 June 1986. The stations are shown in Figure 1.1. I processed the data using methods described in Freeland and Farmer (1980) and Wetton (1981) and I obtained estimates of the relevant parameters by these methods and by using the standard equations described in Chapter 2.

I decided that the momentum equation should be evaluated at each station rather than estimating one value for each term for the entire inlet. This was partly due to the limited data set, but also to see how the values of the terms in the momentum equation changed along the inlet. However, the gradients, such as $\frac{\partial u_1^2}{\partial x}$, which needed to be computed, necessitated that I use sections between every two stations in the final analysis. Therefore, some of the parameters were computed for each station, and then an average was computed for the midpoint between stations. CTD data collected on 10 June 1987 and 11 June 1987 were processed in the same

manner for comparison.

3.2.1 Estimating the inertial terms

depth of interface

To obtain the depth of the interface, $h(x)$, at each station, I utilized a method described by Freeland and Farmer (1980). The observations of the density structure given by my CTD data were used to find all three of these parameters.

In their method, Freeland and Farmer computed the internal wave speed and the potential energy from continuous density distributions using formulae that are described later. They set the computed values equal to formulae representing potential energy and internal wave speed for a two-layer model. These formulae were:

$$c_1^2 = g'(\sigma_2 - \sigma_1)h(H - h)/H \tag{3.2}$$

and

$$\chi_{obs} = \frac{1}{2}(\sigma_1 h^2 + \sigma_2(H^2 - h^2))/H^2 \tag{3.3}$$

where c_1 is the internal wave speed for the first mode computed from observed densities; $g' = g/\rho_2$, where $\rho_2 = 1024.5\,kgm^{-3}$ from density profiles; H is the bottom depth; χ is the observed potential energy; and σ_1 is the σ_t value at 2 m depth. These two equations were solved for h and σ_2 by Freeland and Farmer with the additional condition that σ_1 be set equal to the value of σ_t at $2\,m$ depth.

This procedure gave two-layer the model the same potential energy and internal wave speed as observed in the continuous situation. This approach was only appropriate in the months when there is high runoff and stratification is strong (Wetton, 1981).

The choice of σ_1 by Freeland and Farmer seemed to be a rather subjective choice for an otherwise objective approach. If the total mass had been preserved as well as the potential energy and the phase speed, then the result would have been a system of three nonlinear equations with three unknowns: h, σ_2, and σ_1 (P. H. LeBlond, personal communication). The

observed mass of the system could have been found from

$$M_{obs} = \int_0^H \sigma_t(z)dz.$$

If this quantity had been set equal to the total mass of the two-layer system, then

$$M_{obs} = \sigma_2 H + (\sigma_1 - \sigma_2)h$$

would have been the third equation in a nonlinear system already consisting of equations 3.2 and 3.3. The difficulty that this new dimension would have added to the approach is that the final equation reached for h would have been a cubic and the computation of h would have become more complicated. Freeland and Farmer tested the stability of their approach by choosing σ_1 values at depths other than $2\,m$. They found that their calculated h's varied by less than 10% as long as σ_1 values were chosen from above the pycnocline. I decided to follow their approach so that I could compare my results for h with theirs.

The equation that Freeland and Farmer derived to find h and that I used is:

$$h = (c_1^2/g')/(2\chi - \sigma_1 - c_1^2/(g'H)) \tag{3.4}$$

I do not know whether the surface layer defined by the computed boundary , h, (based on density), is the same as the surface layer defined by the velocity structure, but in the absence of current measurements I will assume that it is so.

internal wave speed

The internal wave speed was found by solving for the eigenvalues of the following equation:

$$Z_n''(z) + \frac{(N^2(z) - \omega^2)}{c_n^2} Z_n(z) = 0 \tag{3.5}$$

with the boundary conditions:

$$Z(H) = 0$$

which is the bottom condition and

$$Z'(0) - Z(0)/h_n = 0$$

which is the free surface condition. H is the total depth.

Equation 3.5 represents the vertical structure of the vertical component of motion of a stratified fluid. A derivation of the equation is given in section 5.2 of Phillips (1966). In his derivation, Phillips assumed that a mean shear was not present. The implied oscillatory motion is that of the internal tide present in Knight Inlet with angular frequency, ω, and amplitude $Z(z)$.

$N^2 \doteq -\frac{g}{\rho}\frac{\partial \sigma_t}{\partial z}$ is the Brunt-Väisälä frequency and its distribution, calculated with the observed densities, is representative of the stratification. If $N^2 - \omega^2 < 0$, the wave amplitude, $Z(z)$, will decrease exponentially with depth, and only surface waves will be described. For $N^2 - \omega^2 > 0$, not only are there surface modes, but there exist an infinite number of internal modes. $N(z)$ usually has its maximum in the pycnocline since the density gradient is the greatest there. It seems logical that the condition of $\omega^2 < N^2$ would more likely be met in this region of the water column.

A lower limit for the angular frequency, ω, is given by the dispersion relation $\omega^2 = f^2 + c_n^2(k^2 + l^2)$ where f is the Coriolis parameter, and k and l are horizontal wavenumbers. If the tide is semi-diurnal, as is the case in Knight Inlet, then $\omega = 1.405 \times 10^{-4}\, s^{-1}$. This is greater than $f = 1.13 \times 10^{-4}\, s^{-1}$ given for Knight (Farmer and Freeland, 1983).

If the tide travels internally as an internal Kelvin wave, as is suggested by Farmer and Freeland (1983), then it is non-dispersive and obeys the relation, $\omega^2 = c_n^2 k^2$. Therefore, the eigenvalues of the modal equation are phase speeds for a propagating internal Kelvin wave in Knight Inlet. For the zero-th mode, $c_0^2 = gH$, and for the baroclinic modes, $c_n^2 = gh_n$ where h_n is the equivalent depth.

Vertical displacements of the surface caused by internal waves are generally very small so that a rigid lid condition could have been used in this analysis. However, the existing program that I used for the calculations of the phase speeds used a free surface and I did not think that there would be a big difference in either case.

Farmer and Freeland estimated $c_1 \approx 1.0\, ms^{-1}$ during the summer in Knight Inlet. The

Station	c_1 (ms^{-1})	χ_{obs} $(kg\,m^{-3})$	h (m)	u_1 $(cm\,s^{-1})$	Fr	σ_1 $(kg\,m^{-3})$	σ_2 $(kg\,m^{-3})$	wind speed $(knots)$
1986								
1.5	0.55	12.12	14.51	25.25	0.438	21.87	24.25	27.5
3	0.53	12.07	6.71	28.26	0.520	19.57	24.15	27.5
5	0.86	12.12	7.41	11.04	0.126	13.58	24.25	32.5
7	1.08	12.22	7.17	7.11	0.065	7.17	24.44	25.0
9	1.10	12.18	6.36	6.79	0.061	4.07	24.38	25.0
11	1.24	11.90	7.19	5.09	0.040	0.38	23.86	12.0
1987								
1	0.58	12.23	8.91	14.65	0.248	20.41	24.47	24.0
3	0.49	12.14	2.34	20.53	0.408	13.24	24.28	20.0
5	0.68	12.12	3.47	10.80	0.157	10.25	24.25	20.0
7	0.84	12.21	3.67	7.15	0.084	4.27	24.41	7.0
9	0.99	12.14	4.38	5.05	0.050	0.53	24.29	14.0
11	0.70	11.98	2.14	10.16	0.143	0.12	23.96	0.0

Table 3.2: Table of c_1^2, χ, h, u_1, Fr, σ_1, σ_2, and wind speed in Knight Inlet in 1986 and 1987.

calculated wave speeds for my study were all close to this value. They are listed in Table 3.2.

potential energy

I found the observed potential energy by performing the numerical integration:

$$\chi = \frac{1}{H^2}\int_0^H \sigma_t(z) z\, dz$$

where σ_t are obtained from the observed σ_t density values and H is the total fluid depth. In the calculation of c_1, I set H equal to the bottom depth. A spline fit was used to fill in the missing data from the maximum depth measured to H. This step was already incorporated into the existing computer program. In the calculation of χ, however, the H that I used was the maximum depth measured for each cast. It was assumed that the bottom density structure was fairly constant so that it would not make much difference whether H was the bottom depth or the maximum measured depth for this particular computation. The values of χ were all approximately $12\,kg\,m^{-3}$ and are also listed in Table 3.2.

The h values that I computed are shown in Figure 3.5. The interface deepens very quickly

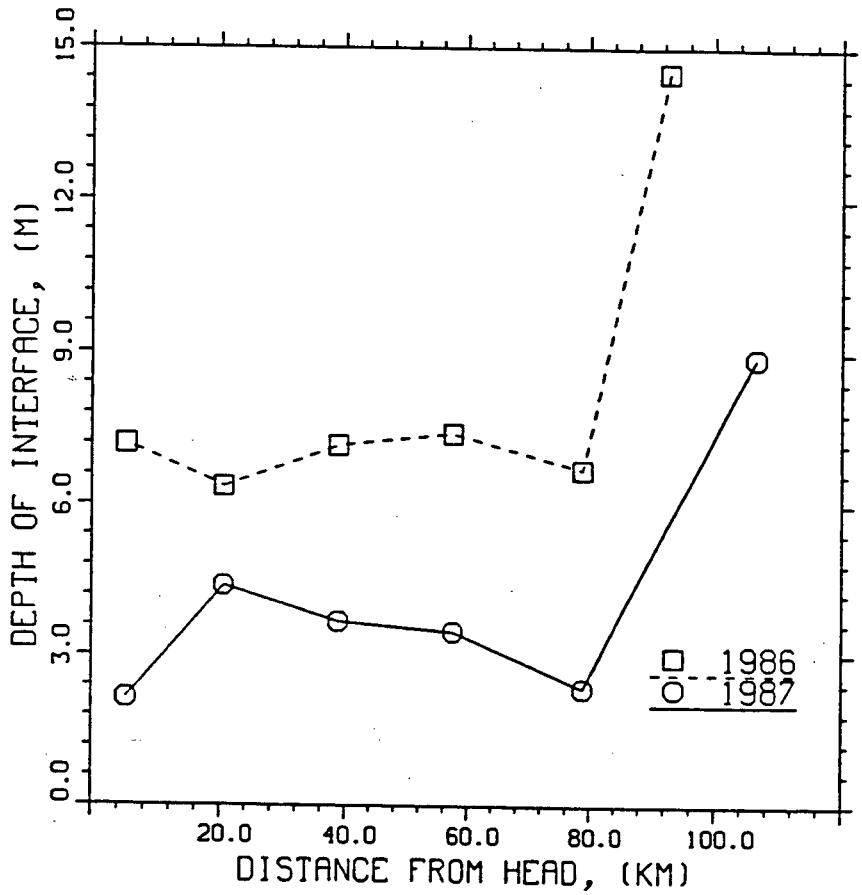

Figure 3.5: Depth of the interface at different points in Knight Inlet.

near the mouth and is at a fairly constant depth from station 3 through to the head.

This constant interface depth region includes the winding half of the inlet. Freeland and Farmer (1980) observed that deepening was more gradual in the sinuous section and their plots bear a resemblance to the plot in Figure 3.5. To refer to both halves of the inlet as separate entities in this study, as Freeland and Farmer did in theirs, did not seem practical due to the small size of the data set. Since stations 1.5 and 1 are well seaward of the sill, I felt that the anomalous h was probably due to outside processes. Pearson and Winter (1978) found that the upper layer thickness increased from $6\,m$ or $7\,m$ at the head of Knight Inlet to $20\,m$ seaward of the sill during times of high river discharge. They calculated, though, that h was between $6\,m$ and $10\,m$ for most of the inlet, and only reached the greater depth of $20\,m$ on the seaward side of the sill. The average h of the other five stations was $6.97\,m$ in 1986 and $3.20\,m$ in 1987 and these were the values that I used to represent the lower boundary of the surface layer in other later computations.

inflowing layer density: σ_2

I determined the density of the second layer from equation 3.2.

$$\sigma_2 = \sigma_1 + \frac{c_1^2 H}{g' h (H - h)}$$

Figures 3.6, 3.7, 3.8, and 3.9 show how the densities computed for the two-layer model fit the observed continuous density profile. In the deeper water the computed densities fit quite well. For station 11 in 1987, the computed interface seems to be much shallower than the pycnocline in the observed distribution (Figure 3.9).

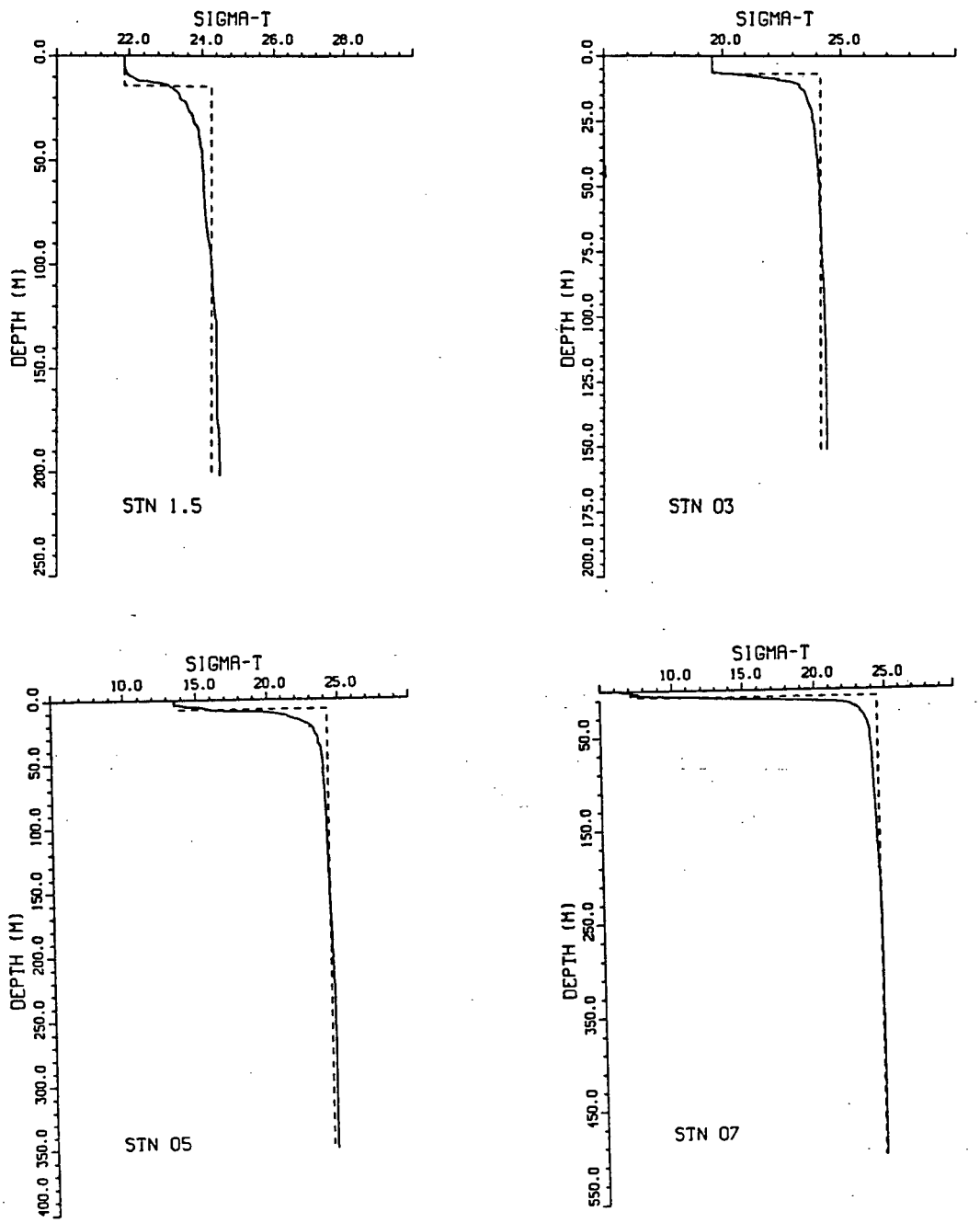

Figure 3.6: Representative density profiles for the two-layer model and the observed continuous density distributions for 1986, stations 1.5 to 7. The dashed line shows the density distribution represented in the two-layer model and the solid line shows the observed density profile.

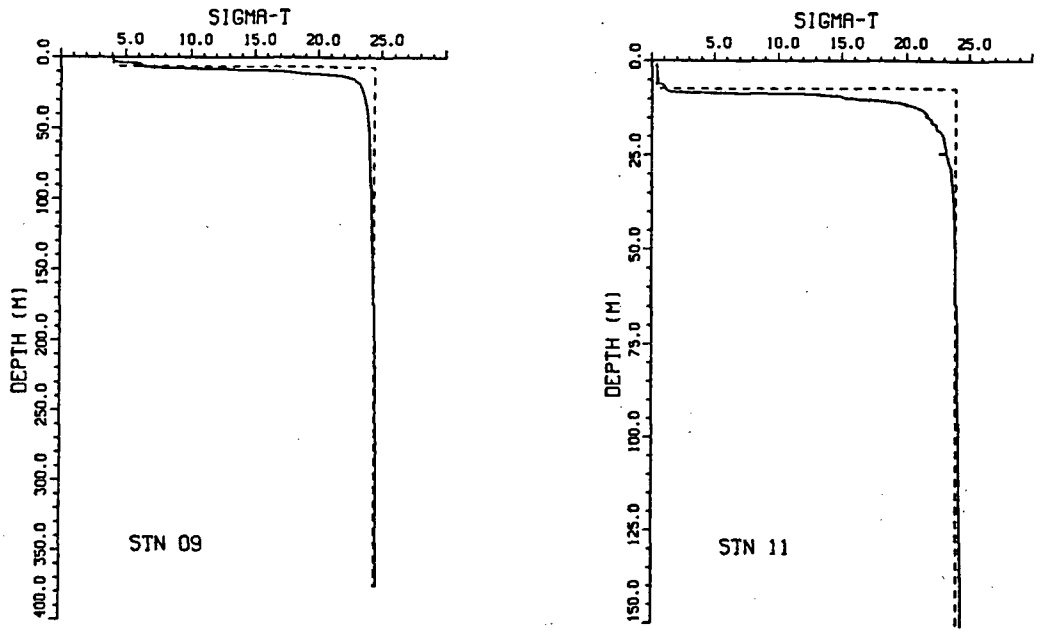

Figure 3.7: Representative density profiles for the two-layer model and the observed continuous density distributions for 1986, stations 9 and 11. The dashed line shows the density distribution represented in the two-layer model and the solid line shows the observed density profile.

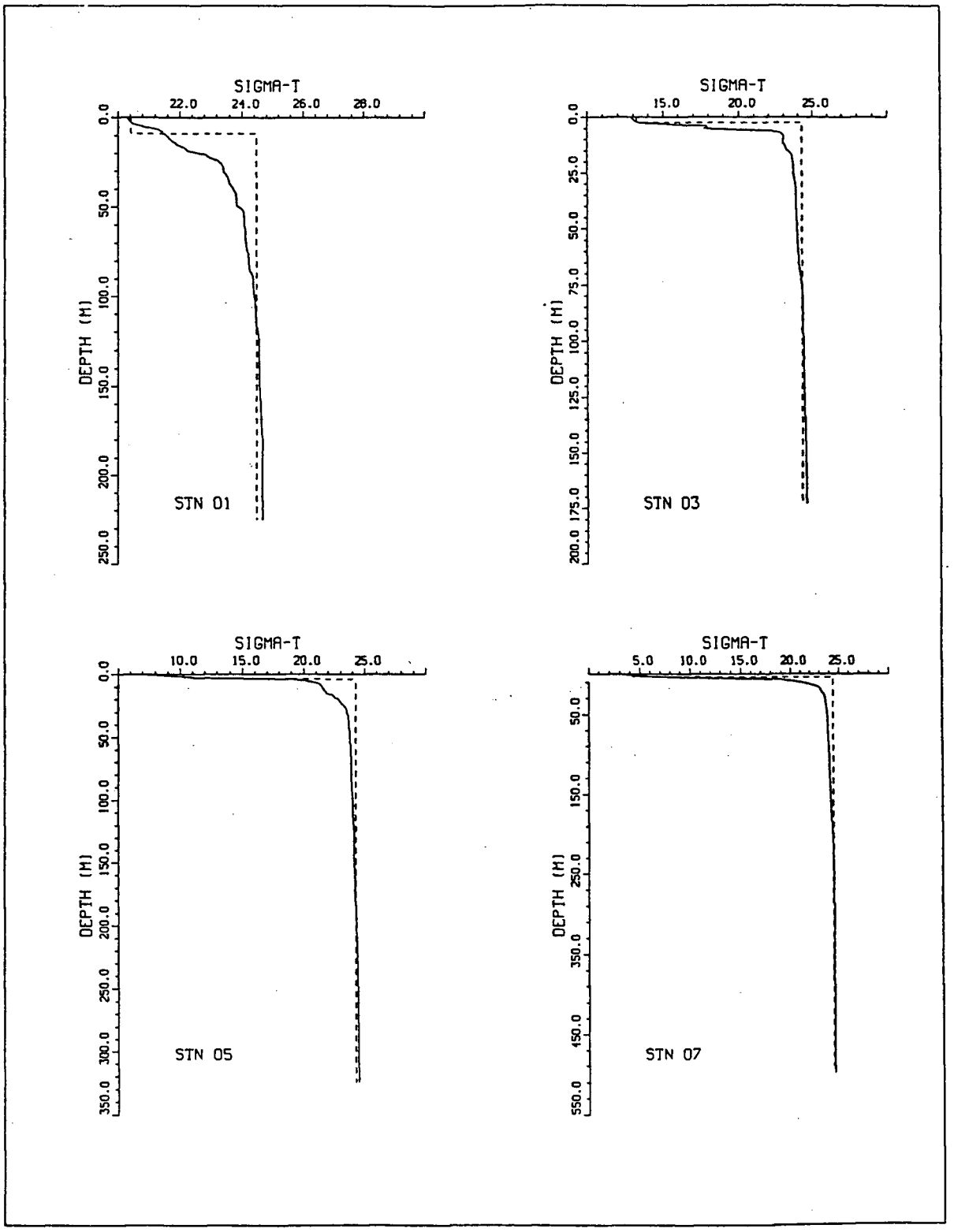

Figure 3.8: Representative density profiles for the two-layer model and the observed continuous density distributions for 1987, stations 1 to 7. The dashed line shows the density distribution represented in the two-layer model and the solid line shows the observed density profile.

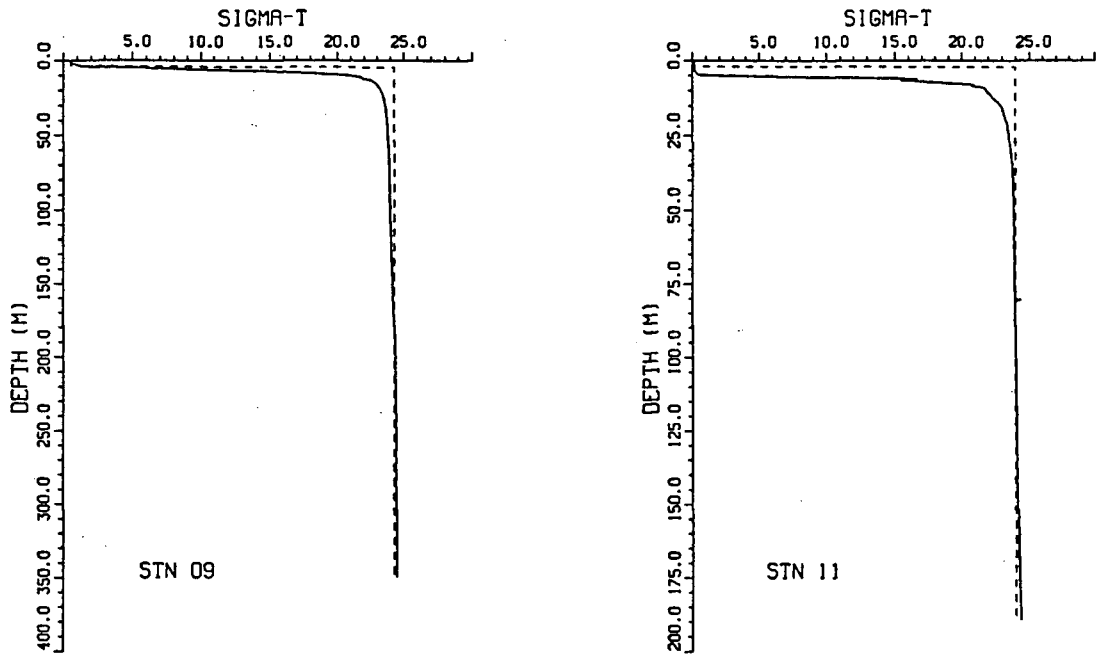

Figure 3.9: Representative density profiles for the two-layer model and the observed continuous density distributions for 1987, stations 9 and 11. The dashed line shows the density distribution represented in the two-layer model and the solid line shows the observed density profile.

velocity of the surface layer

I obtained fresh water runoff data for the Klinaklini River from water survey data of the Inland Waters Branch of Environment Canada. The daily mean discharge for 31 May 1986 was $920\,m^3s^{-1}$, and, for 1 June 1986, it was $880\,m^3s^{-1}$. An average value of $900\,m^3s^{-1}$ was used for R in equation 2.10. In 1987, the mean discharge for the two days that the data were collected was $541.5\,m^3s^{-1}$. I took the width of the inlet, B, to be $2.5km$. I determined the upper layer velocity by using the above values, and the densities used and computed previously, in the following equation derived from equations 2.10 and 2.11:

$$u_1 = \frac{R}{Bh}\left(\frac{\sigma_2}{\sigma_2 - \sigma_1}\right). \tag{3.6}$$

These values are listed in Table 3.2 and shown in Figure 3.10.

Froude numbers

I calculated the interfacial Froude numbers for each station with the use of the surface layer velocity values.

$$Fr = \frac{u_1}{\sqrt{gh\Delta\rho/\rho_1}}$$

In the above definition (from Freeland and Farmer, 1980), $\Delta\rho$ is the difference in densities across the interface, ρ_1 is the density of the upper layer and was given the value of $1000 + \sigma_1$ at $2\,m$ for each station. The Froude number compares the flow velocity with the phase speed of an internal wave. If $Fr >> 1$, supercritical flow occurs, and if $Fr << 1$, subcritical flow occurs. At $Fr = 1$, flow is critical. A hydraulic jump, as well as barotropic forcing, may occur when flow changes from supercritical to subcritical and it can be induced by the presence of a sill as in Knight Inlet. The transition from super- to subcritical flow is important to energy-exchange processes in Knight Inlet. Freeland and Farmer found that $Fr < 1$ at the mouth of Knight Inlet, and the Froude numbers that I calculated for both years agreed with their result. The Froude numbers, for my study, in the sill area were larger than for regions up-inlet of the sill, but they still satisfied the criterion for subcritical flow. They concluded, then, that Knight Inlet

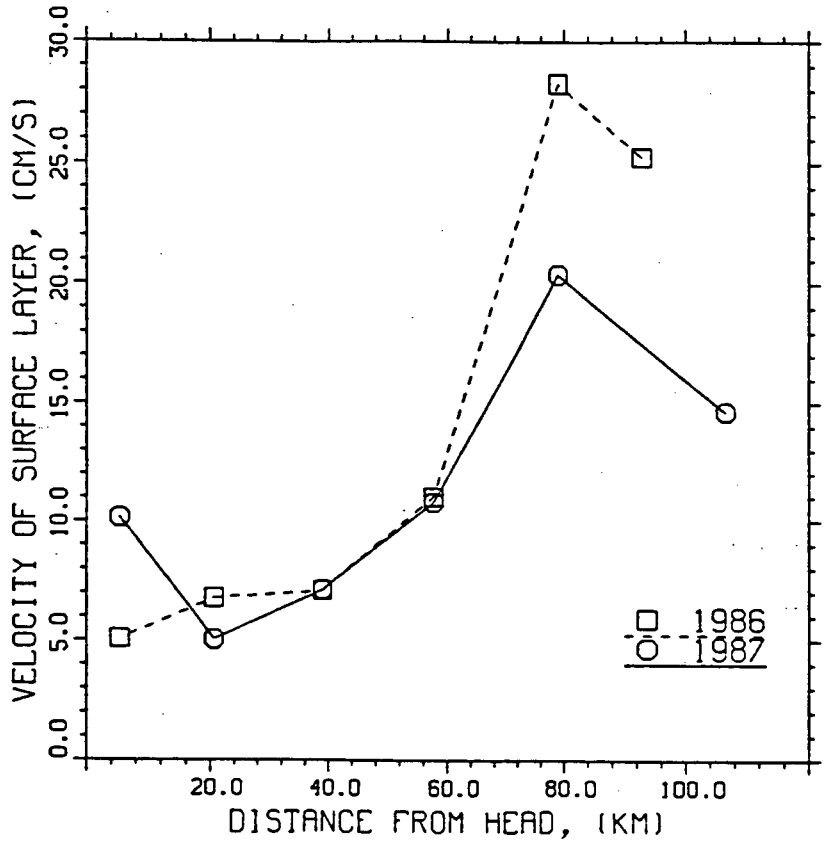

Figure 3.10: Surface layer velocity for Knight Inlet in 1986 and 1987.

Station Sections	$w \times 10^{-4}$ $(cm\,s^{-1})$	Δu $(cm\,s^{-1})$	k_e $\times 10^{-4}$
1986			
3 – 5	56.36	5.34	10.6
5 – 7	14.65	4.71	3.1
7 – 9	1.19	5.36	0.2
9 – 11	7.76	5.38	1.4
1987			
3 – 5	14.38	9.05	1.6
5 – 7	6.26	5.78	1.1
7 – 9	3.66	5.31	0.7
9 – 11	−10.68	7.51	−1.4

Table 3.3: Table of entrainment velocity, (w), Δu for $h_2 = h$, and the entrainment coefficient, (k_e), for $h_2 = h$ in Knight Inlet for 1986 and 1987.

was not hydraulically controlled by the critical condition, $Fr = 1$, at the mouth as purported by Long (1975), although a hydraulic jump is a periodic phenomenon in Knight Inlet. Pedersen (1978) stated that a small Froude number, in a first order analysis, means that the shear stress is balanced by the longitudinal pressure gradient. If the flow velocity is small compared to the phase speed, then the Froude number will be much less than one and the inertial terms will also be small. It can be seen from Table 3.2 that the Froude numbers are less than one, and that stations 7, 9, and 11 have Froude numbers which are much less than one.

velocity of the inflowing layer

I found the velocity of the lower, inflowing layer from a rearrangement of equation 2.11.

$$u_2 = u_1 h(\frac{\sigma_1}{\sigma_2})\frac{1}{h_2} \tag{3.7}$$

In a two-layer model, normally $h_2 = H - h$ with respect to the density structure, I was not sure what value of h_2 to use to define the layer with respect to the velocity, u_2. Pickard and Rodgers (1959) sometimes observed a weak downstream current below the obvious inflow. Previously, I stated that I would assume that h based on the density structure would define the

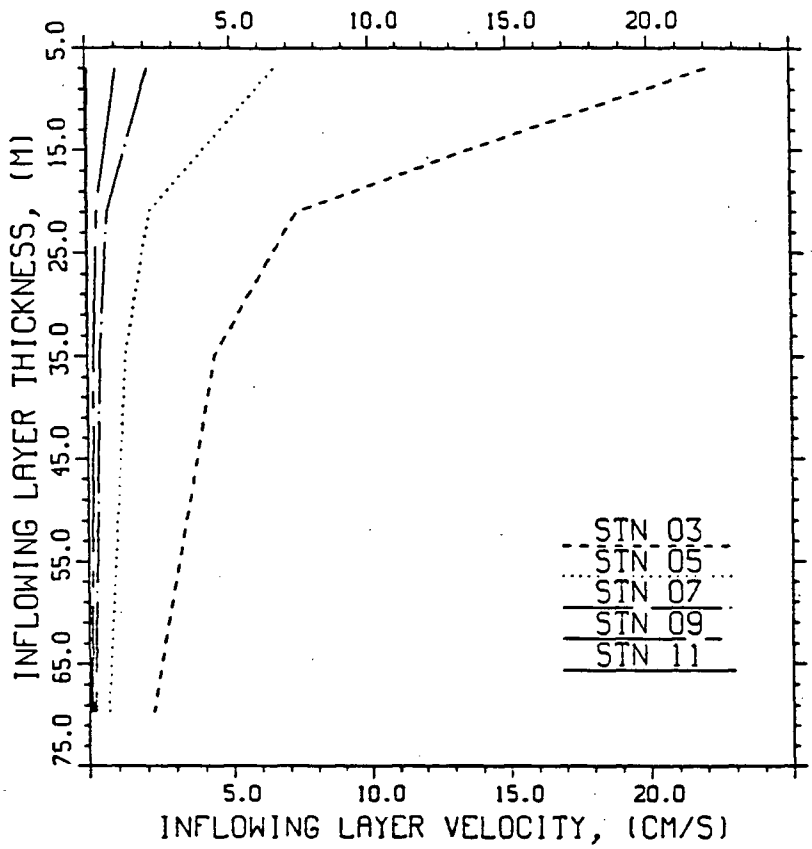

Figure 3.11: Inflowing layer velocity as a function of inflowing layer thickness for Knight Inlet for 1986.

boundary between u_1 and u_2, but for u_2 I wanted to see how different values of h_2 would effect u_2 and, ultimately, k. I computed u_2 for values of h_2 in the range: $h \leq h_2 \leq H - h$; h_2 was set equal to h, $3h$, $5h$, and $10h$. It was expected that the magnitude of u_2 should be very close to the magnitude of u_1 for $h_2 \approx h$ (ie. outflowing layer thickness equal to the inflowing layer thickness) and that the magnitude of u_2 should decrease as h_2 increases towards $H - h$. Figure 3.11 shows how u_2 decreased. The h_2 and corresponding u_2 estimates are listed in Table 3.4. Figure 3.12 shows the inflowing layer velocity for $h_2 = h$.

To estimate the values of the two inertial terms, I had to calculate $\frac{\partial u_1^2}{\partial x}$. I did this calculation for sections found between every two stations. Ultimately, then, there would be only five

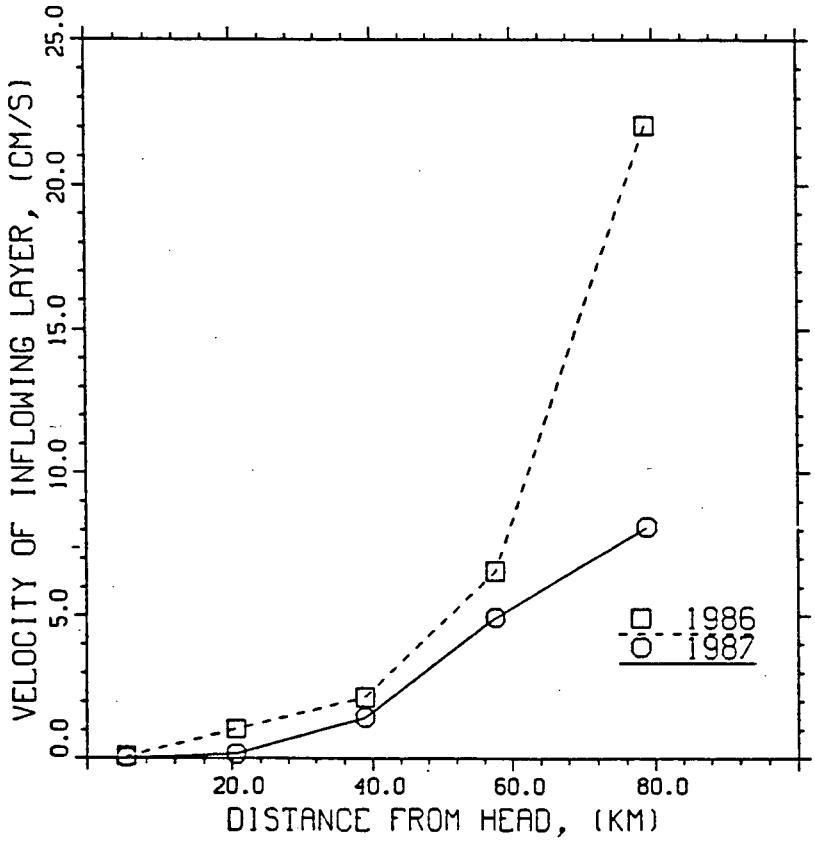

Figure 3.12: Inflowing layer velocity for $h_2 = h$ in Knight Inlet in 1986.

estimates for k. The estimates for these two inertial terms are listed in Table 3.5.

entrainment velocity

Out of interest, I found the entrainment, w, for the entire layer, between pairs of stations from equation 2.8 with h constant and equal to the value of the average interface depth ($\overline{h}$).

$$w = \overline{h}\frac{\partial u_1}{\partial x} \tag{3.8}$$

Pedersen (1978) listed two effects of entrainment on fjord dynamics. It influences the longitudinal pressure gradients, and hence, the shear stress due to longitudinal density gradients. Entrainment also affects the momentum created by the upward flow across the longitudinal surface flow, which creates more shear stress. It can occur as a result of breaking internal gravity waves. The entrainment velocities are listed in Table 3.3. It seems that the entrainment is much larger in the straight portion of Knight Inlet (stations 3-7) than in the sinuous section. This is consistent with what Freeland and Farmer (1980) found. From the entrainment values, I calculated an entrainment coefficient, k_e, like Cordes, *et al.* (1980) did, where $w = k_e \Delta u$. Δu is the difference between the upper layer velocity and the lower layer velocity and was calculated using u_2 computed with $h_2 = h$. From station 11 to station 3, I estimated w to be $((0.2826 - 0.0509)/73600) \times 6.97 = 21.94 \times 10^{-4}\, cm\, s^{-1}$ for 1986 and $4.51 \times 10^{-4}\, cm\, s^{-1}$ in 1987. The entrainment coefficients along the inlet are mostly on the order of 10^{-4} which is a result that is consistent with Cordes, *et al.*'s $k_e = 2 \times 10^{-4}$.

3.2.2 Pressure Gradient Acceleration

I calculated the slopes of isobaric surfaces in Knight Inlet by finding the dynamic heights of the surfaces at every station relative to a $100\, m$ level of no motion. This assumption is only reasonable inland of the sill (Wetton, 1981), so that in the final analysis, I left out station 1.5. It can be seen from the previous results, that this station is associated with a few anomalous values; most obviously, the interface depth. A least squares fit through stations 3 to 11 provided me with the isobaric slopes that I needed. The profiles of these slopes are shown in Figure

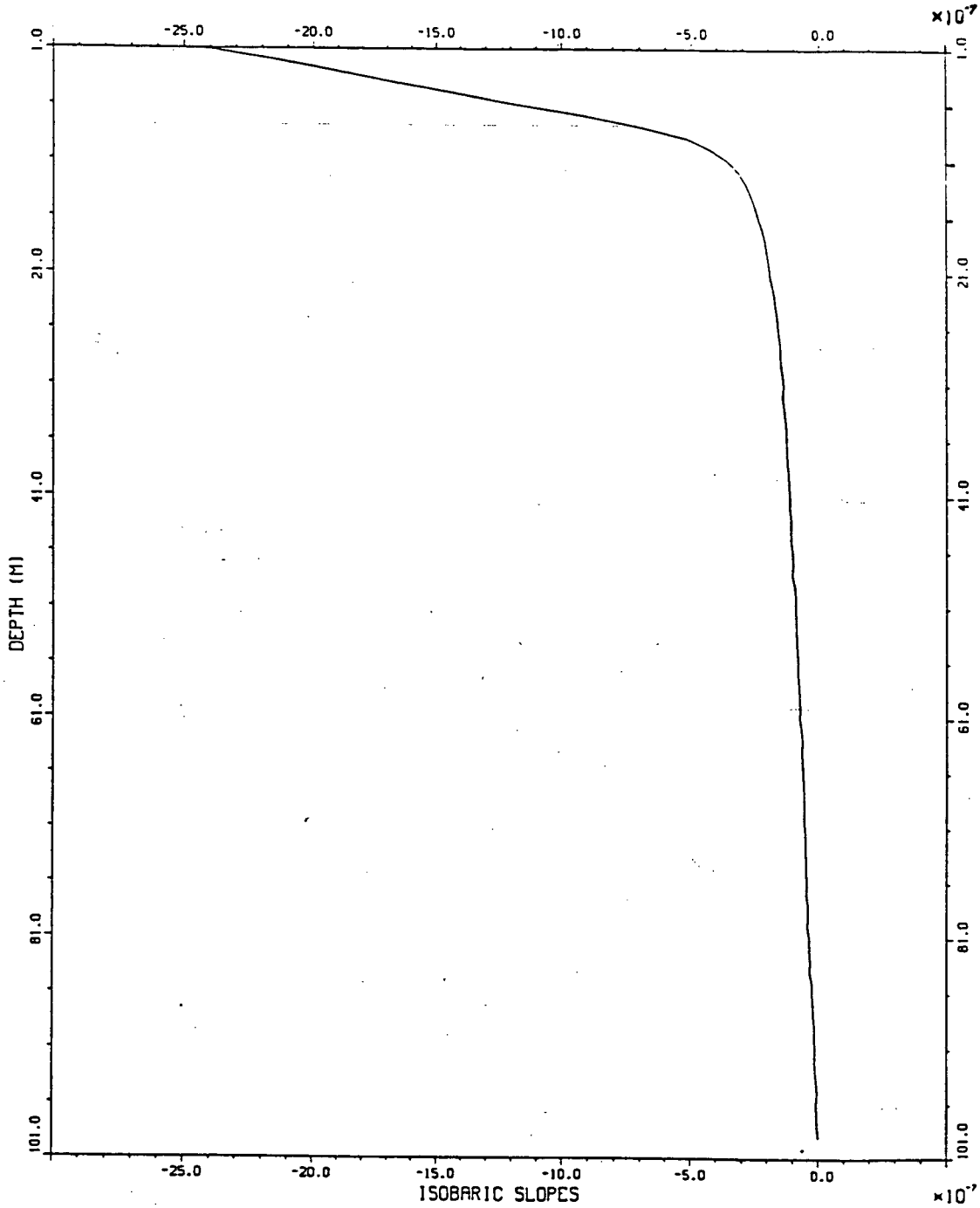

Figure 3.13: Isobaric slope profile in dynamic meters per meter for Knight Inlet, 1986.

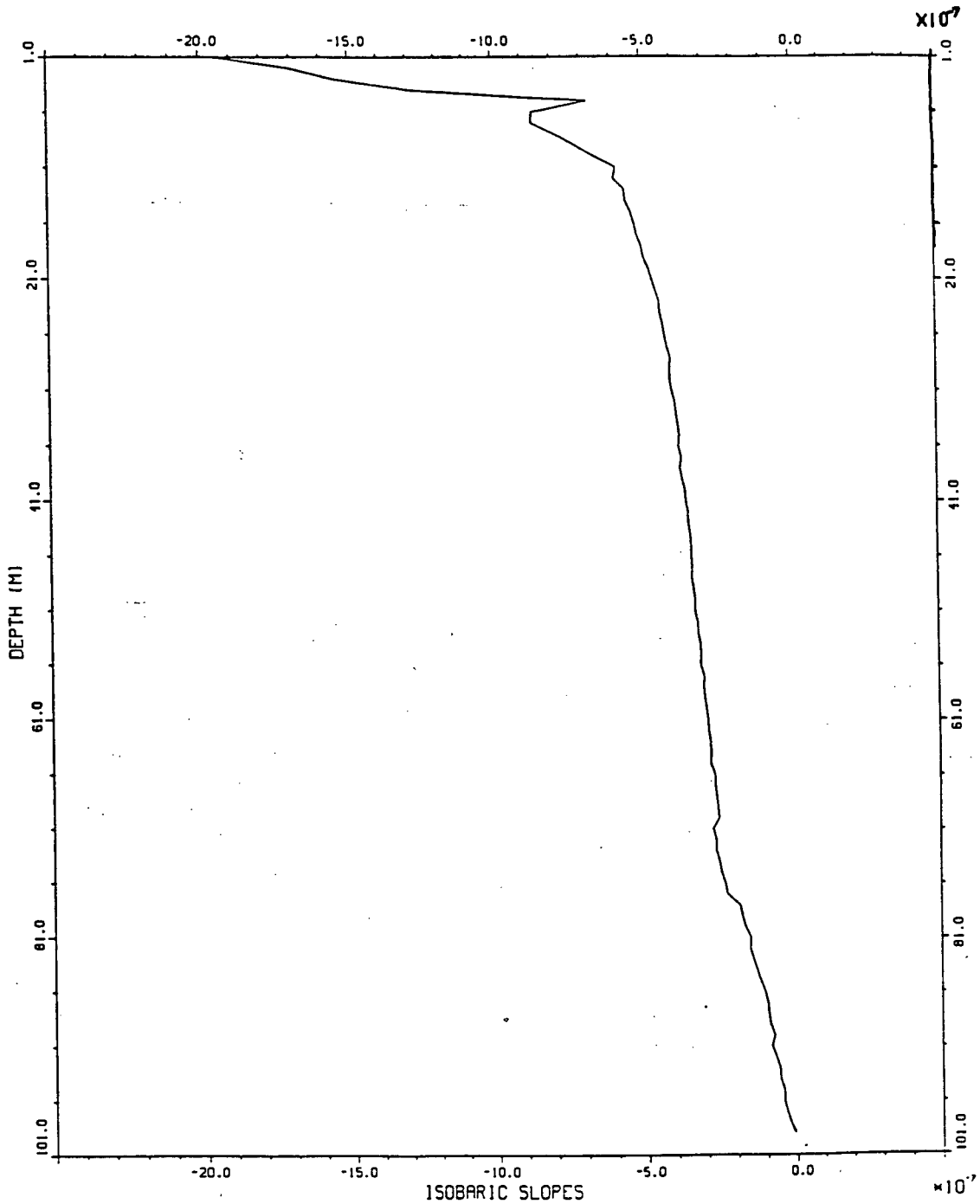

Figure 3.14: Isobaric slope profile in dynamic meters per meter for Knight Inlet, 1987.

3.13 and Figure 3.14 for Knight Inlet data sets gathered during cruises in 1986 and 1987 respectively. There are no zero crossings in either profile. The implication is that the pressure gradient at depth is not zero. Webb(1985) showed that there are weak deep residual flows up channel of the sill. If the zero of the isobaric slope were shifted to zero at some intermediate depth, say below $20\,m$, the near surface isobaric slopes would not be changed much so that the calculation of the near surface momentum terms would not be greatly changed. Wetton (1981) found only one zero crossing in his isobaric profiles. One may speculate that these weak flows and small pressure gradients are associated with residuals driven by non-linear effects on the tidal currents. Further studies are necessary.

The dynamic heights shown in Figure 3.15 were fitted with a linear regression to compute $\frac{\partial \eta}{\partial x}$. Wetton (1981) suggested that the deviation from the linear fit in the straight portion of the Knight Inlet was due to the internal tide which is generated at the sill. Research of the internal tide in Knight Inlet has been carried out by Webb (1985) and Farmer and Smith (1980). The sea surface slope was the uppermost isobaric slope calculated, $\frac{\partial \eta}{\partial x} = -2.43 \times 10^{-6}\, m m^{-1}$ in 1986 and $\frac{\partial \eta}{\partial x} = -1.95 \times 10^{-6}\, m m^{-1}$ in 1987 (Figure 3.15). I assumed that the sea surface was at $1\,m$ depth because the data sets for each station did not have equivalent starting points. These values for $\frac{\partial \eta}{\partial x}$ are consistent with those calculated by Wetton (1981), which were typically of the order $10^{-6}\, m\, m^{-1}$.

The integrated value of the pressure gradient term was $-10.00 \times 10^{-5}\, m^2 s^{-2}$ in 1986 and $-3.50 \times 10^{-5}\, m^2 s^{-2}$ in 1987 with the interface depth equal to $7.0\,m$ in 1986 and $3.2\,m$ in 1987.

3.2.3 Friction coefficient

The equation that I used to solve for k was:

$$k = -(\Delta u)^{-2}(0.9h\frac{\partial u_1^2}{\partial x} + 1.8h\frac{\partial u_1^2}{\partial x} + \int_{-h}^{0} \frac{1}{\rho}\frac{\partial p}{\partial x} dz) \tag{3.9}$$

The terms on the righthandside are the inertial accelerations and pressure gradient acceleration integrated over the surface layer as shown in Chapter 2 (see equations 2.7, 2.9, and 2.22). The

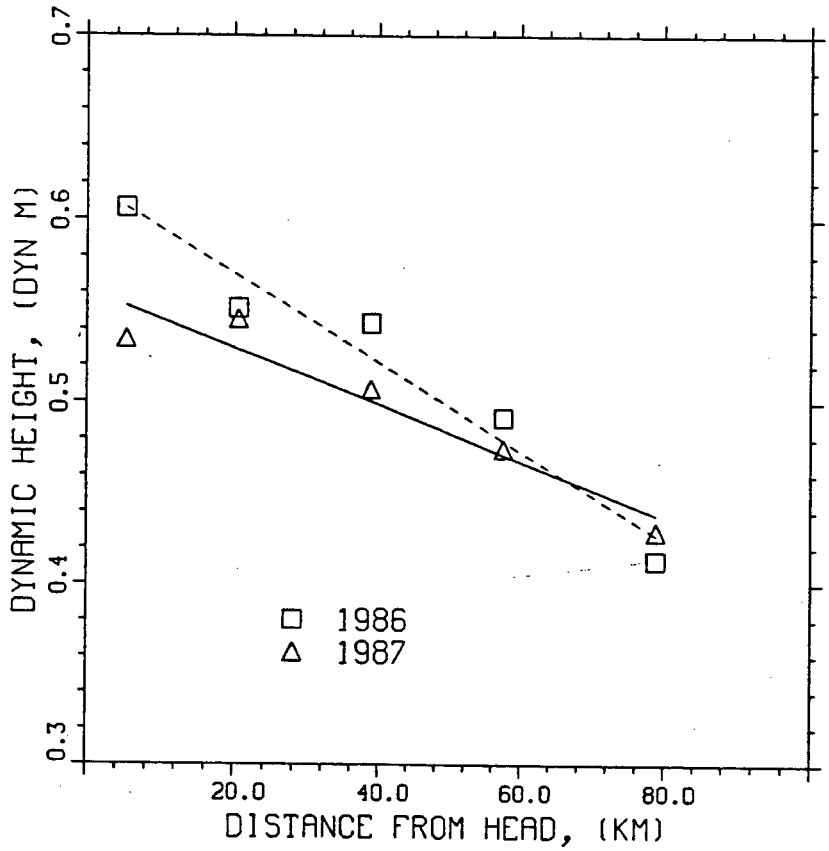

Figure 3.15: Sea surface slope for Knight Inlet in 1986 and 1987.

Station Sections	$h_2\,(m)$	$u_2\,(cm\,s^{-1})$	$k \times 10^{-3}$	$k_w \times 10^{-3}$
1986				
3 – 5	6.97	14.31	14.11	133.21
	20.91	4.77	1.82	17.14
	34.85	2.86	1.43	13.47
	69.69	1.43	1.21	11.43
5 – 7	6.97	4.36	41.79	184.20
	20.91	1.45	15.99	70.48
	34.85	0.87	13.81	60.85
	69.69	0.44	12.45	54.86
7 – 9	6.97	1.59	34.67	117.02
	20.91	0.53	24.16	81.54
	34.85	0.32	22.64	76.41
	69.69	0.16	21.59	72.87
9 – 11	6.97	0.56	33.67	84.02
	20.91	0.19	29.44	73.47
	34.85	0.11	28.69	71.59
	69.69	0.06	28.15	70.24
1987				
3 – 5	3.20	6.53	2.80	21.16
	9.61	2.18	1.27	9.64
	16.01	1.31	1.12	8.50
	32.02	0.65	1.03	7.77
5 – 7	3.20	3.20	9.58	34.91
	9.61	1.07	5.11	18.64
	16.01	0.64	4.60	16.78
	32.02	0.32	4.27	15.57
7 – 9	3.20	0.79	12.00	28.52
	9.61	0.26	9.92	23.59
	16.01	0.16	9.57	22.76
	32.02	0.08	9.32	22.16
9 – 11	3.20	0.09	6.98	****
	9.61	0.03	6.87	****
	16.01	0.02	6.84	****
	32.02	0.01	6.83	****

Table 3.4: Table of inflowing layer velocities, u_2, and friction coefficients, k, for various values of h_2 for 1986 and 1987. Also listed are the friction coefficients calculated with the wind effect, k_w, for 1986 and 1987 in Knight Inlet.

Station Sections	$\int_{-h}^{0} u\frac{\partial u}{\partial x}dz$	$\int_{-h}^{0} w\frac{\partial u}{\partial z}dz$	$-\int_{-h}^{0}\frac{1}{\rho}\frac{\partial p}{\partial x}dz$	$-\frac{1}{\rho}\tau_i$	Stresses (with wind)	
					$-\frac{1}{\rho}\tau_i$	$\frac{1}{\rho}\tau_w$
1986						
3 – 5	199	397	1000	−402	−3795	3393
5 – 7	24	48	1000	−928	−4091	3163
7 – 9	1	3	1000	−995	−3360	2364
9 – 11	8	17	1000	−975	−2433	1458
1987						
3 – 5	40	81	350	−229	−1733	1504
5 – 7	10	20	350	−320	−1166	846
7 – 9	4	8	350	−338	−803	465
9 – 11	−15	−29	350	−394	*****	****

Table 3.5: Estimates of terms in integrated momentum equation, $\times 10^{-7}\ m^2 s^{-2}$, with and without wind effects in Knight Inlet for 1986 and 1987.

stress term, which contains k, is estimated by $-k\Delta u^2$ as was explained in Section 2.1.3. The final resolution of k required that the difference, Δu, be calculated for every between station section. To do this, I calculated an average u_1 value and an average u_2 value for every two stations. I used the difference between these two "average" velocities to give Δu for each section. I did this procedure for every u_2 corresponding to a different h_2 and then I found the coefficient of friction for every one of these values. Table 3.4 lists the k values for each h_2. k did not differ greatly when h_2 was equal to a few times h.

The estimates of k that I have discussed thus far were calculated with the mean wind stress set to zero. I re-computed k and the balance of terms in the momentum equation out of curiosity as to what effect the inclusion of the wind stress term would have had on the final results. I used wind data that was recorded at the time of sampling. The wind was strongest at the mouth ($27.5\,knots$ at stations 1.5 and 3), and weakest at the head ($12\,knots$ at station 11) (Table 3.2). The average wind speed for the sampling period was $25\,knots$. The direction was generally down-inlet. The values of k that I re-computed with the influence of the wind included were done so with the h_2 and u_2 values that I used previously. These new coefficients are listed in Table 3.4 and are much larger than the previous k values computed with the condition of no wind.

I realize that the wind's effects on the surface layer do not only stem from the wind field present during the time of sampling, but also from the state of the wind field for many hours preceding. These rough approximations, then, are just that and should not be taken as conclusive.

The estimates of the terms for the integrated momentum equation are listed in Table 3.5. The estimates are given in $m^2 s^{-2} \times 10^{-7}$ for 1986 and 1987. The interfacial stresses are listed for no wind conditions and wind conditions. The calculated wind stress is also listed.

Chapter 4

Discussion of Surface Layer Dynamics Problem

4.1 Discussion

The estimations of the terms in the integrated horizontal momentum equation that I made for Knight Inlet (Table 3.5) lead to some interesting results and intriguing comparisons.

The inertial terms in equation 2.1 decreased in importance relative to the pressure field and the turbulent stress as the distance from the mouth increased. The two integrated inertial terms were larger (almost 25 times larger) near the mouth (sill area), where the surface layer was moving the fastest, than at the head (Table 3.5). The noticeable significance of the inertial terms in the sill area could be due to processes only there. The sill is where internal gravity waves are generated and is an active region for mixing due to tidal flow. In 1987, the two terms were generally smaller than in 1986 especially at the sill where the 1986 results were five times larger than those of 1987. Since the river discharge in 1986 was almost twice as much as in 1987, the surface layer velocity for 1986 was larger, so this result was hardly surprising. In both years, the first inertial term was one half as large as the second, which was expected from the integrated representations of those two terms shown in equation 2.7 and equation 2.9. The negative values in 1987 were due to the deceleration of u_1 between station 11 and station 9.

I calculated the coefficient of interfacial friction for various values of u_2 which were, in turn, calculated from different h_2 values. The smallest k found for each section was found

with $h_2 = 10h$; values for $h_2 = 3h$ and $5h$ were comparable to the $h_2 = 10h$ values. The $h_2 = h$ values are large, but, as h_2 is likely a few times h, the smaller values are probably more representative. For this h_2, u_2 was the least and Δu was the most. It seemed that, provided h_2 was at least a few times h, k did not vary much.

The estimates of the friction coefficient, k, that I found were considerably larger than the presumption made by Freeland and Farmer (1980) that $k < 1.7 \times 10^{-3}$. They concluded that interfacial friction was not important in the circulation of Knight Inlet. They obtained the best fit between observation and theory in the inviscid limit when $k = 0$. Long (1980) stated that a small drag coefficient does not imply that friction is unimportant. He demonstrated that the Reynolds' stress is appreciable compared to the longitudinal inertial acceleration by using typical estimates for the surface layer velocity and for his parameter that represented the interfacial friction. My estimates were also outside the range, 2.0×10^{-3} to 5.0×10^{-3} given by Dyer (1973). Long (1975) considered $k = 1$ to be appropriate for Knight Inlet, which, when compared with my estimates and those of Freeland and Farmer, seemed to be a large overestimation. Gade and Svendsen (1978) applied Long's two-layer model to Sognefjord in Norway and found that the friction coefficient was of the order 10^{-3}. Considering the variation in the k estimates between the years 1986 and 1987, it was difficult to provide a single estimate for k, or even a small, viable range as Dyer did. It appeared that k for 1986 was of the order 10^{-2}, and, for 1987, k was of the order 10^{-3}. The value of k will probably change as the dynamic processes in Knight Inlet change seasonally and daily with the tide.

If wind effects were considered, the estimates of the friction coefficients were even larger. Wetton (1981) stated that the pressure gradient is reactive to the wind on the surface layer of the inlet; it modifies the pressure gradient by increasing the sea surface slope which drives the flow. An increase in the pressure field would increase the stress term in order to maintain a balance between forces. The assumption of little or no wind, in my case, may not have been valid, in light of the strong wind velocities recorded at the time of sampling, but for lack of more extensive wind data, the assumption was made.

In low wind or no wind conditions, it seemed that the interfacial stress balanced the pressure field. This is especially true inland of the sill. If wind effects were calculated from recorded wind velocities and included into the analysis, the stress due to the wind would seem to account for a significant amount of the stress term. Wetton also found this fact to be true. However, my analysis, as well as Wetton's, assumed that $\frac{\partial u}{\partial t} = 0$. This is unlikely to be true if the wind had not been blowing steadily for some time; it would be a bad assumption. Although, the wind data that I used was somewhat questionable as to whether it could accurately represent the wind field effects on the surface at the time of sampling, I believe that underestimating the importance of wind effects when trying to obtain an estimate of the stress could result in misleading estimates of the friction coefficient, and perhaps my estimates of k and interfacial stress which considered those effects provide a better representation of the system.

The Reynolds' stress was least important at the mouth and increased up-inlet. This fact is not surprising considering the earlier analysis of the inertial terms would have lead to the same conclusion. In 1986, the value of $\frac{1}{\rho}\tau_i$ was about 2.4 times larger than at the mouth, and, in 1987, it was 1.7 times larger at the head than at the mouth.

Although my work in the Fraser River plume was, by no means, extensive, it did prove useful in providing a more precise estimate of the friction coefficient for that area. Cordes, *et al.*, (1980) concluded that entrainment can account for about one half of the observed deceleration in the Fraser River plume, but that the deceleration caused by interfacial stress and balanced by pressure gradient effects is more important. My estimation of the pressure gradient for the plume resulted in a much smaller estimate of the interfacial stress so that all three effects are comparible. The values of the entrainment coefficients calculated for Knight Inlet were, surprisingly, of the same order as those found by Cordes, *et al.* ($O(10^{-4})$).

McAlister, *et al.*, (1959) analyzed the dynamical balance for Silver Bay, Alaska and their study is summarized in Dyer (1973). They used the same horizontal momentum equation as I did, but obtained estimates for the terms at several depths rather than along the fjord. For their high runoff season (July), they found that there was a strong pressure gradient associated

with the surface slope. The largest gradient was limited to $5\,m$ depth. Below their level of no net motion at $9\,m$, the dynamical balance was between the pressure gradient and the Reynolds' stress term. In their summer analysis, they found that the pressure field did not reverse and that the field was greater inside the bay than outside. The inertial term, $u\frac{\partial u}{\partial x}$, dominated the inertial terms at the surface for the high runoff season, and was balanced by the pressure gradient and vertical stress gradient. In Knight Inlet, the inertial terms were important between stations 3 and 5 so perhaps in this area, the results are more comparible to Silver Bay since their data were gathered near the mouth of Silver Bay. In both seasons, the pressure gradients were very strong and probably directed the flow process. This last statement at first seemed contradictory to my result that the inertial terms were generally not important relative to the pressure field and turbulent stress, but I noted that Silver Bay has very different hydrography to Knight Inlet, and that this difference must affect the circulation in both fjords. Rattray (1967) stated that exceptions to the balance of the horizontal pressure gradient and vertical gradient of turbulent stress could occur because of bathymetric effects. Silver Bay is shallower than Knight Inlet with its average depth equal to approximately $70\,fathoms \approx 128\,m$, and Silver Bay is also much shorter.

Pedersen (1978) stated that the pressure gradient and interfacial stress must be balanced in the deeper counterflow, which agrees with the findings of McAlister, *et al.* "These pressure gradients can be established only by longitudinal density gradients originating from the weak transport of brackish water downwards, combined with the up-estuary convective transport" (Pedersen, 1978). He went on to say that a lack of balance was not significant as long as friction was very small (Farmer and Freeland, 1983). I did not consider recirculation of the surface layer water in my analysis, but Pedersen considered it to be important for distribution of pollutants. Pedersen suggested that "K-Theory" was an improvement over models of circulation that use a one way momentum flux through the interface. K-Theory incorporates eddy diffusivity and eddy viscosity and is briefly described by Farmer and Freeland (1983). However, determination of the eddy coefficients is difficult and limits the validity of that approach.

Wetton (1981) concluded that the dynamical balance in the surface layer was between the horizontal pressure gradient and the stress term, which agrees with my result, but it must be noted that his stress term considered only the wind acting on the surface layer and not the turbulent shear stress at the interface and so it was not a complete balance.

4.2 Conclusions

Knight Inlet was represented as a fjord with two-layer circulation. Estimates of terms in the horizontal momentum equation were made for the steady state. The coefficient of interfacial friction, k, was estimated to be of the order 10^{-2} for 1986 and of the order 10^{-3} for 1987 for the time period sampled.

The interface depth, h, was fairly constant inland of the sill and deepened rapidly seaward of the sill as the mouth of Knight Inlet was approached. In 1986, h was $6.97\,m$, and, in 1987, h was $3.20\,m$.

I found that the inertial terms were important only in the sill area relative to the pressure and stress terms. In other regions of Knight Inlet, it was shown that the balance of forces in the horizontal momentum equation representing a simple two-layer model is dominated by the pressure gradient and stresses acting on the surface layer for little or low wind conditions.

During periods of light winds the stress term can be estimated by using just the interfacial stress, but when dealing with periods of strong winds, the addition of these effects will give a truer account of the balance. Other outside processes, especially those found at the sill (*eg.* tidal mixing and the generation of the internal bore), will also influence any results obtained from this kind of analysis and these other effects should also be considered.

Chapter 5

Introduction to the Finestructure Problem

"Structure", in a physical oceanographic sense, pertains to the arrangement of water properties or the relationship between properties. Characteristic forms that physical oceanographers concern themselves with are, for example, steps or staircase structures found in vertical profiles of temperature, salinity, or density, and inversions occurring in the property values (Coachman and Charnell, 1977). Processes that give rise to structure are associated with turbulent mixing and so structure can be thought of as a manifestation of these mixing processes.

Mixing is an important aspect of oceanic research. It affects the distribution of the different water properties which can determine what organisms can inhabit certain regions of the ocean; it affects the distribution of pollutants; and it can affect circulation by altering density gradients. Specifically, as an example of the last effect listed, Farmer and Freeland (1983) stated that mixing is central to the problem of gravitational circulation since it is responsible for altering density gradients that drive the flow in estuaries.

Mixing in a fjord is a sink for energy which comes from mechanical input, such as the wind acting on the surface layer, tidal action, turbulent gravity currents at depth, and shear flows which arise from river runoff. Thermal convection can be important in the winter when surface temperatures and river discharge are lower, and double diffusion may be important in the deep basins (Farmer and Freeland, 1983). These authors described key processes that they deemed

relevant to fjord oceanography in their review of the physical oceanography of fjords so I will not detail mixing processes here.

The two CTD surveys of Knight Inlet provided much data on water properties of that inlet, and, although my original intention was to use the data to study dynamical processes, the fine resolution attained by the instrument made the idea of investigating fine scale features seem feasible also.

Finestructure is defined by Osborn and Cox (1972) as structure with scales greater than $1\,m$ (microstructure has scales that are less than $1\,m$), and many researchers have used conductivity and temperature profilers to study finestructure, as well as microstructure (eg. Mack, 1985; Schmitt, *et al.*, 1986; Imberger, 1985; Coachman and Charnell, 1977; Gregg, 1975). If equipped with special fast response thermistors and conductivity cells, these instruments can obtain information on features with resolutions of several millimeters. The Guildline instrument used to collect the data in Knight Inlet appeared to have a resolution of several centimeters so that these data seemed suitable for investigating the finestructure present.

The purpose of this study was to determine where most of the activity occurred in Knight Inlet, and to what degree or extent it occurred. Therefore, this study of finestructure in Knight Inlet will not be an in-depth quantitative analysis, but a qualitative description of activity observed during the two cruises in 1986 and 1987. The collection of the data was described in the first part of this thesis. Discussion of the data processing and results will follow in the next chapter. A comparison was made between the 1987 data and measurements made by Dr. A. E. Gargett of the Institute of Ocean Sciences at Patricia Bay, British Columbia. Dr. Gargett used a microprofiling "Yo-Yo" instrument called FLY (Fast Light Yo-Yo).

Since I had never been exposed to a CTD probe before I started my research, it was necessary for me to understand how the instrument is used, and what problems could arise in data collection and processing. What follows in the next section is a description of the instrument that was used to collect my data with special attention to sampling problems common to all CTD's. These sampling problems limit the instrument's effectiveness as a finestructure probe.

5.1 CTD Probes

The CTD (Conductivity, Temperature, and Depth) probe is a continuously profiling instrument. It makes *in situ* measurements of temperature and conductivity (which lead to a salinity profile), and it measures depth in terms of pressure. It is attached to an electrical cable and lowered into the water by a winch. The instrument is usually dropped vertically or towed behind the ship. The data is transmitted through the cable to a control unit on deck where it is recorded. The conductivity sensor is either inductive or an electrode cell, which is more popular because of its simpler calibration (less calibration space required) (Pickard and Emery, 1984).

Two manufacturers of CTD's are Neil Brown Instrument Systems in the United States and Guildline Instruments in Canada. The University of British Columbia Department of Oceanography owns a Guildline Model 8705 Digital CTD probe with a Model 87102 control unit and it is with these two units that the data used in this thesis were collected.

5.1.1 Problems with sampling

To accurately determine what spatial resolution can be achieved by the instrument, it is necessary to know the characteristics of the dynamic response of the sensors used. Much work has been done in this area (eg. Fozdar, *et al.*, 1985; Gregg and Meagher, 1980; Horne and Toole, 1980; and Gregg, *et al.*, 1982). These studies were all done on Neil Brown instruments.

temperature response

Temperature is sensed most commonly in a profiling instrument by changes in electrical resistance, which is a function of temperature. Any signal that is received must diffuse through the fluid boundary layer that is set up around the sensor, and through the sensor's coating. The time required to do this will limit the spatial resolution of the sensor. If the signal

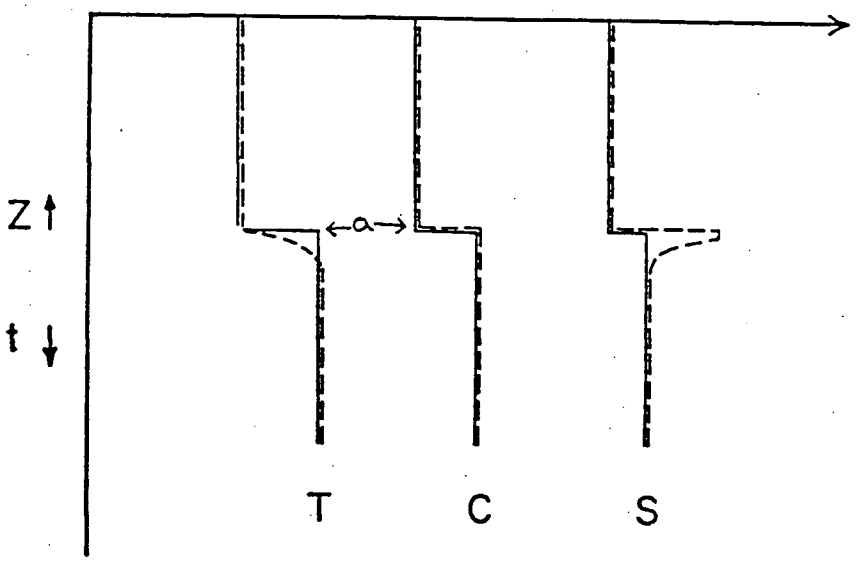

Figure 5.1: Figure showing response of sensors on CTD (from Horne and Toole, 1980).

received is recorded before the true temperature is actually sensed, then there is an error in the recorded (observed) temperature. In Figure 5.1, the true temperature change is represented by a sharp gradient, and the observed temperature is shown by the dashed line. The observed temperature at point *a* is actually cooler than the real temperature because of the time needed for the thermistor to respond to the change.

Corrections to the observed temperature can be made in physical space or frequency space depending on what is to be studied. Corrections in physical space are necessary for accurate salinity data and corrections in frequency space are necessary for microstructure and dissipation measurements (Horne and Toole, 1980). Knowledge of the differential equation that governs the behavior of the sensor and the transfer function (assuming that the transfer function is linear) allow corrections of the temperature spectra in frequency space (Osborn and Cox, 1972).

Differential equations have also been determined that model the behavior in physical space.

One of the most commonly used filtering models is

$$\frac{dT_O}{dt} = \frac{1}{\tau}(T_T - T_O)$$

where τ is the response time constant and T_T and T_O are the true and observed temperatures, respectively (Horne and Toole, 1980, after Gaul, 1968; and Pingree, 1969). This is called a single-pole filter model. The solution is a description of the change in temperature as a logarithmic response.

$$\frac{T_T - T_0}{T_O - T_i} = e^{-\frac{t}{\tau}}$$

where T_i is the initial temperature at $t = 0$. The response time is the time required for $e^{-\frac{t}{\tau}}$ to become e^{-1}. For a 99% response to the signal, $e^{-\frac{t}{\tau}}$ should equal 0.01; $t = 4.61\tau$.

A technique for correcting data using a single-pole filter is summarized in Horne and Toole (after Fofonoff, *et al.*, 1974). They stated that data corrected using this method could still be in error for two reasons. The differential equation is only an approximation of the sensor's response and errors can arise due to estimation of the terms in the equation. They present an alternative technique that assumes that the observed temperature is a convolution of the true temperature and the response function of the sensor. However, Horne and Toole's filtering model assumes that the response is constant, but the response function of the temperature sensor is often dependent on the lowering rate of the instrument, which is generally not uniform due to various reasons discussed later.

conductivity response

The response of the conductivity cell is a function of the flushing rate of the cell which is also dependent on the lowering rate of the instrument. The cell walls also develop fluid boundary layers which can inhibit its response. The length of the cell and the sampling rate can determine what scales can be resolved. For example, if the cell is 5 cm long and the flushing time is 0.05 s, with a lowering rate of 1 ms^{-1}, there will be 20 samples per second and each will

be independent of the other. If scales of less than $5\,cm$ are to be studied then the response of the conductivity cell becomes important.

Errors in conductivity can also occur if the cell is angled to the direction of motion of the instrument. Gregg, *et al.*, (1982) stated that the angle will be significant if the relative lateral velocity between the ship and the water is large, or if the flow field near the probe is distorted by the flow field around the ship. Either can occur if the probe is towed behind the ship to obtain horizontal maps of water properties. They also stated that recirculation around the cell has a minor effect, but the viscous boundary layer produced tails in the step-response function.

If contaminants find their way into the conductivity cell, then the recorded data will also be in error. The cell must be kept clean. The error will usually appear as a spike in the salinity profile.

sensor response mismatch

The major problem in studying finestructure in the ocean with a CTD probe is the difference in the dynamic responses of the temperature and conductivity sensors. It was explained in previous paragraphs that no sensor responds instantaneously to the quantity that it must measure and that the amount that it lags depends on the response function that governs its behavior and a time constant, which is a characteristic of the type of sensor. If one sensor lags behind the other, then spiking can occur in the salinity profile since salinity is derived from the temperature and conductivity data.

Figure 5.1 shows how a salinity spike can occur due to the faster response of the conductivity cell. The conductivity cell senses the sharp gradient well, but the thermistor is slower so that just below the step the temperature recorded is cooler than the true temperature and this difference will produce the error in the salinity at this point. The result is seen as a spike (an overestimation of the true salinity variance).

aliasing

A low frequency signal can have the same values at points in time which are Δt apart as one of higher frequency. As a rule, the sampling interval, Δt, should be one-half of the shortest period present in the data record (Neumann and Pierson, 1966). This leads to a range (from 0 to $1/2\Delta t$ within which the frequency spectrum can be estimated. The frequencies in the data will be interpreted correctly. The frequency, $f_N = 1/2\Delta t$, is called the Nyquist frequency.

If Δt is too large, the frequency range will not be wide enough and frequencies in the data that are greater than the maximum angular frequency, $2\pi/2\Delta t$, will be aliased into the range given above. Higher frequencies will be reported at lower frequencies.

If Δt is too small, the Nyquist frequency will be greater than the highest frequency of any real significance in the data record. This can result in costly processing of data that is not really important in the first place.

With a CTD, the sampling rate depends on the response of the sensors. It is hoped that the instrument will sample quickly enough to make it possible to study the fine-scale features of interest without the risk of misinterpreting the data because of aliasing. To eliminate the effects of aliasing, the data can be filtered to frequencies low enough to remove any aliased frequency. This is explained in more detail in Gregg, *et al.*, (1982).

fall rate

Irregular fall rates can result from ship roll, wire angle, and state of the sea. If pressure is plotted against time for a single CTD cast, the irregular rate appear as bumps in what should be a linear profile.

A ship-board "motion compensation system" like the one described by Mack (1985) can eliminate much of the problem. His experiment required that the CTD be "Yo-Yo"ed from the ship while the ship drifted. His system achieved a near-uniform descent rate for the CTD so

that the thermistor frequency response and the conductivity cell spatial response were nearly matched.

In the absence of such a sophisticated system, the data can be filtered to eliminate the effects of ship roll, etc. A simple technique would be to delete from the record any data points that are not increasing in depth. For casts in which his compensation system did not work, Mack used a "threshold increment" equal to one-quarter of the depth increment expected for a $1\,ms^{-1}$ drop rate and his sampling rate. However, Gregg, *et al.* (1982) stated that this standard technique would not remove effects of any upward motions from the net downward portions of the data record. They showed that just the descending portion of the record was sufficiently variable in velocity that the resulting data made their subsequent analysis seem hopeless. Instead, they determined the wavenumber at which irregularities in the drop rate would have little effect on the resultant salinity and then they low-passed filtered the data to remove higher wave numbers in the temperature and conductivity record.

5.1.2 The Guildline CTD

All facts about the Guildline CTD probe which was used for data acquisition used in my thesis are taken from the Model 8705 Digital CTD Probe and Model 87102 Control Unit Technical Manual, Volume 1 (with permission).

Data is transmitted from the Guildline CTD probe in blocks, each consisting of a scan of sixteen channels. Fifteen channels each have a twelve bit binary word and one channel remains blank. It is used for synchronization. Each scan of these sixteen channels is repeated at a $40\,ms$ update interval. The desired resolution for each conductivity, temperature, and depth record is eighteen bits so each parameter is given two twelve bit words for a total of six words and a total of twenty-four bits.

The conductivity sensor is a four electrode conductivity cell. The cell is a Pyrex tube and the electrodes are mounted in side arms in an "H" configuration. The spatial resolution is about $5\,cm$. The temperature sensor is a resistance thermometer made of fine copper wire

encased in an oil-filled stainless steel capillary tube. The pressure sensor is a strain gauge type transducer.

The response time constant is less than $50\,ms$ for all channels, including all sensors and associated electronics. For a drop rate of $1\,ms^{-1}$ the resolution of the instrument sensors is $5\,cm$. The cycle time is $40\,ms$, so that for the same drop rate, 25 samples per second will be taken or one sample every $4\,cm$. With respect to resolution, this instrument seemed more than adequate to use to study the finestructure in Knight Inlet.

The accuracy of the temperature is $\pm 0.005\,\mathrm{deg}\,C$ and the resolution is $\pm 0.0005\,\mathrm{deg}\,C$. The accuracy of the conductivity is $\pm 0.005\,ppt$, in terms of the equivalent salinity, and the resolution is $\pm 0.001\,ppt$. The accuracy of the pressure is $\pm 0.15\%$ of full scale pressure, and the resolution is $\pm 0.01\%$ of full scale pressure.

Chapter 6

Analysis of Finestructure Data

6.1 Analysis

In order to detect inversions or fluctuations of temperature and salinity, I took the difference between every two points in the temperature and salinity record. I subtracted the lower point (with respect to depth) from the upper point. Since temperature normally decreases with depth, a "normal" temperature record of these first differences, (ΔT), would contain mostly positive values, and, since salinity normally increases with depth, a normal ΔS record would contain mostly negative values . An inversion would show up as a change of sign, from a positive value to a negative value or negative to positive.

I filtered the raw data for "bad" (erroneous) points by discarding any triplet of depth, temperature, and salinity for which there existed a difference for any of the three that was greater than a certain threshold value, called ϵ. The ϵ criteria that I used were $5.0\,m$ for depth, $0.5°C$ for temperature, and $0.5\,ppt$ for salinity. These thresholds are fairly liberal, but in the thermocline/halocline region the gradients were so sharp (Figures 6.1 and 6.2) that I wanted to be sure that I did not delete any "good" (real) points (variations) from the record. I also discarded any triplet where the difference in the depth between any point and its succeeding point was less than $0.0125\,m$ and where the difference showed that the depth was decreasing (*i.e.* a negative difference in the depth). This last criterion eliminated any effects of an uneven descent rate perhaps caused by ship roll (Mack, 1985).

The approach that I used appears to be very simple, but I had spent considerable time before I settled on this method trying a more complex, systematic, and objective statistical procedure that filtered out any triplet that was outside a certain number (4 or 5) of standard deviations from the mean first difference. After I reviewed the plots of the first differences that were "despiked statistically", I felt that this method was too strict and was eliminating points that may not have been errors. Thus, I turned to the simpleminded approach which I refined until I decided upon the method that I described in the previous paragraph.

6.1.1 1986

Figures 6.1 and 6.2 show the temperature and salinity profiles for the six Knight Inlet stations for 1986. Station 11 showed a large inversion in temperature from $5\,m$ to $10\,m$. Smaller inversions appeared in temperature at stations 5, 7, and 9 in the surface water ($< 10\,m$), and in the salinity at stations 7 and 9. The deeper water showed small minima in temperature at station 7 at $\approx 175\,m$ and at station 9 at $\approx 160\,m$. A small spike appeared in the temperature for station 9 at $\approx 220\,m$. This spike produced spikes at the same position when the data was processed further. Most of these other spikes were removed manually to make plotting easier. The features described above can be better seen in Figures 6.3 and 6.4 which show temperature profiles separately for the upper $30\,m$ and for $30\,m$ to the bottom, respectively, and in Figures 6.7 and 6.8 which show salinity profiles for the upper and lower water.

Figures 6.5, 6.6, 6.9, and 6.10 show the results of my first differencing for the six stations in Knight Inlet for the 1986 data. The top $20\,m$ to $30\,m$ had the largest range of activity for all the stations in both temperature and salinity with the largest variations concentrated in the region of the interface (about $10\,m$) and above. I plotted the upper $30\,m$ separately from the deeper sections (below $30\,m$) to better see what activity existed in the deep water of Knight Inlet. The temperature and salinity records for the upper $30\,m$ were plotted on different scales because the ΔT's were smaller than the ΔS's for that portion of the water column.

The temperature record had the most variation for the upper $30\,m$ (Figure 6.5) in the sill

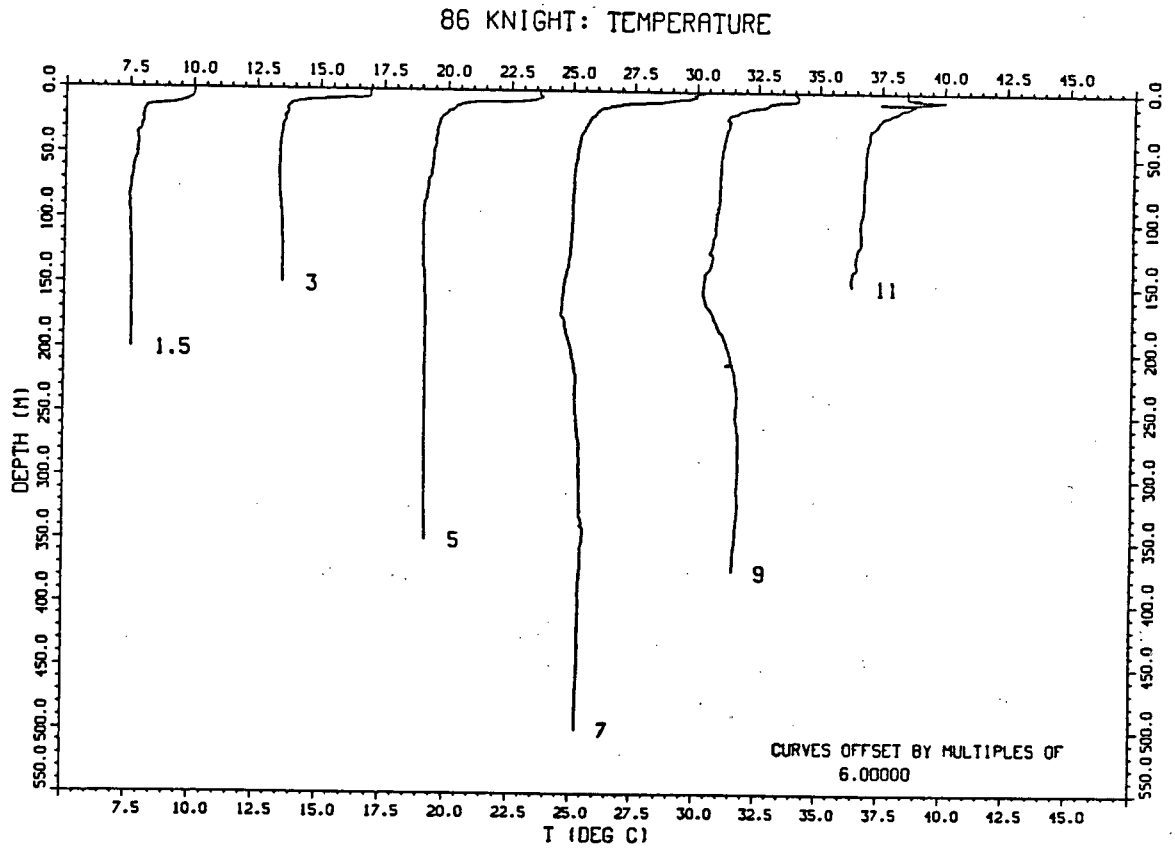

Figure 6.1: Temperature profiles for 1986 Knight Inlet stations.

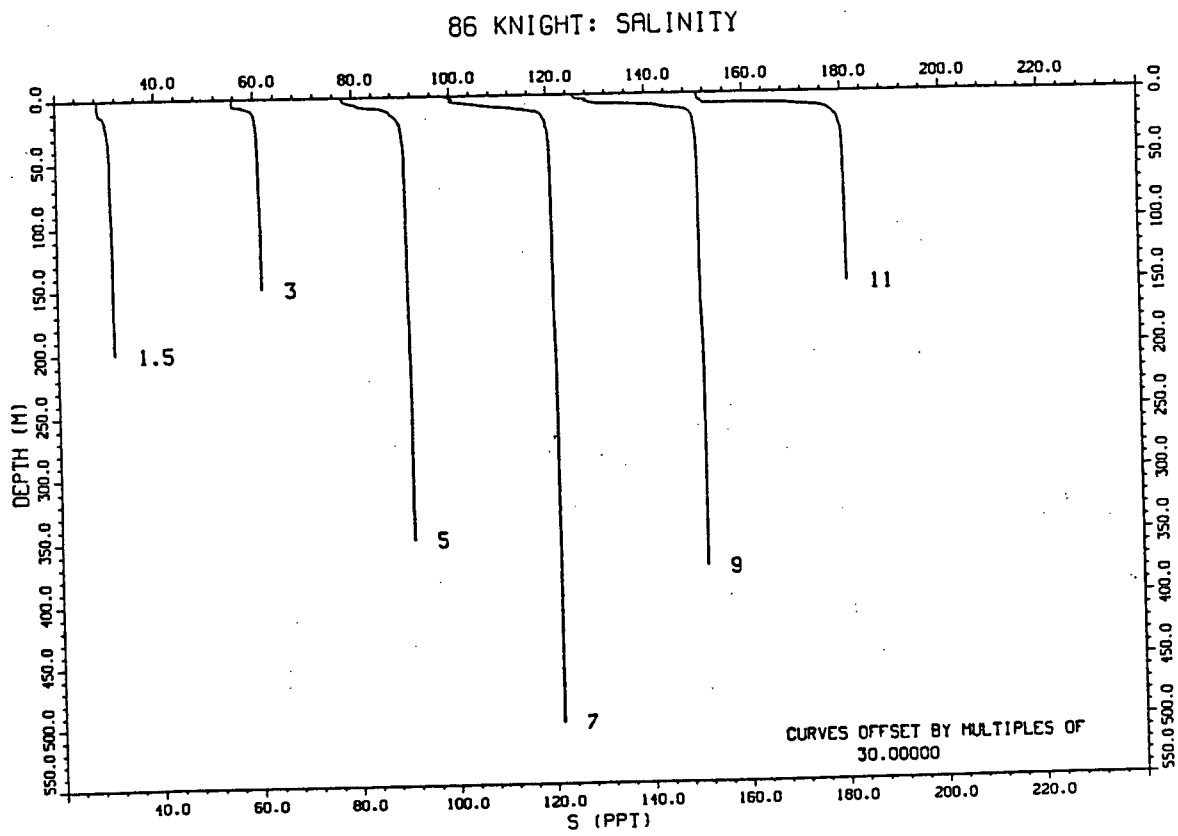

Figure 6.2: Salinity profiles for 1986 Knight Inlet stations.

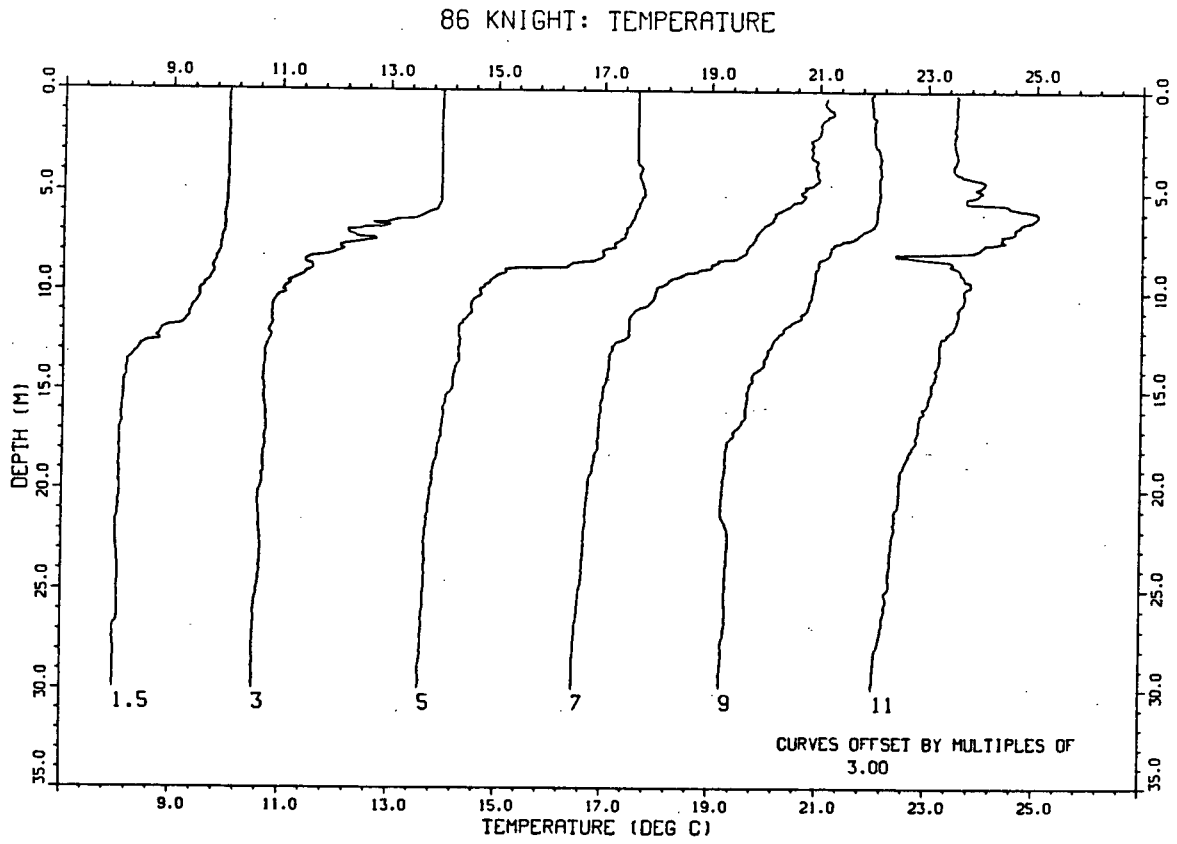

Figure 6.3: Temperature profiles for 1986 Knight Inlet stations for $0\,m$ to $30\,m$.

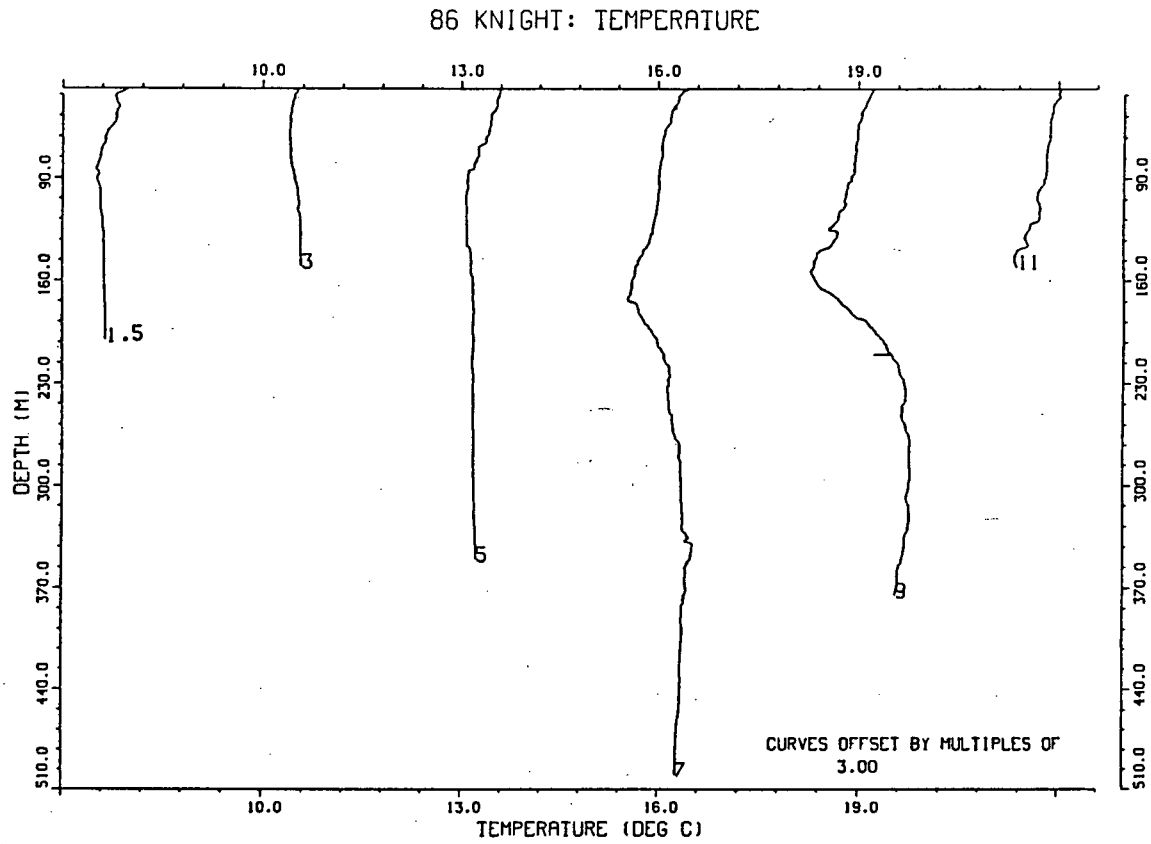

Figure 6.4: Temperature profiles for 1986 Knight Inlet stations for $30\,m$ to the bottom.

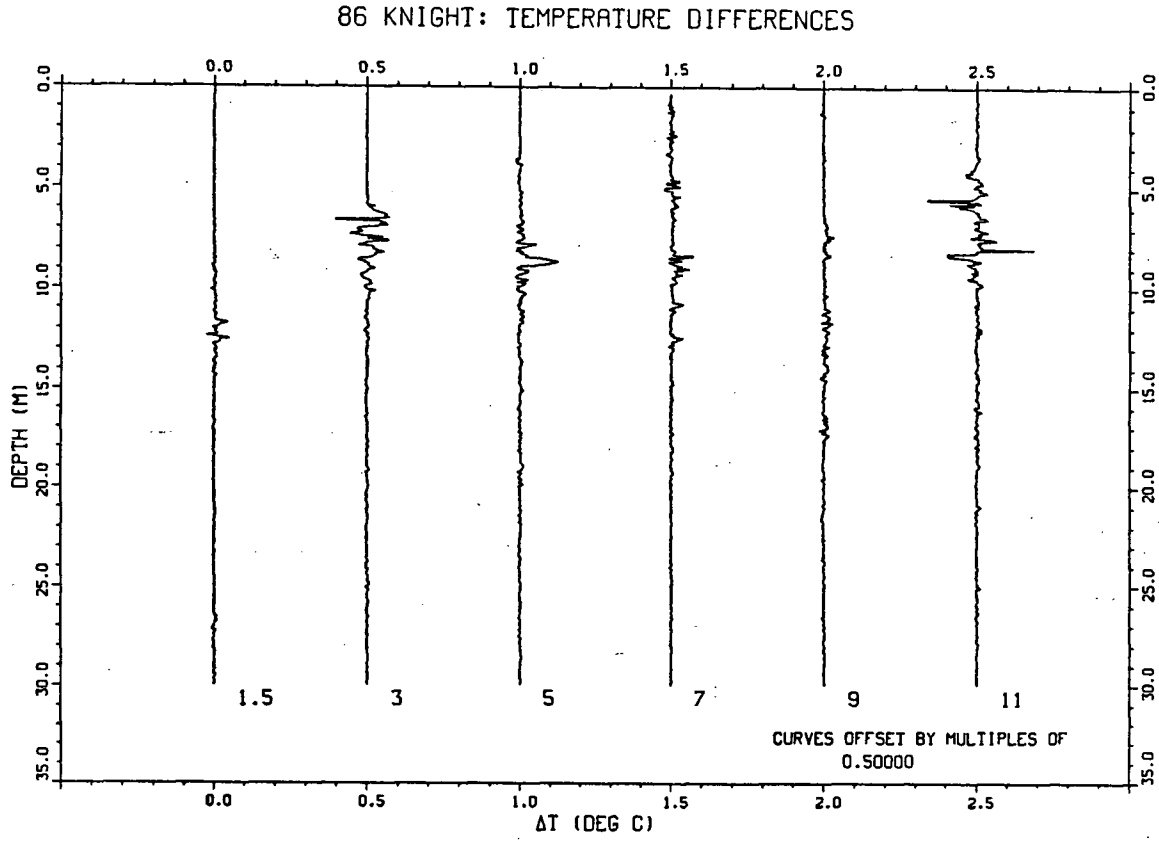

Figure 6.5: Profiles of first differenced temperature record from 0 to 30 m for 1986 Knight Inlet stations.

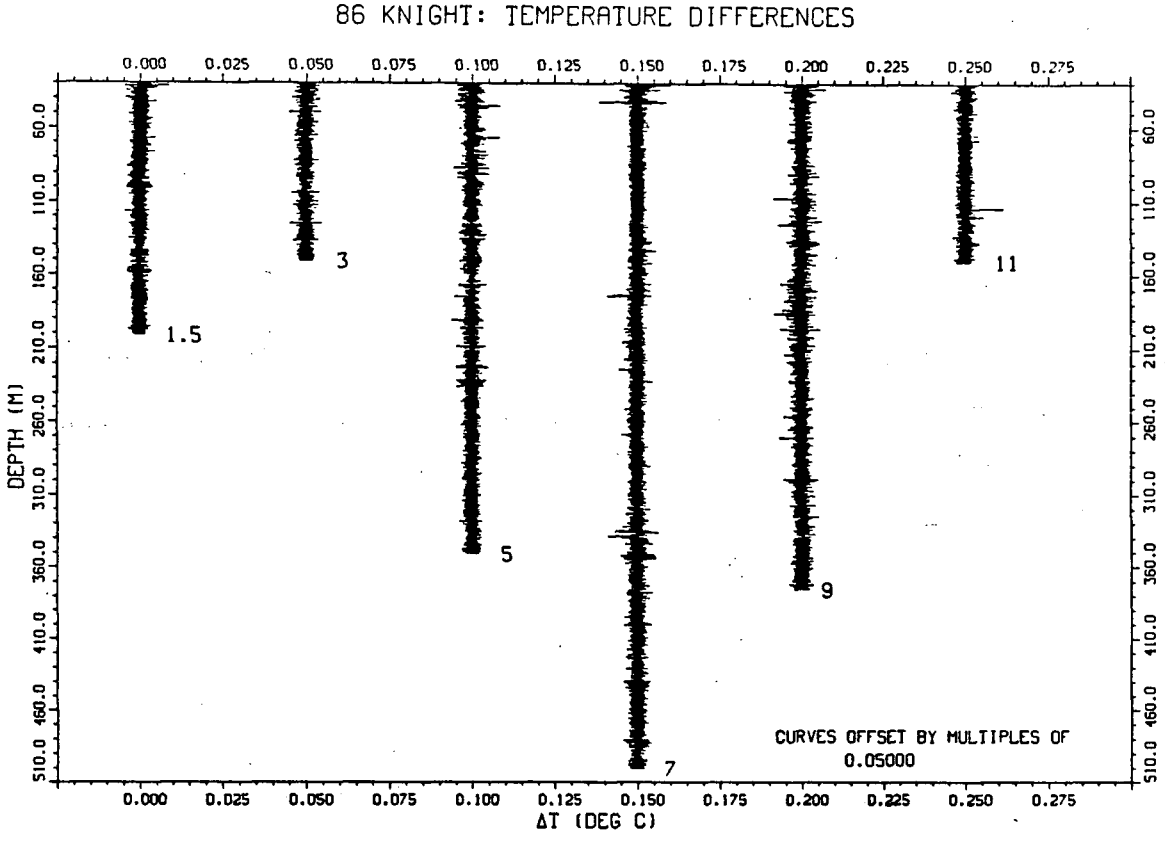

Figure 6.6: Profiles of first differenced temperature record from 30 m to the bottom for 1986 Knight Inlet stations.

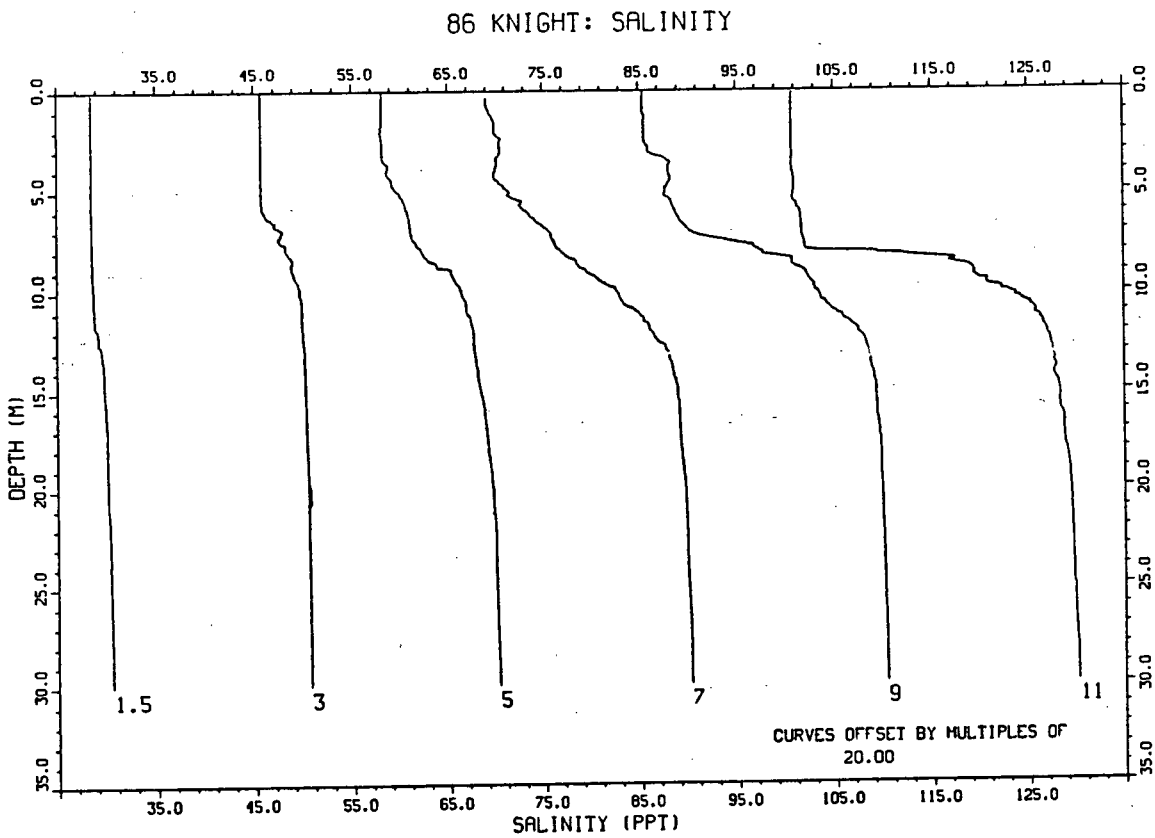

Figure 6.7: Salinity profiles for 1986 Knight Inlet stations for $0\,m$ to $30\,m$.

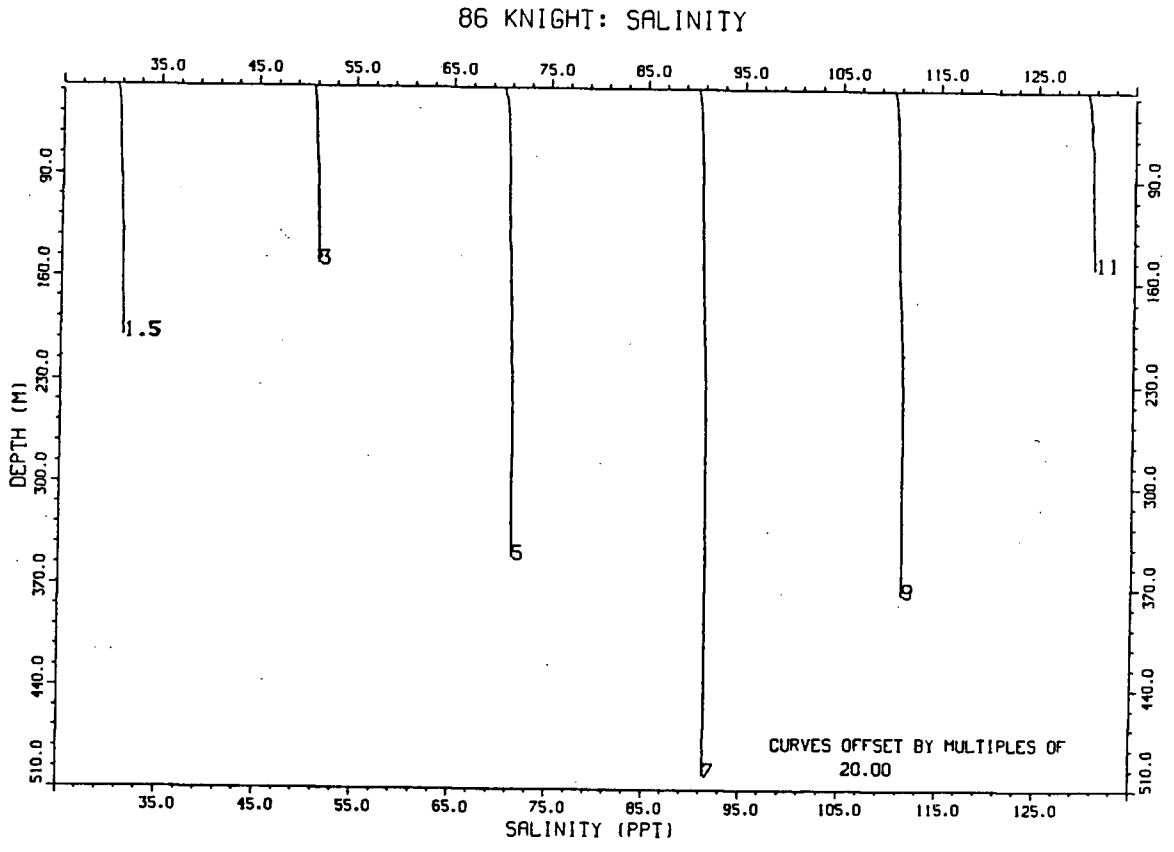

Figure 6.8: Salinity profiles for 1986 Knight Inlet stations for 30 m to the bottom.

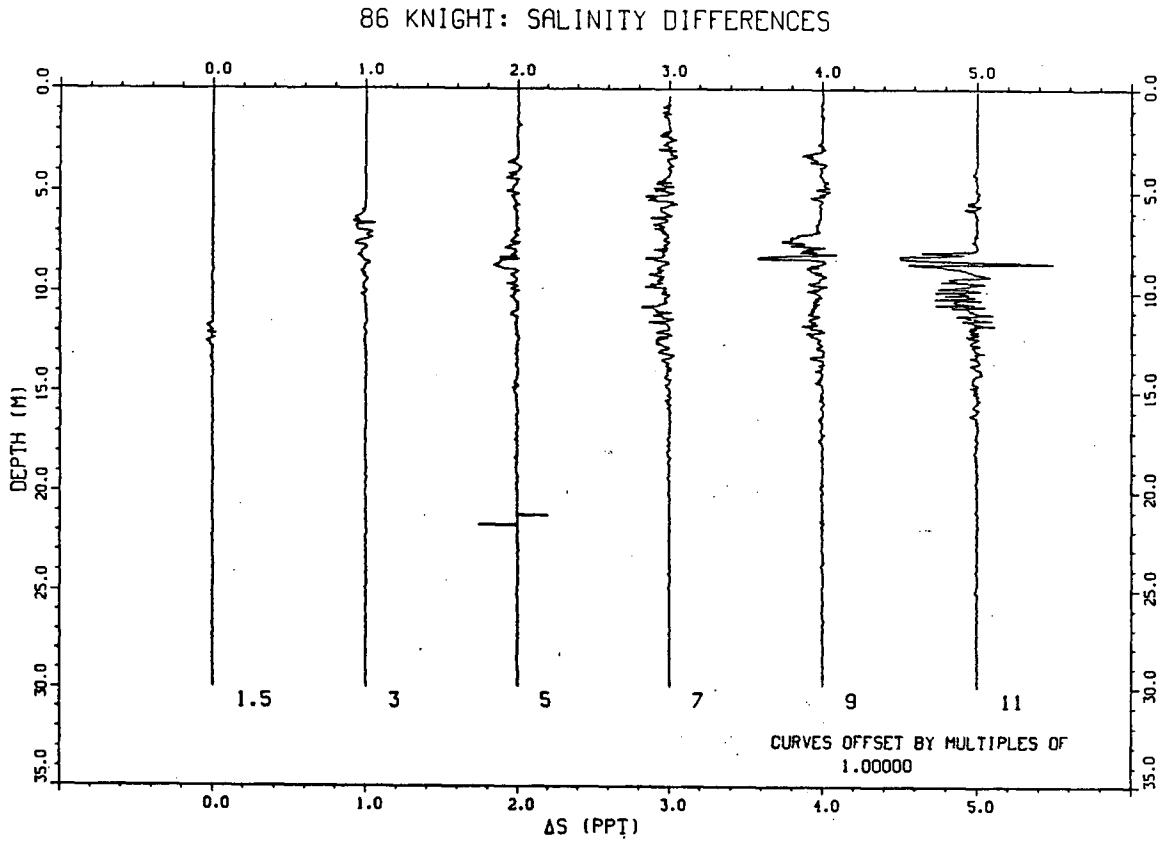

Figure 6.9: Profiles of first differenced salinity record from 0 to 30 m for 1986 Knight Inlet stations.

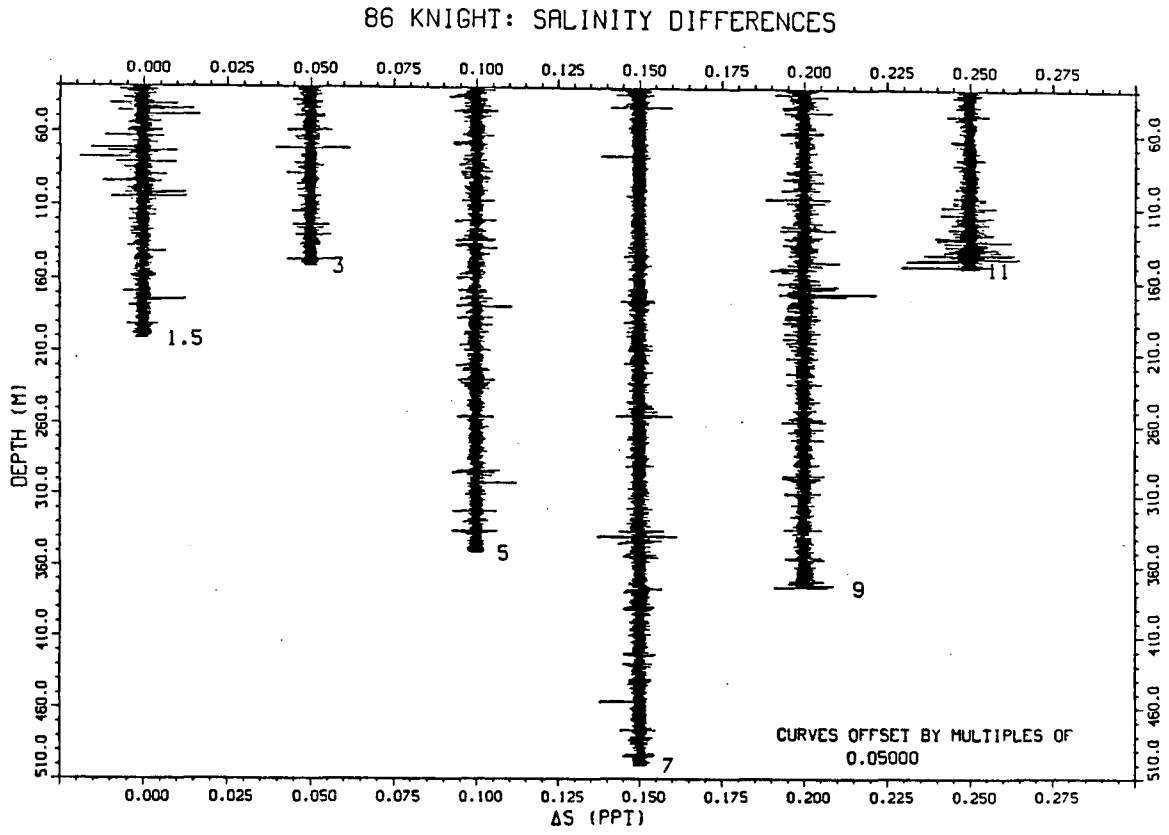

Figure 6.10: Profiles of first differenced salinity record from 30 m to the bottom for 1986 Knight Inlet stations.

area (station 3 ranged from $-0.10°C$ to $+0.08°C$; station 5 ranged from $-0.13°C$ to $+0.13°C$), and at the head (from $-0.16°C$ to $+0.19°C$). The ΔT values tended to be more positive with large negative values appearing at station 3 at $7\,m$, and at station 11 at $5\,m$ and $8.5\,m$. These negative values I associated with temperature inversions that occurred in these regions. The inversions at the head may have been caused by the intermingling of two different water masses (fresh river water and brackish inlet surface water).

The salinity record for the upper water (Figure 6.9), however, showed smaller variations, relative to the other stations, in the sill area (station 3 ranged from $-0.09\,ppt$ to $+0.06\,ppt$; station 5 ranged from $-0.26\,ppt$ to $+0.21\,ppt$), and the most variation was at the head (from $-0.50\,ppt$ to $+0.49\,ppt$). The ΔS values tended to be negative with large positive values at station 11 at $8.5\,m$ (corresponding to the same temperature structure for that area), and small positive values from $6\,m$ to $7.5\,m$ at station 3 (as in temperature). Entrainment of salty water into the surface layer and wind mixing makes the surface water more saline down-inlet, so that near the entrance of the inlet, the inlet's surface water is almost as dense as the sea water that it meets and little salinity variation will occur. The water at station 1.5 appeared to be well-mixed judging from the absence of large variations in salinity there. Gregg (1975) stated that a completely well-mixed region would have no fluctuations about the mean, but without adequate velocity information, what can be inferred about these regions is limited, since turbulent motions could be present without producing a signal (in his case, a temperature signal).

It should be noted that some points in these two plots (Figures 6.5 and 6.9) could have been spikes, but there was no definite objective way to be sure that these points were not real fluctuations either. For example, in the ΔS profile shown in Figure 6.9, between $21\,m$ and $22\,m$ for station 5, there appeared two "spikes". If the two, however, are compared with points in shallower water for the same station, (near $8\,m$), these two spikes are not much larger than some of the points there. I had to make a subjective choice as to whether these were real differences or spikes due to errors in the original data. Herein lies the "fault" in my method. If

I had chosen a smaller ϵ for salinity, then I would have rid the record of these two points, but I also would have lost probable good data from stations 9 and 11. In the end, I decided that, in this case, since no strong variations appeared in the temperature record for the same depths at which the spikes appeared at station 5, these anomalous points probably were indeed errors.

In the lower part of the water column (below $30\,m$), the first difference plots were less clear, especially for the temperature differences (Figure 6.6). This was mostly due to the large number of points that were in each data set. It appeared that I was dealing with data that were very close to the noise level of the instrument. Unfortunately, no attempt was made to accurately determine the noise level of the instrument so that the noise could be filtered out and the structure could be more clearly seen. Numerous small spikes appeared in both the temperature and salinity records, and these were removed manually so that the scales of the plots could be expanded and the finer features revealed. Both plots (Figures 6.6 and 6.10) are scaled similarly so that a comparison of the activity in each record could more easily be made. The salinity record (Figure 6.10) showed more areas of small activity than the temperature record in the deeper water, and the magnitude of the variations appeared to be larger in the salinity record than in the temperature record for these small active regions.

In the ΔT plot (Figure 6.6) at station 7 there were small bursts of activity at $\approx 175\,m$, $\approx 330\,m$, and at $\approx 360\,m$ which are associated with "blips" in the temperature profile for this station (Figure 6.4. No station appeared to be any more active in temperature than another. There existed several interesting "gaps" in the ΔT profiles, for example, at $\approx 120\,m$ at station 5 and at $\approx 350\,m$ at station 9. I have no explanation for the presence of these sporadic "quiet" patches.

The ΔS profiles for the deeper water (Figure 6.10) revealed bursts of activity that appeared in patches that were several meters thick. For example, at station 7 between $320\,m$ and $330\,m$, and at station 9 between $170\,m$ and $180\,m$. The gaps that were present in the ΔT profiles are also reflected in the ΔS profiles (*eg.* at station 5 at $120\,m$). There was a large concentration of fluctuating salinity near the bottom of station 11 ($\approx 140\,m$ to $\approx 150\,m$).

6.1.2 Testing sensor response mismatch

I mentioned earlier that spikes in the data record were a cause for concern throughout my analysis. Were the variations that I was seeing real or spikes that were possibly artifacts of mismatch of the temperature and conductivity sensor responses (subsection 5.1.1)? I decided to perform a cursory check to see how much mismatch affected my data. I used data that had already had the "obvious spikes" removed. I assumed that these errors (the obvious spikes) were due to outside interference, such as organisms contaminating the conductivity cell. I plotted temperature, salinity,and conductivity versus depth for station 11 from $0\,m$ to $40\,m$ (Figures 6.11, 6.12, and 6.13, respectively). I used the raw data from the CTD eliminating any points that were outside the following ranges: $0°C$ and greater than $40°C$, less than $0\,ppt$ and greater than $40\,ppt$, and less than $0\,m$ and greater than the bottom depth. I chose Station 11 because of the high activity observed in its surface water.

The salinity and conductivity plots (Figures 6.12 and 6.13) were virtually identical in appearance, which implied that changes in salinity were due mostly to changes in conductivity. What if the conductivity had been fixed? Then the variations in salinity would be entirely due to changes in the temperature. If the temperature response had been completely off, and the conductivity were fixed, then the apparent change in salinity would have been

$$\Delta S_{app} = (\frac{\Delta S}{\Delta T})\Delta T. \tag{6.1}$$

I recalculated the salinity with conductivity equal to a constant. The constant value that I used was the average conductivity found between $5\,m$ and $20\,m$ at station 11. The temperature and resulting salinity profiles are shown in Figures 6.14 and 6.15.

At $6\,m$, the temperature changed from $\approx 8.7°C$ to $\approx 10.1°C$, a change of $1.4°C$. At the same point, the salinity went from $13.68\,ppt$ to $13.16\,ppt$, a change of $0.52\,ppt$. $\frac{\Delta S}{\Delta T}$ was $\approx 0.4\,ppt°C^{-1}$. Between $6\,m$ and $8\,m$, the temperature went from $\approx 10.1°C$ to $\approx 7.4°C$, a change of $2.7°C$, and for the same region, the salinity change was $1.04\,ppt$. $\frac{\Delta S}{\Delta T}$ for this region was also $\approx 0.4\,ppt°C^{-1}$. The largest ΔT shown for station 11 in Figure 6.5 is $\approx 0.2°C$. This would give a variation

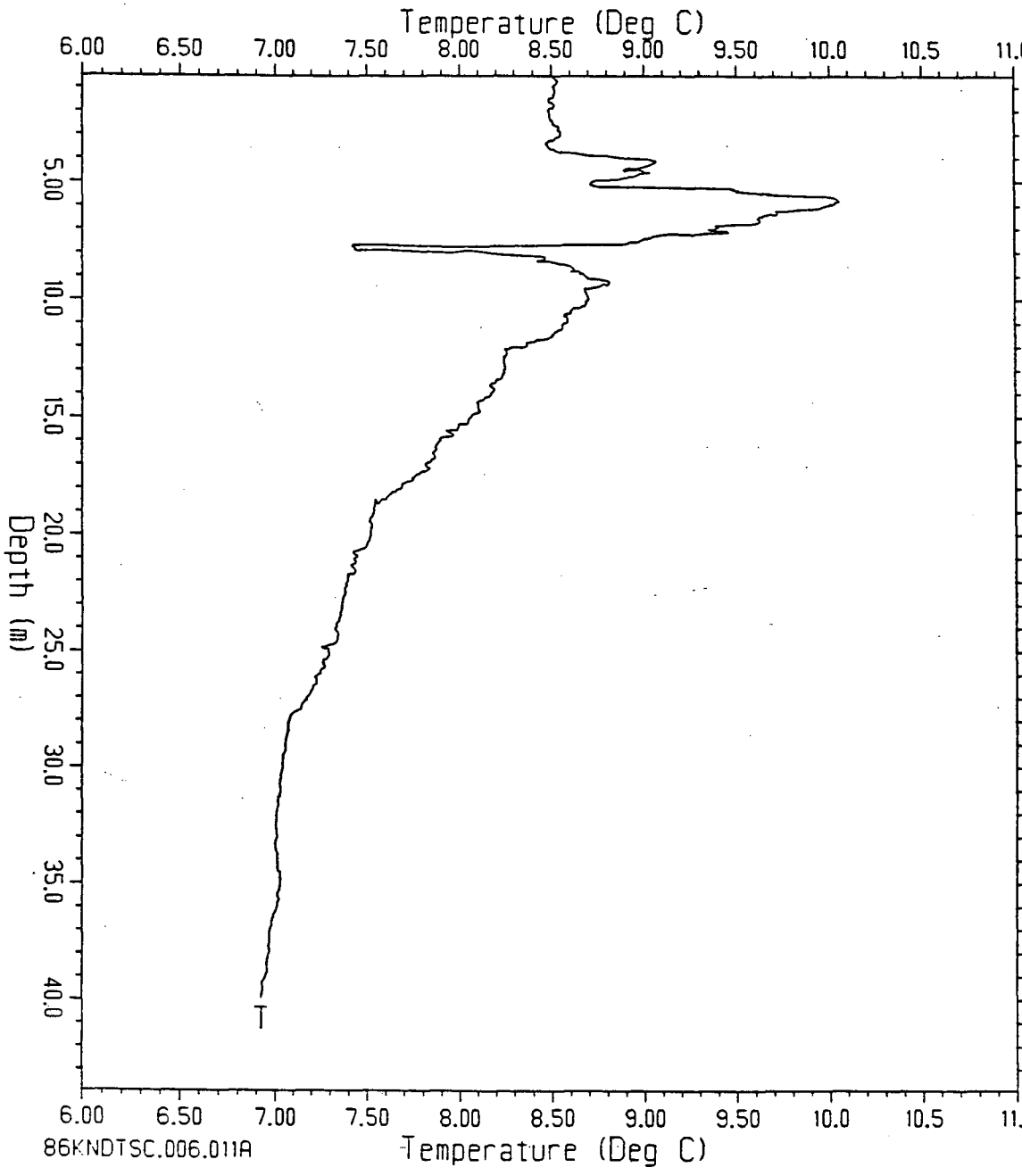

Figure 6.11: Profile of temperature from $0\,m$ to $40\,m$ for 1986 Knight Inlet station 11.

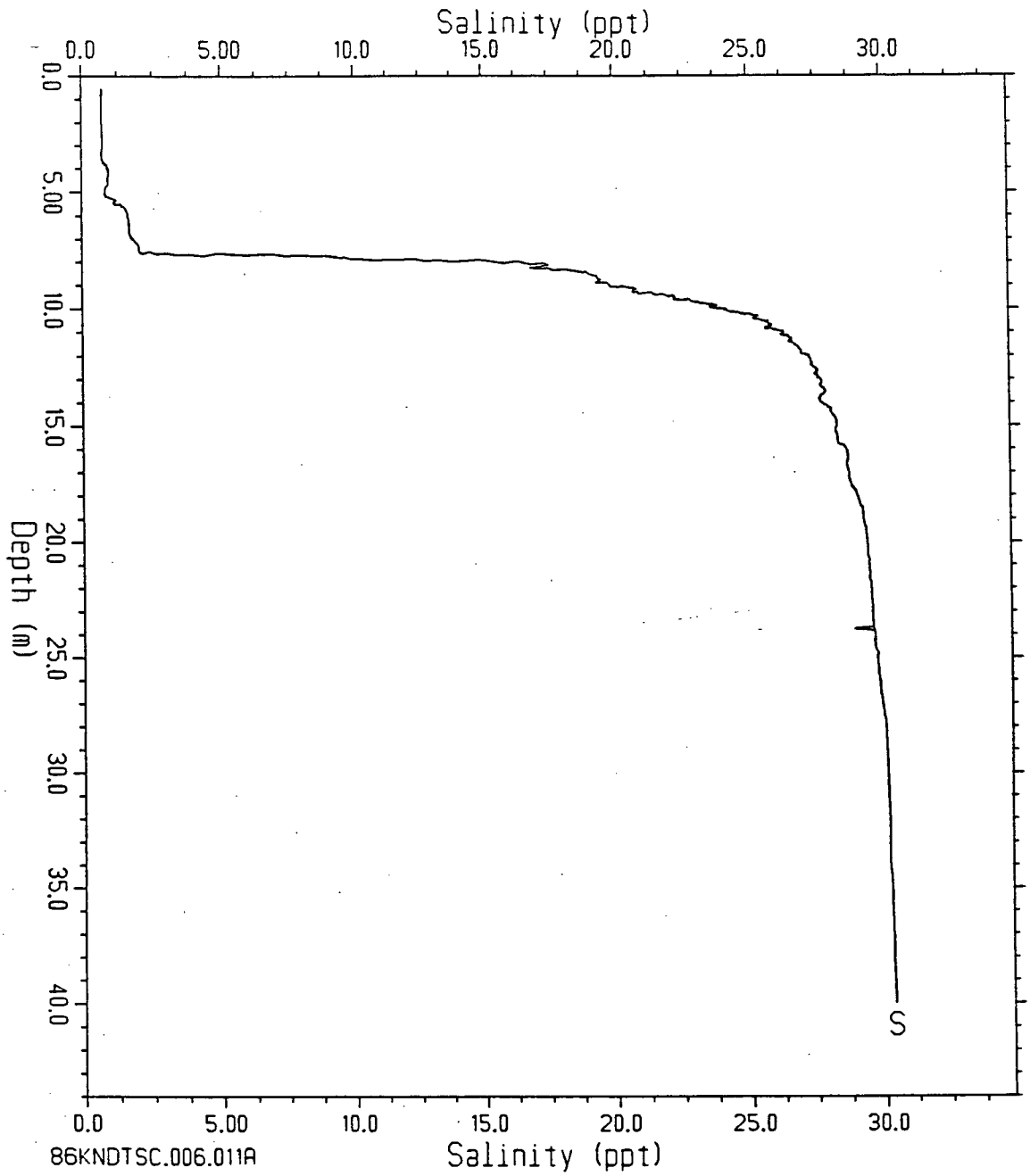

Figure 6.12: Profile of salinity from $0\,m$ to $40\,m$ for 1986 Knight Inlet station 11.

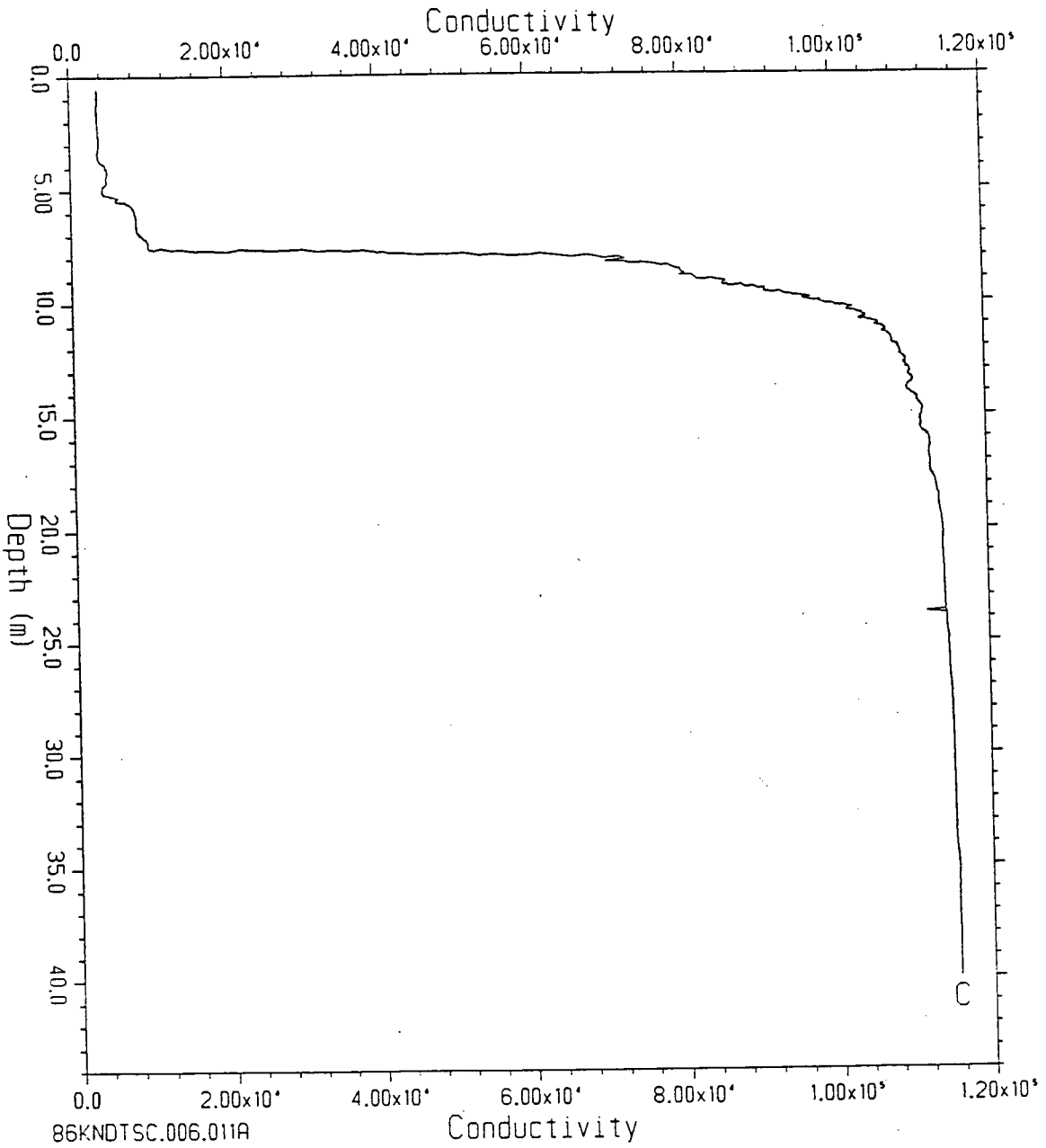

Figure 6.13: Profile of conductivity from $0\,m$ to $40\,m$ for 1986 Knight Inlet station 11.

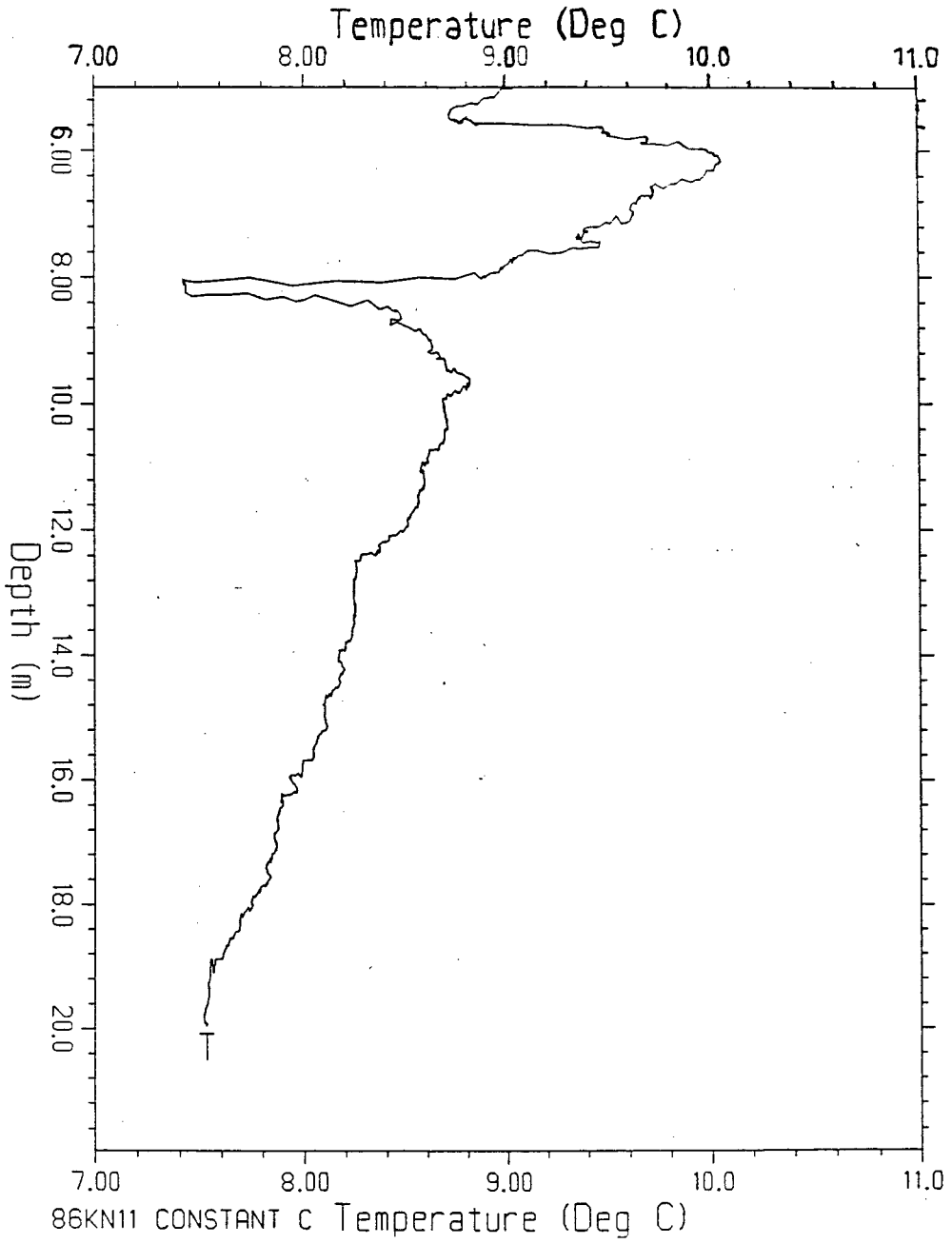

Figure 6.14: Profile of temperature from $5\,m$ to $20\,m$ for a constant conductivity for 1986 Knight Inlet station 11.

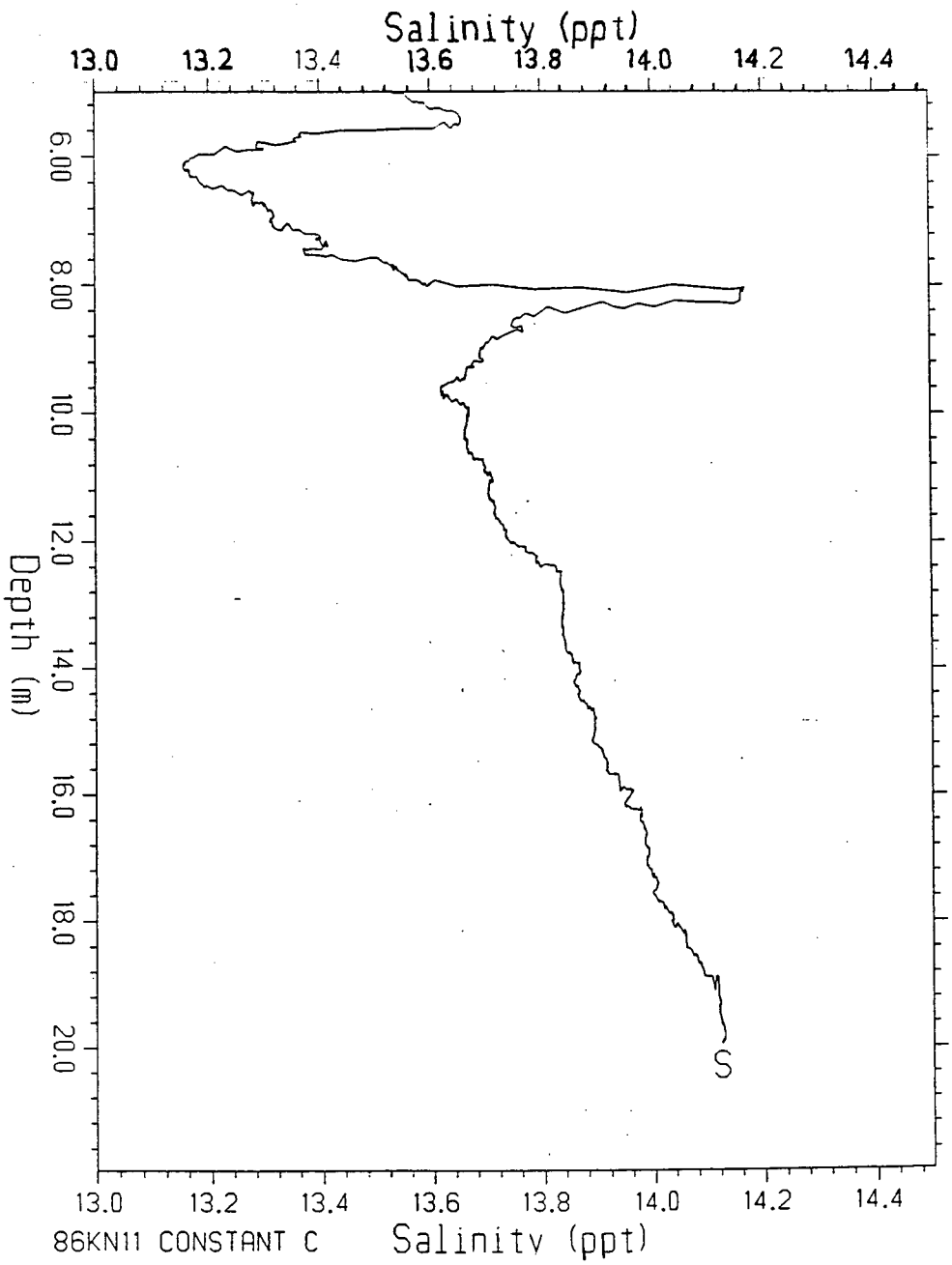

Figure 6.15: Profile of salinity from $5\,m$ to $20\,m$ for a constant conductivity for 1986 Knight Inlet station 11.

of $\approx 0.08\,ppt$ in salinity. The largest ΔS shown for station 11 in Figure 6.9 is more than ten times this amount so I concluded that these salinity variations, as well as the others, were real and were not a result of sensor response mismatch.

6.1.3 1987

I processed the 1987 CTD data in the same way as I processed the 1986 data. The temperature and salinity profiles are shown in Figures 6.16 and 6.17, and blow-ups of these profiles for the upper and deeper water are shown in Figures 6.18, 6.19, 6.22, and 6.23. The 1987 data showed large changes in temperature and salinity in the shallow water ($< 10\,m$ deep) (Figures 6.18 and 6.22). Minima occurred in the temperature data at station 5 at $50\,m$ and at station 3 at $\approx 25\,m$ (Figure 6.16). A temperature "maximum" (inversion) ranging from $100\,m$ to $150\,m$ appeared at station 5, and there occurred a small maximum at station 9 at $\approx 100\,m$. The salinity profile revealed the halocline to be from $5\,m$ to about $10\,m$.

The ΔT and ΔS profiles for the upper and lower waters are shown for the 1987 data in Figures 6.20, 6.21, 6.24, and 6.25. The plots of ΔT and ΔS for the upper water are on different scales once again to better see the temperature variations which were much weaker than the salinity variations. There appeared to be much more temperature activity in 1987 than in 1986 for both the upper and lower sections. The shallower water ($< 30\,m$) showed much stronger variations than the deeper water ($> 30\,m$). However, in 1987 there appeared to be strong activity throughout the inlet except at station 1, which is well outside the sill area. For stations 5 and 7 the variations in temperature and salinity began closer to the surface (Figures 6.20 and 6.24) than for the other stations. This is especially apparent in the salinity record. Figure 6.18 shows that stations 5 and 7 had step-like features in the shallow water.

ΔT for the upper water showed large fluctuations from positive to negative values at station 3 at $5\,m$. At station 5, the ΔT values tended to be positive for the top $10\,m$. Station 7 had small inversions throughout its depths, but the values tended to be positive. At station 9, the values tended to be negative, but at $5\,m$ they switched to positive due to the sudden decrease

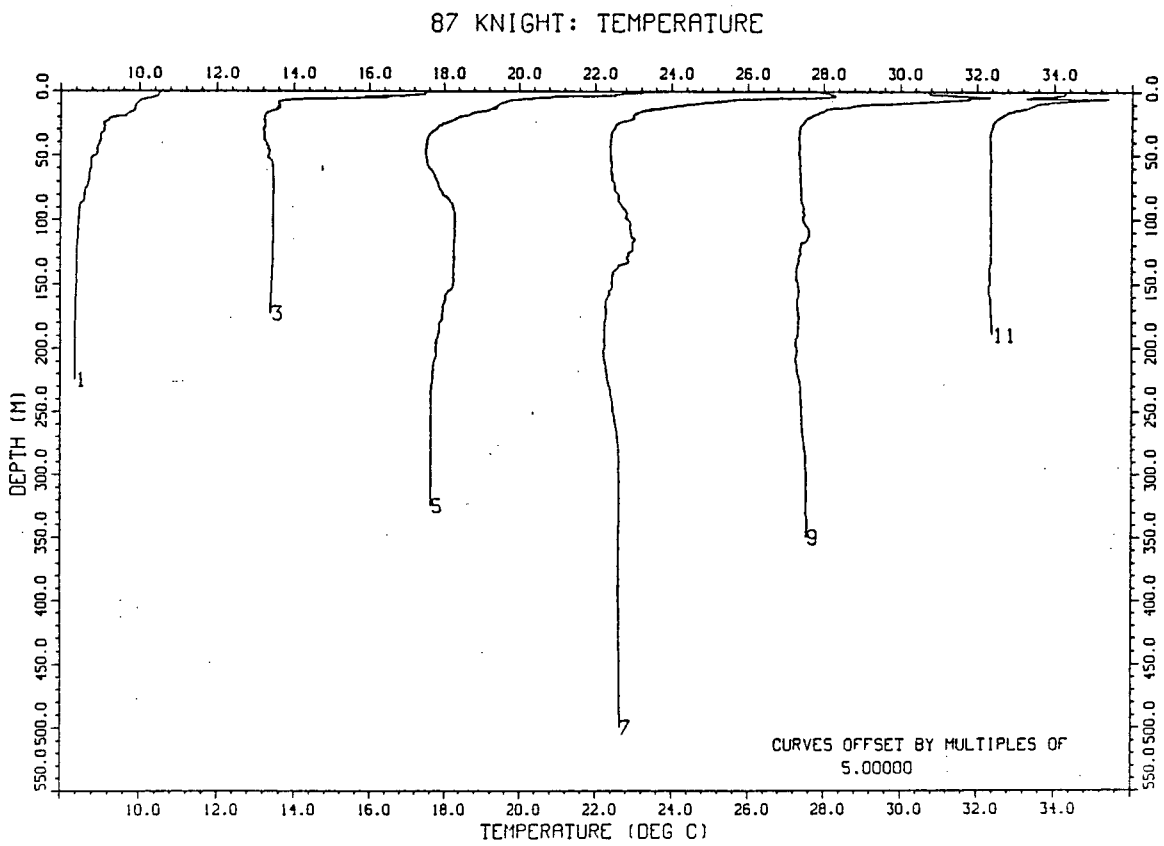

Figure 6.16: Temperature profiles for 1987 Knight Inlet stations.

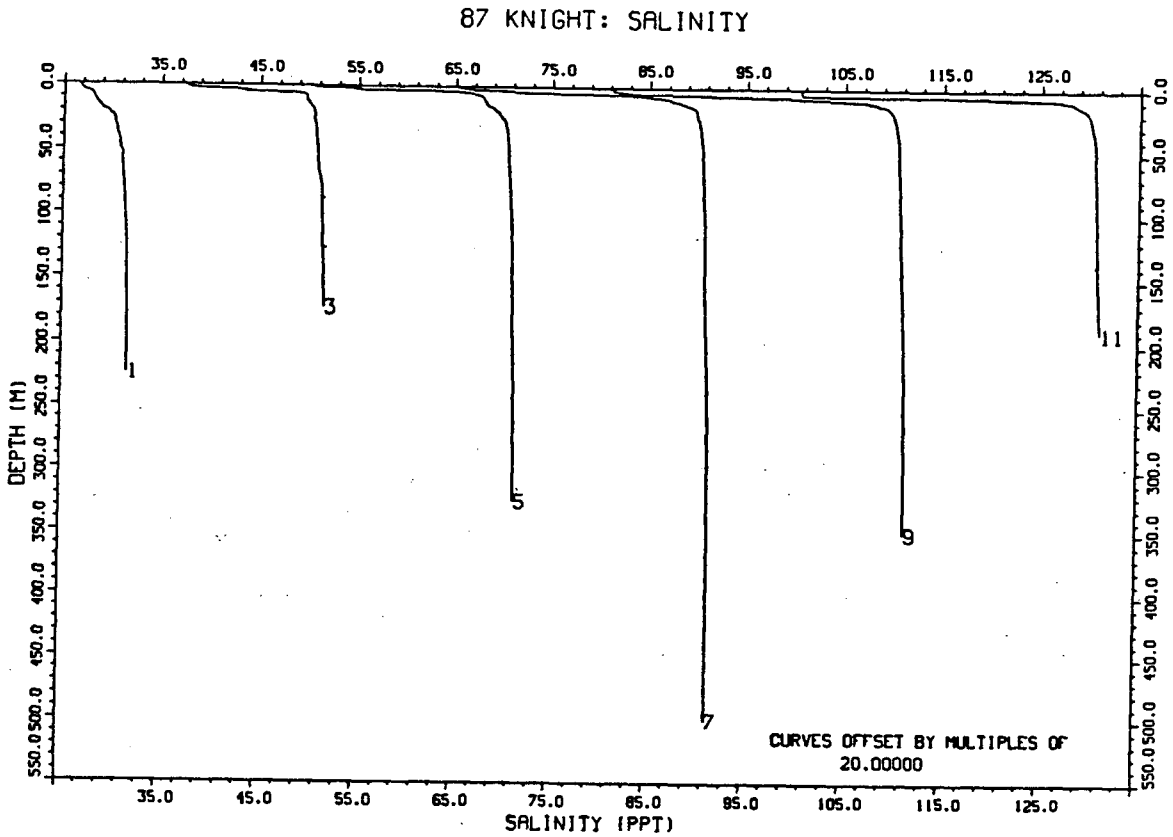

Figure 6.17: Salinity profiles for 1987 Knight Inlet stations.

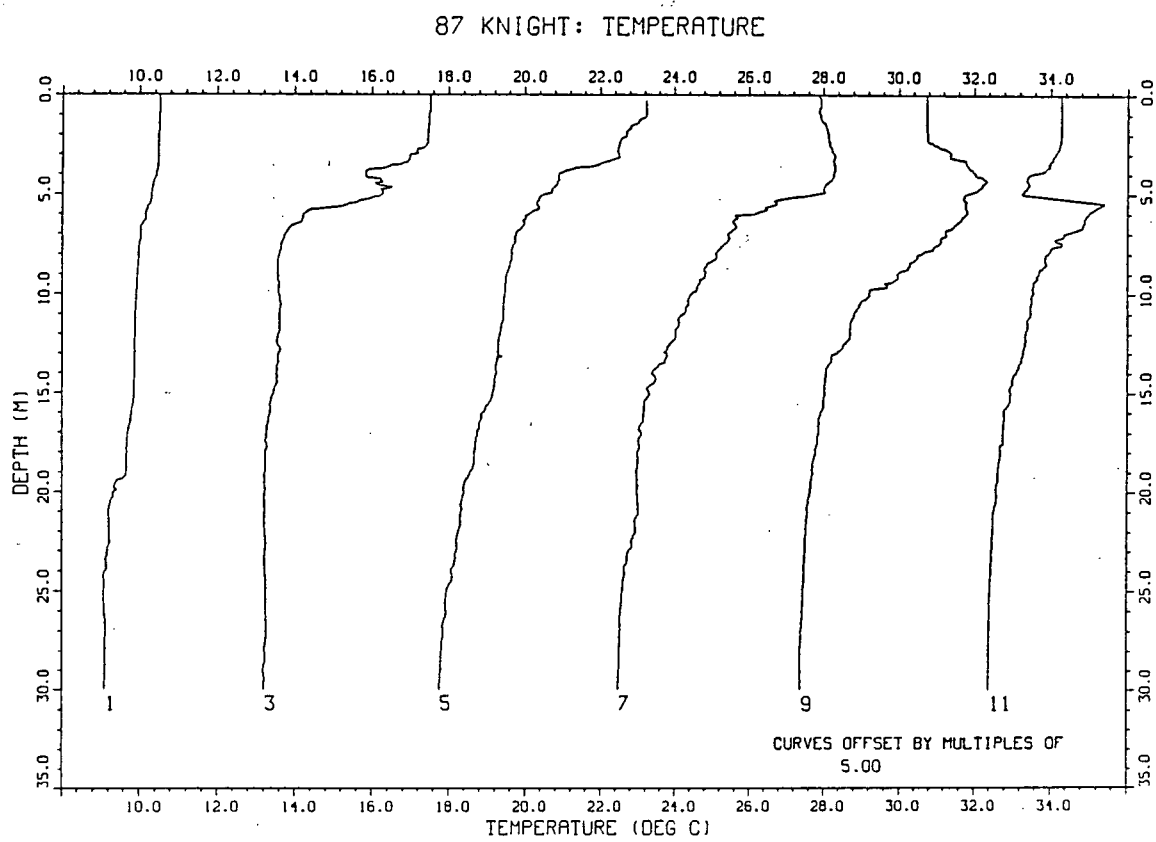

Figure 6.18: Temperature profiles for 1987 Knight Inlet stations for $0\,m$ to $30\,m$.

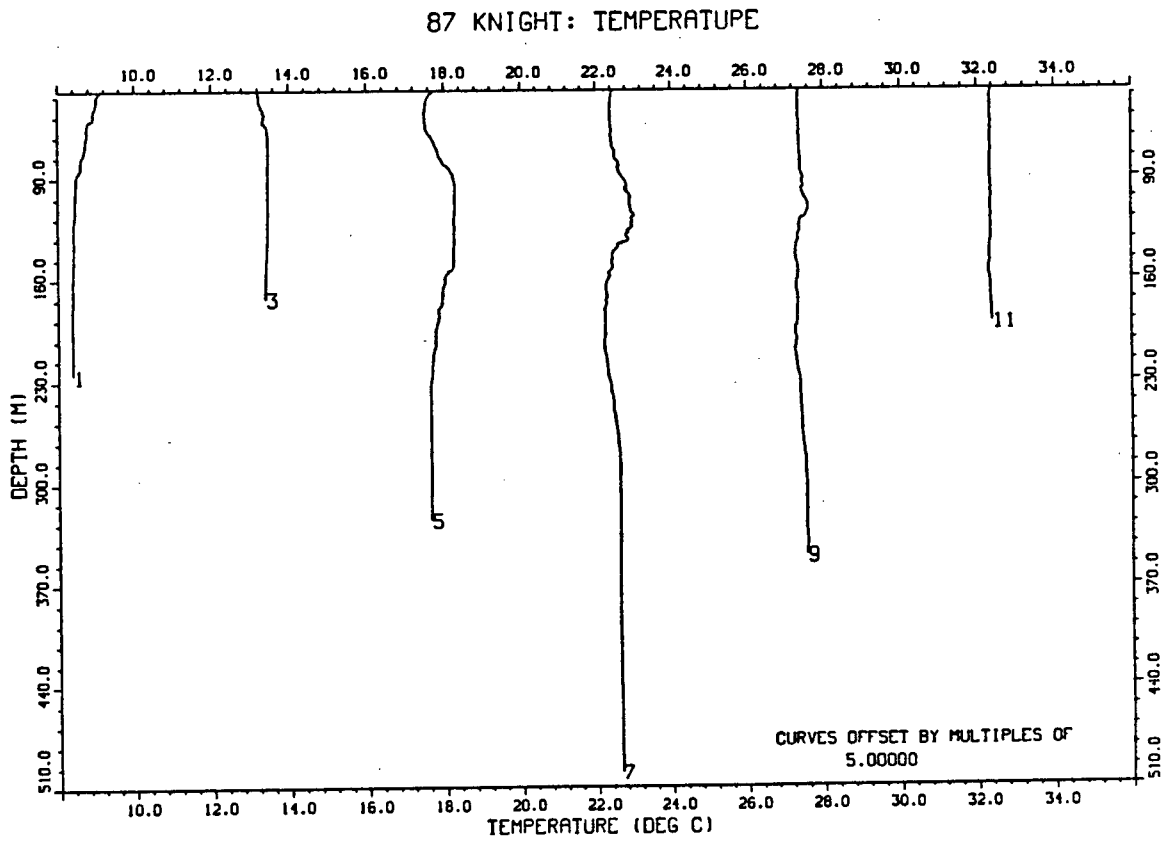

Figure 6.19: Temperature profiles for 1987 Knight Inlet stations for 30 m to the bottom.

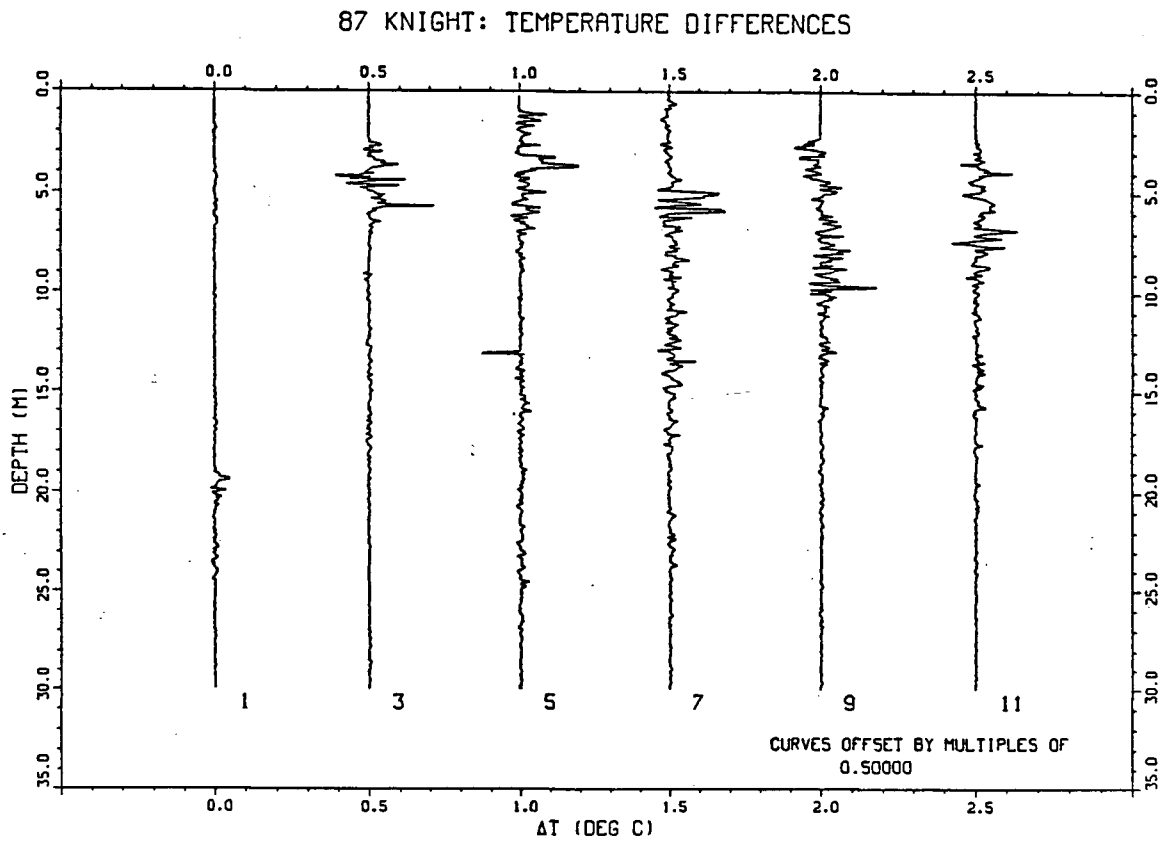

Figure 6.20: Profiles of first differenced temperature record from 0 to 30 m for 1987 Knight Inlet stations.

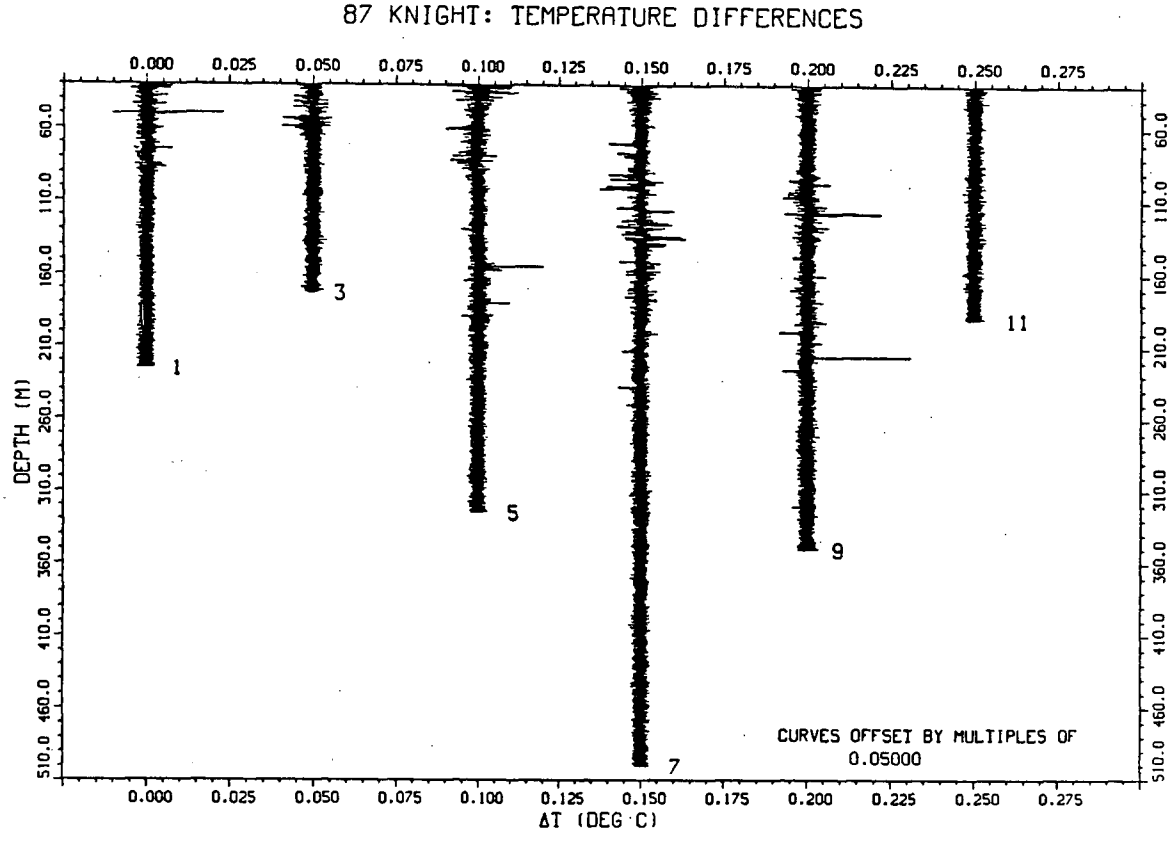

Figure 6.21: Profiles of first differenced temperature record from 30 m to the bottom for 1987 Knight Inlet stations.

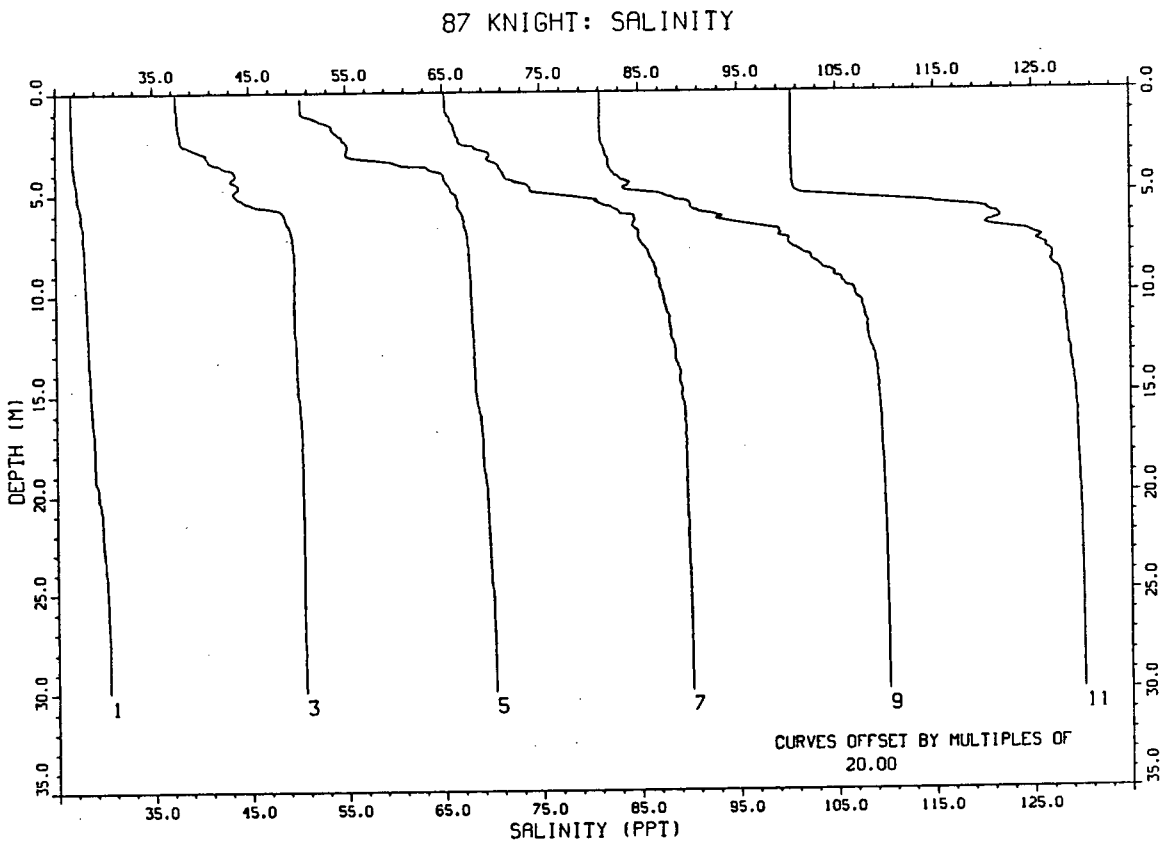

Figure 6.22: Salinity profiles for 1987 Knight Inlet stations for 0 m to 30 m.

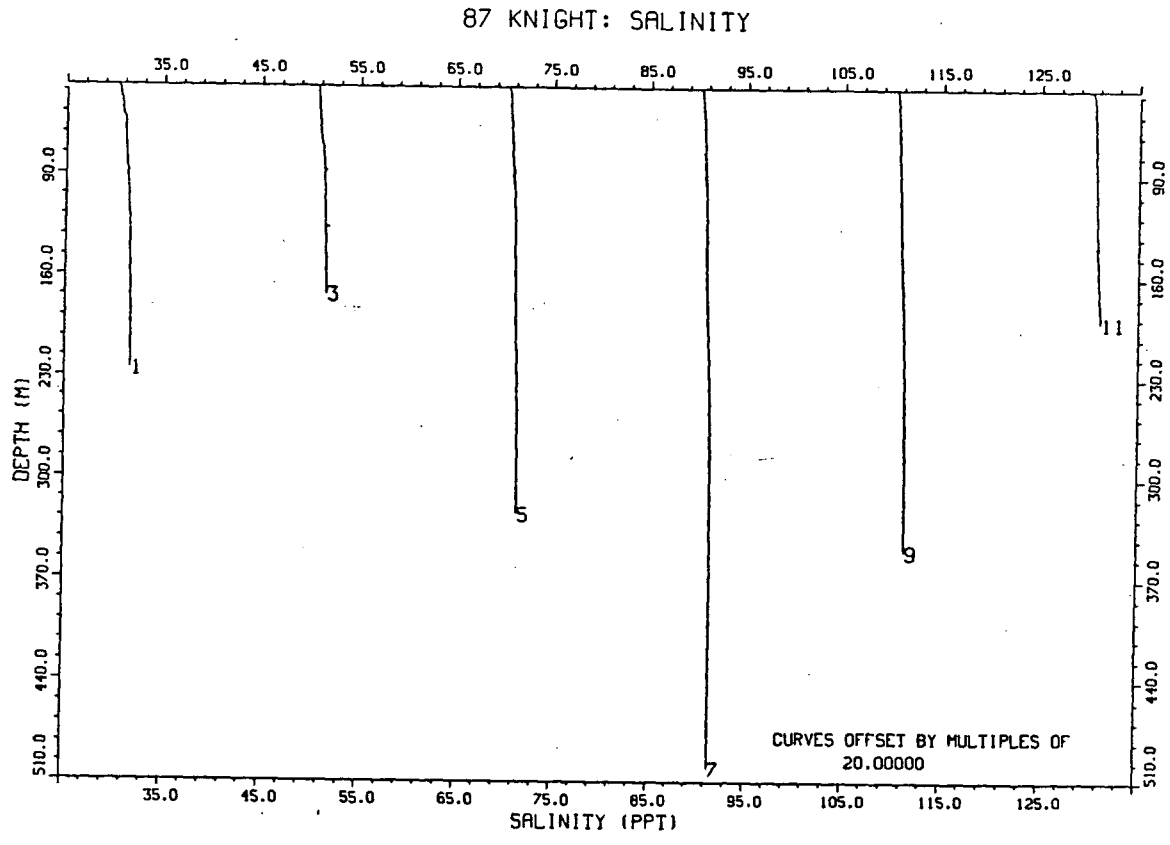

Figure 6.23: Salinity profiles for 1987 Knight Inlet stations for 30 m to the bottom.

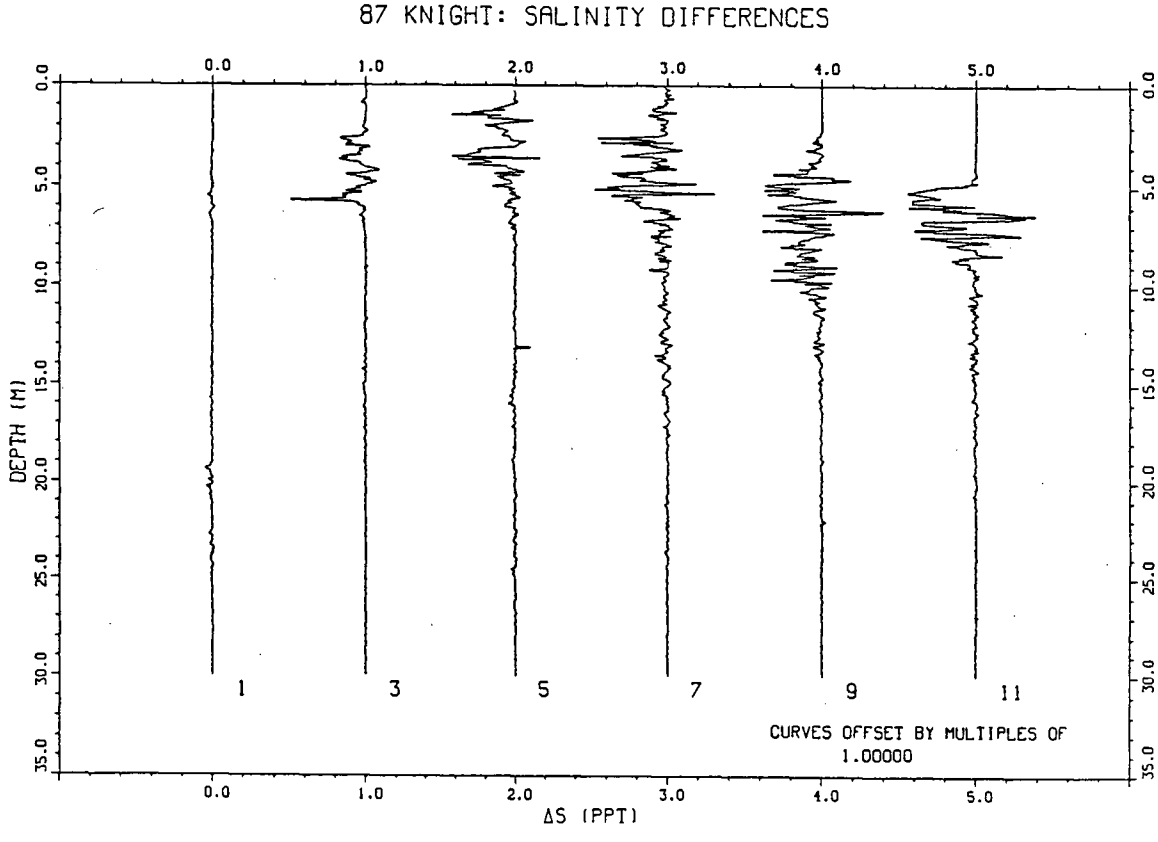

Figure 6.24: Profiles of first differenced salinity record from 0 to 30 m for 1987 Knight Inlet stations.

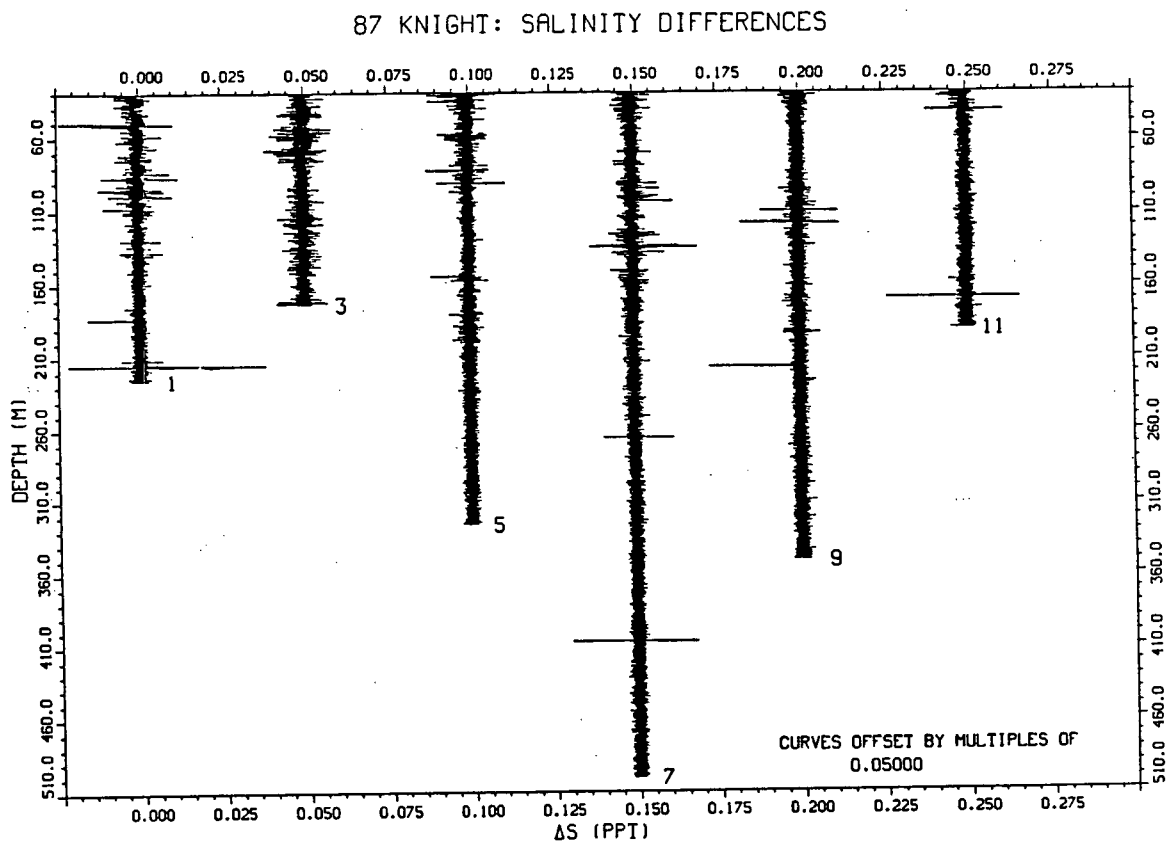

Figure 6.25: Profiles of first differenced salinity record from 30 m to the bottom for 1987 Knight Inlet stations.

of temperature that occurred in that area. The ΔT values fluctuated from positive to negative and *vice versa* from $2\,m$ to $8\,m$ depth at station 11.

The ΔS profiles for the upper water showed much activity from $0\,m$ to $8\,m$ for stations 5 and 7, and from $3\,m$ to $10\,m$ for stations 9 and 11. The ΔS values for stations 3 and 5 tended to be negative whereas for stations 7, 9, and 11, there existed large, sporadic jumps to positive values.

The profiles of ΔT and ΔS (Figures 6.21 and 6.25) for the deeper water did not show very well the structure of that region since the variations appeared to be close to the noise level of the instrument again. It must be noted that many spikes were present in both the ΔT and ΔS records which I removed by hand so that the data could be plotted on the scales that are shown.

The ΔT profile for the deeper water (Figure reffigure:87delTl) at station 5 revealed a small patch of activity at $\approx 80\,m$ where the increasing temperature suddenly stabilized, and another small patch occurred at $160\,m$ where the temperature suddenly decreased. The region between $80\,m$ and $160\,m$ at station 5 was relatively quiet. Several thin layers of fluctuations appeared at station 7, *eg.* at $\approx 100\,m$ and at $\approx 130\,m$. Thicker layers of fluctuations occurred at station 5 (from ≈ 140 to $\approx 145\,m$, and from $80\,m/$ to $100\,m$), and at station 3 (from $50\,m$ to $60\,m$) which I attributed to sharp increases/decreases of temperature. These layers appeared more numerous and stronger in 1987 than in 1986.

The deeper ΔS record for 1987 (Figure 6.25) appeared almost as active as in 1986. The level of activity when compared to the 1987 ΔT profile for the deeper water appeared to be the same as well, except for stations 1 and 3. Layers of strong salinity variations can also be seen in the profile, *eg.* station 5 at $\approx 60\,m$, station 7 at $\approx 120\,m$, and station 3 from about $50\,m$ to $60\,m$ and from $70\,m$ to $75\,m$.

6.1.4 Comparison of 1987 CTD data with FLY microprofiler data

The trouble with looking at first differences the way that I did was that there were too many

data points (at times there were as many as 20 per meter), which made processing and plotting very expensive. Since finestructure is structure at scales larger than $1\,m$, these large data sets were not necessary. I needed to average my differenced data into representative intervals of one or more meters. I did this for the 1987 temperature data and compared the resulting profiles with those produced by an instrument designed specifically for measuring microstructure.

Dr. A. Gargett of the Institute of Ocean Sciences had measured temperature structure with a microprofiling instrument (FLY) at the same time as the 1987 CTD data was measured for Knight Inlet. She averaged her data into 3 meter intervals ("bins") (Figure 6.26) and plotted the temperature gradient as a centered first difference (Figure 6.27), the log of the mean-square differentiated temperature (log MSQ dT) (Figure 6.28), and the log of MSQ dT normalized by the average temperature gradient squared. These final two quantities are principal measures of microstructure used when studying small scale features. The variance of the temperature gradient, for example, is an indication of the rate of dissipation of temperature fluctuations (Gregg, 1975).

I wanted to compare my 1987 CTD profiles to her plots of the temperature gradient and the log MSQ dT so I averaged the CTD data with a $3\,m$ averaging interval (Figure 6.29) and then I found the centered first differences using this averaged data. To find the gradients, $\frac{dT}{dz}$, I calculated

$$\frac{1}{2}\left(\frac{T_{i+1} - T_{i-1}}{dz}\right) \tag{6.2}$$

where dz was the bin size $= 3.0\,m$, and i is the index denoting each interval point (T_1 would be the temperature at $3\,m$). This calculation gave $\frac{dT}{dz}$ at $3, 6, 9, \cdots m$, and is the same as subtracting the backward difference from the forward difference and then dividing by twice the bin size. For example, to find the gradient at $6\,m$, I subtracted the temperature at $3\,m$ from the temperature at $9\,m$ and divided by $2 \times 3\,m$. The calculations actually gave gradients with mostly negative values since I subtracted a shallower depth from a deeper depth. When I plotted these gradients I multiplied my values by -1 to agree with Dr. Gargett's gradients. The value of $\frac{dT}{dz}$ at $0\,m$ was set equal to the temperature at $0\,m$ subtracted from the temperatue

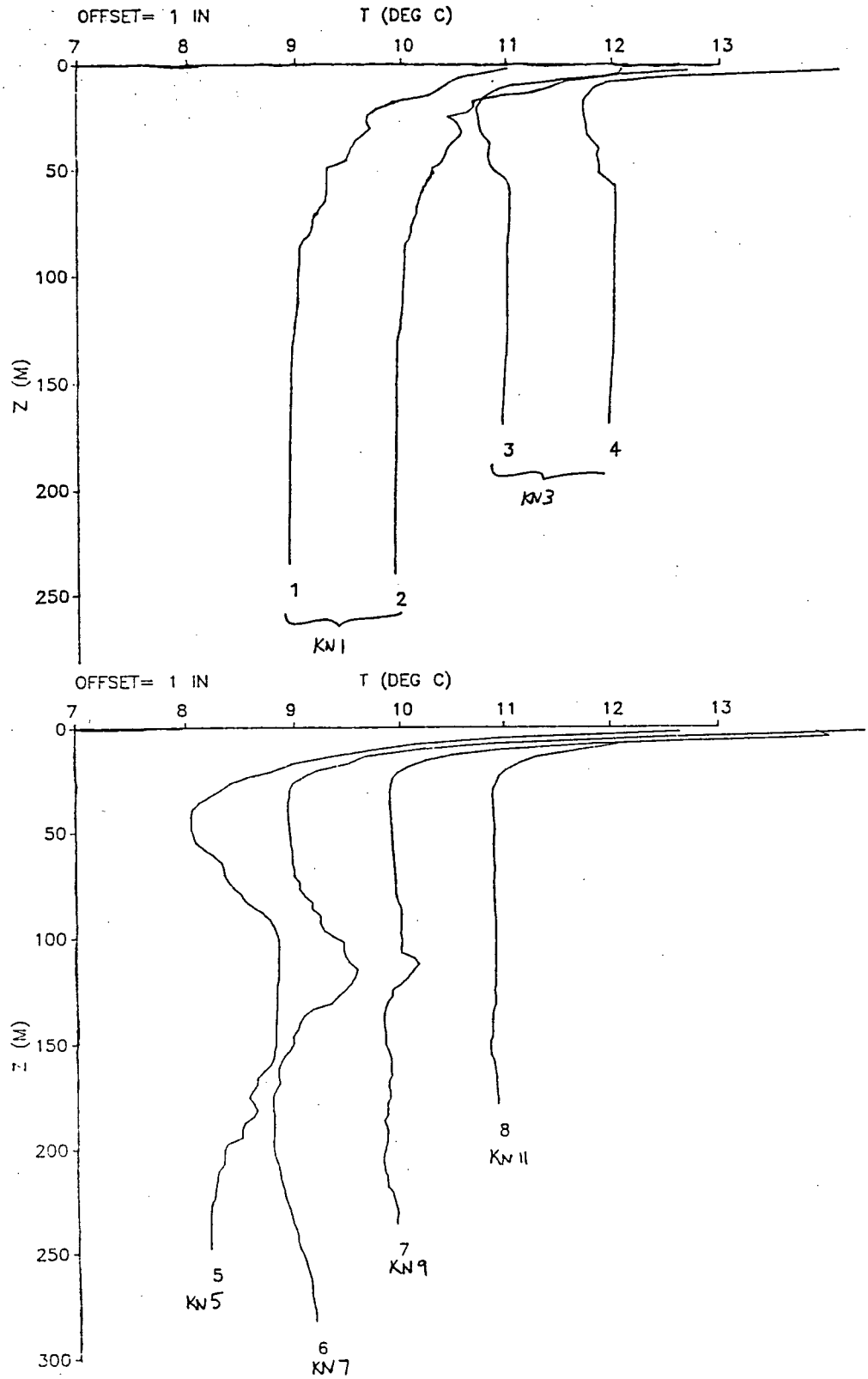

Figure 6.26: Profiles of temperature as measured by FLY for 1987 Knight Inlet stations. Data has been averaged into $3\,m$ bins.

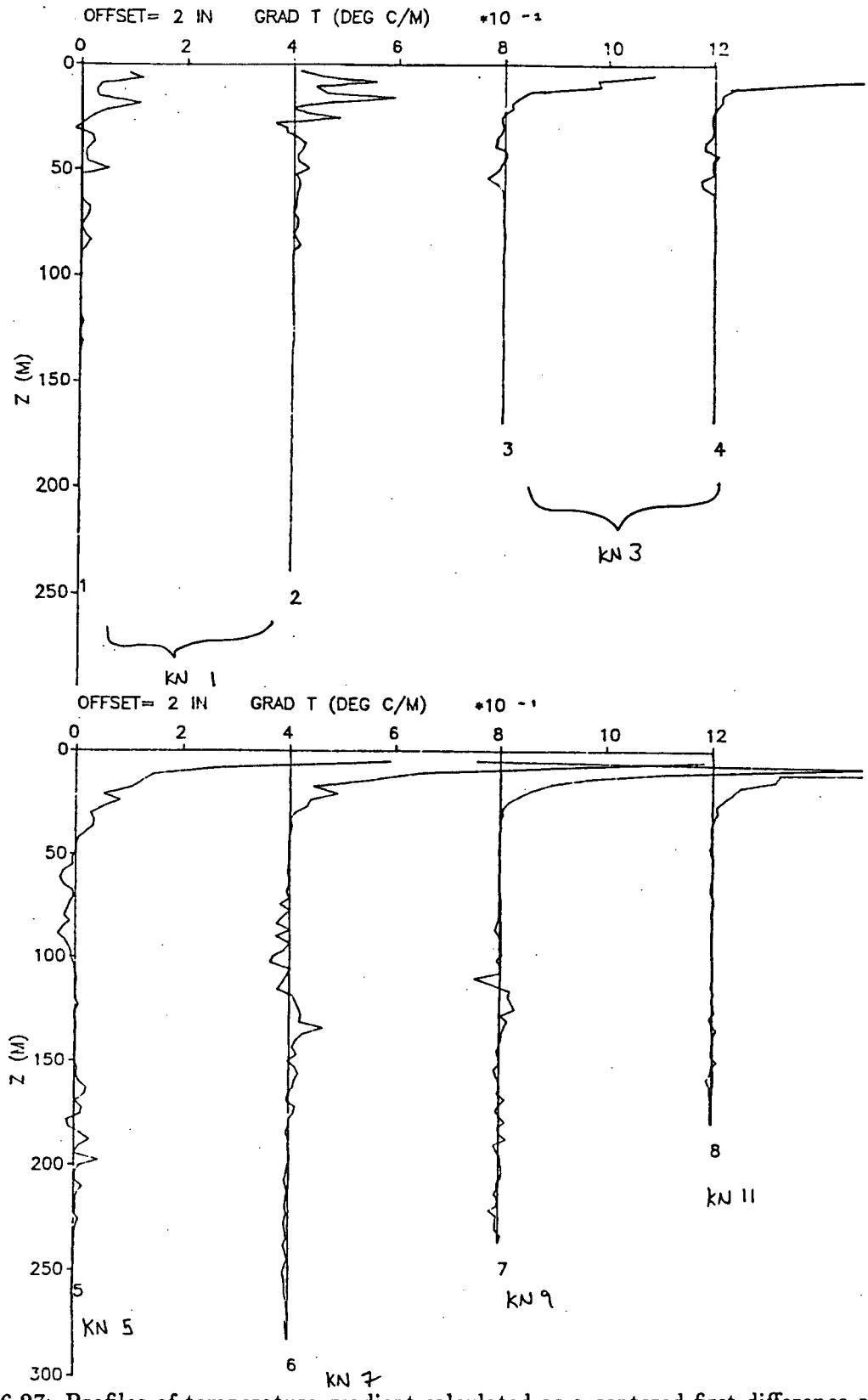

Figure 6.27: Profiles of temperature gradient calculated as a centered first difference as measured by FLY for 1987 Knight Inlet stations.

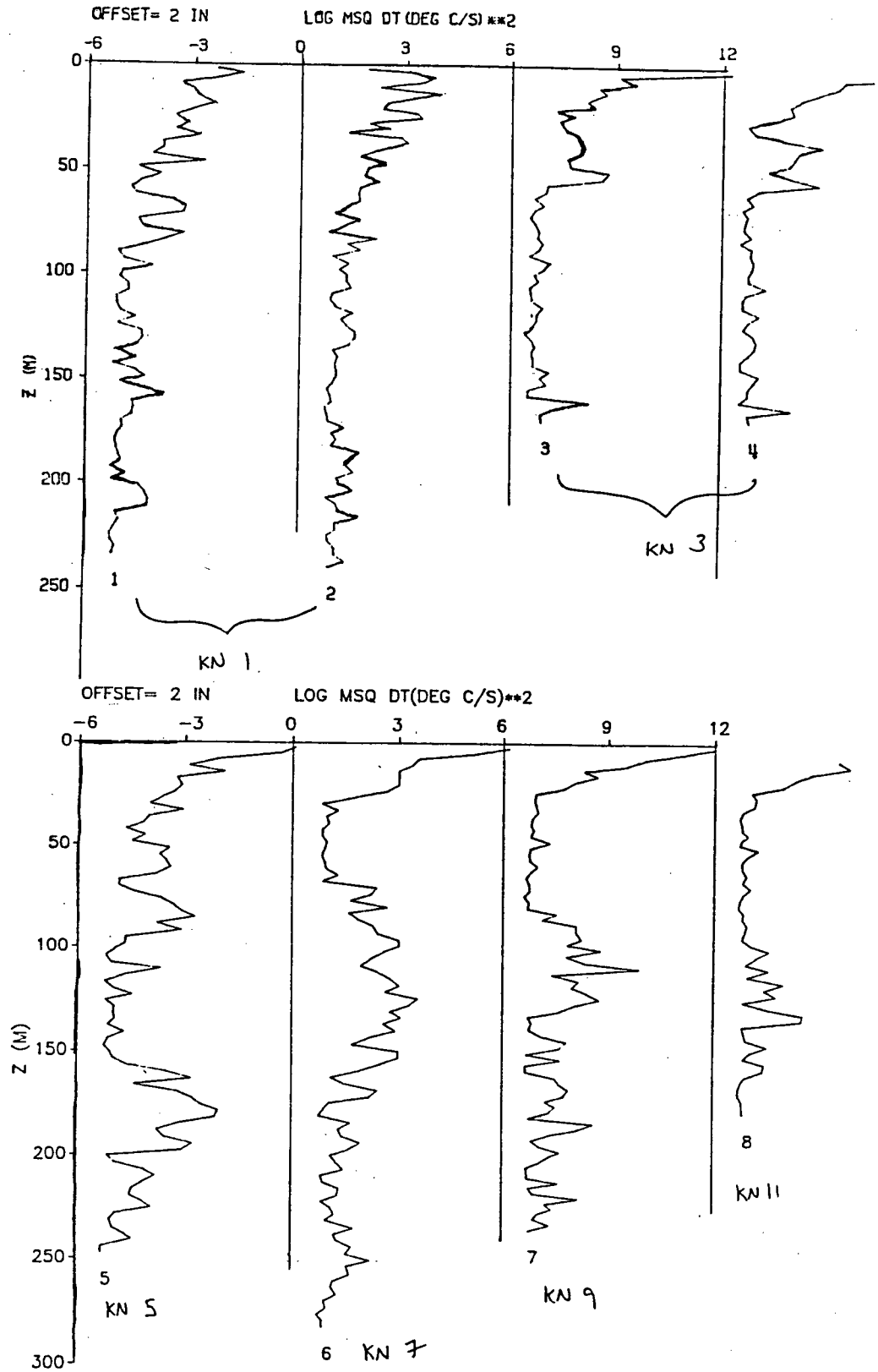

Figure 6.28: Profiles of log mean-square of the differentiated temperature (MSQ dT) as measured by FLY for 1987 Knight Inlet stations.

at $3\,m$ and divided by $3\,m$.

I calculated the MSQ dT (also known as the variance of the temperature gradient) from

$$\sum_{j=1}^{N}((\frac{dT}{dt})_j - \overline{\frac{dT}{dt}})^2 = \frac{\sum_{j=1}^{N}(\frac{dT}{dt})_j^2 - \frac{(\sum \frac{dT}{dt})^2}{N}}{N-1} \tag{6.3}$$

using the 1987 ΔT data that I had processed earlier and shown in Figures 6.20 and 6.21. I divided each ΔT by its corresponding difference in depth to obtain a gradient and these were the gradients I used to find the variances.. The time intervals dt were estimated using an assumed drop rate of $1\,m/s$ so that Δz (the depth difference) and dt would be equivalent numerically. I calculated these mean-squares for every 3 meter interval. The profiles produced from the microprofiler are shown in Figures 6.26, 6.27, and 6.28. The profiles of the CTD data that I used for comparison are shown in Figures 6.29, 6.30, and 6.31. It should be noted that if there was a large spike in the data record, it will alter the true value of the variance. The variances calculated from the CTD data were done so from the data represented in previous plots of ΔT in 1987.

There was trouble with the temperature calibration of the FLY, and the plots of the microprofiler data are uncorrected for this trouble. The thermistor on the FLY could be corrected with an offset change which would affect the temperature profile, but since MSQ dT and CDF depend on the temperature gain and not the offset, those two profiles would not be affected (A. Gargett, personal communication).

I was surprised to see how closely the plots of temperature as measured by the CTD and by the FLY resembled each other (Figures 6.29 and 6.26) despite the calibration problem. Both figures show the same features below the surface ($> 10\,m$), *eg.* the large minimum in temperature at station 3 and the maxima at stations 7 and 9 at $\approx 120\,m$.

The profiles of the temperature gradients (Figures 6.27 and 6.30) do not resemble each other as closely as the temperature profiles did when comparing the FLY gradients with the CTD gradients. However, these profiles also share some features. At station 1, two maxima appeared at $\approx 5\,m$ and $25\,m$ in both the FLY and the CTD profiles. At station 3, two small negative gradients were present between $50\,m$ and $60\,m$ in both profiles. For the other four

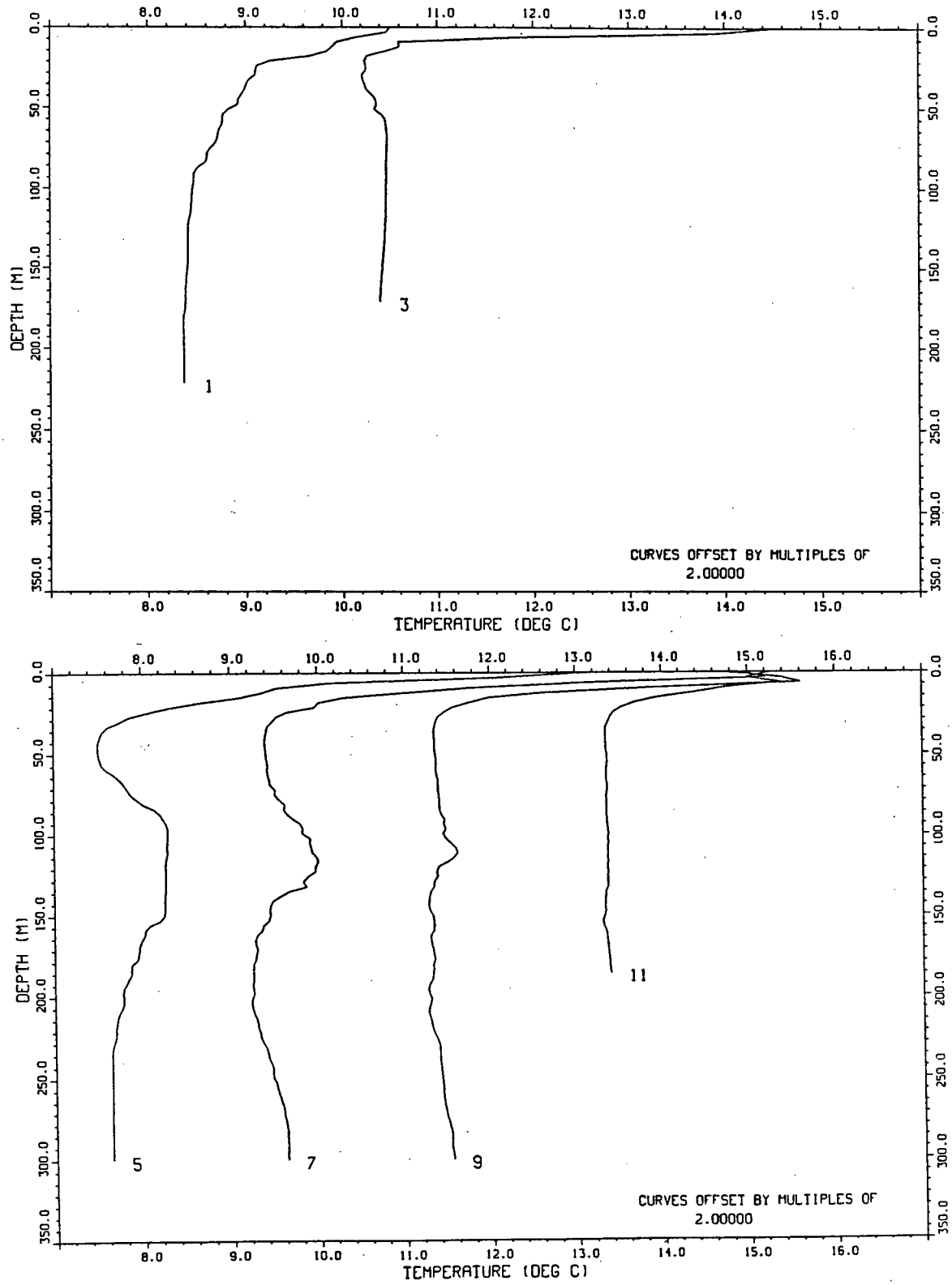

Figure 6.29: Profiles of temperature as measured by the CTD for 1987 Knight Inlet stations. Data has been averaged into $3\,m$ bins.

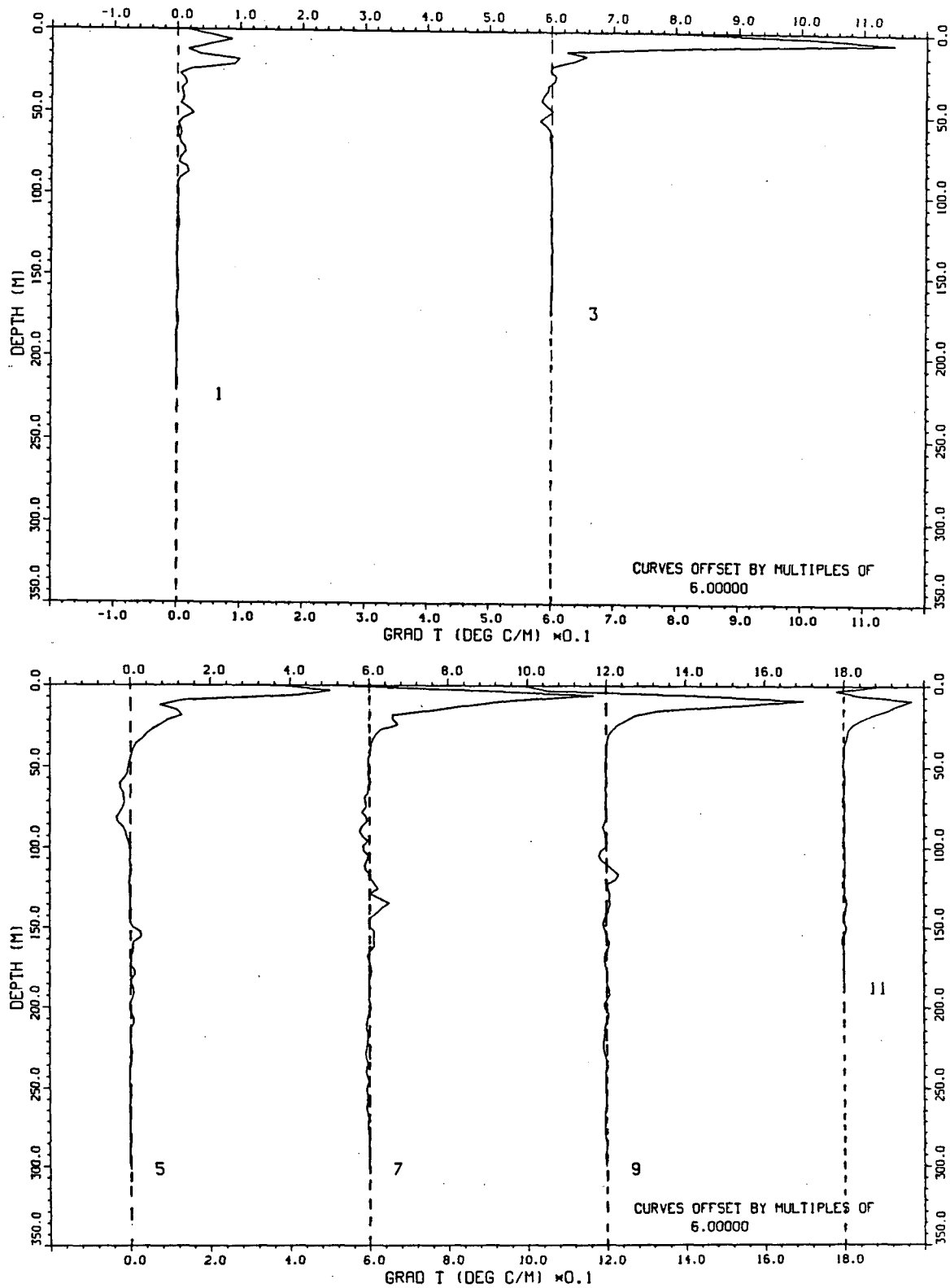

Figure 6.30: Profiles of temperature gradient calculated as a centered first difference as measured by the CTD for 1987 Knight Inlet stations.

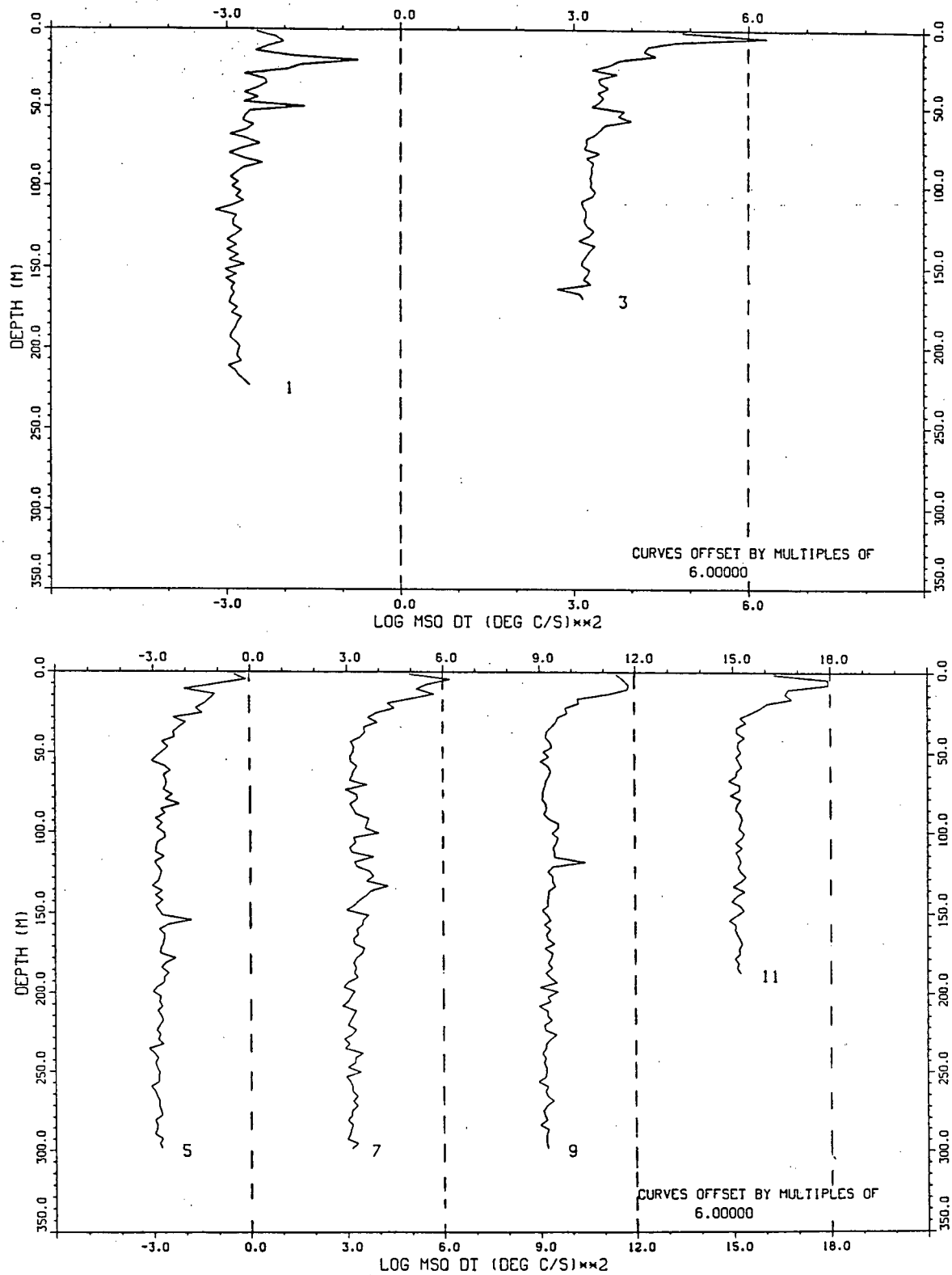

Figure 6.31: Profiles of log mean-square of the differentiated temperature (MSQ dT) as measured by the CTD for 1987 Knight Inlet stations.

staations common features were less evident. Most notable were the maxima at $\approx 130\,m$ at station 7, at $\approx 160\,m$ at station 5, and at $\approx 120\,m$ at station 9. The structure in the shallow water $< 10\,m$ was harder to compare since the FLY did not seem to record this data. The features shown by the CTD seemed to be less sharply defined than for the FLY, especially for the last four stations. The CTD profiles show large fluctuations of temperature to have existed in the shallow water.

The profiles of the CTD MSQ dT, however, showed more clearly the finestructure pressent, and, although they do not closely resemble the FLY profiles, there were also some common features that were picked up by both instruments. For example, at station 9, the variance of $\frac{dT}{dt}$ at $\approx 125\,m$ was comparatively larger than other variances at that station for the CTD profile, and this large variance also appeared in the FLY profile. The CTD seemed to lag a bit behind the FLY since most of the common features appear a bit later in the CTD record. For example, the double-peaked feature from $50\,m$ to $60\,m$ at station 3 for the CTD appeared between $40\,m$ and $50\,m$ for the FLY. The lag is most likely due to the fact that the FLY casts and the CTD casts were not done at exactly the same time, but the FLY was cast after the CTD cast was finished. The FLY is a towed instrument and the CTD casts were performed while the ship was stopped. In the deeper water, the more prominent variations of temperature gradient from the mean, were almost as large as the variations of temperature gradient in the shallower water, *eg.* at station 9 at $100\,m$ and at station 5 at $175\,m$ (Figure 6.28).

The FLY profiles of the temperature gradient (Figure 6.27)show more numerous fluctuations in the shallow water at station 1. Negative gradients appeared, not only at $100\,m$ at station 7, but extended from $\approx 75\,m$ to $125\,m$. Station 9 had a prominent negative gradient at $\approx 100\,m$ which does not appear in the CTD profile (Figure 6.30).

6.2 Summary

I did not extensively investigate the finestructure present in Knight Inlet. My method of processing the CTD data did not lend itself to an in-depth quantitative analysis, but it was

useful as a qualitative indicator of the structure that was present. I will briefly summarize several key features that I found present in the upper and lower waters of Knight Inlet.

The upper water ($< 30\,m$) of Knight Inlet was much more visibly active than the deeper water ($> 30\,m$). The most pronounced fluctuations were concentrated in the thermocline/halocline region, in the sill area, and at the head.

Station 11 exhibited large inversions of temperature in both 1986 and 1987 which I attributed to river discharge meeting brackish inlet surface water.

The sill area is an area of strong mixing whose energy is provided by the tidal forcing. Tidally induced flow over the sill in Knight Inlet can generate large amplitude turbulent internal wave trains (Farmer and Freeland, 1983; Farmer and Smith, 1980a; Farmer and Smith, 1980b). Farmer and Smith (1980a) observed that during strong tides, mode 1 internal waves were generated at the sill and travelled upstream away from the sill. These lee waves or jumps relaxed as the tide slackened, and subsequently they turned into internal bores or surges. The same authors also observed that for summer conditions, there occurred subcritical flow with respect to mode 1 waves, but supercritical flow with respect to higher modes. Smith and Farmer (1980) observed, during a maximum ebb, "large amplitude instabilities in the shear zone that separate the descending supercritical flow from the subcritical fluid above." In the same paper, Smith and Farmer stated that little finestructure would be found in the subcritical layer over the crest and on the down-inlet side of the sill because of the intense turbulence produced by the hydraulic disturbance. They concluded that the mixing caused by the instabilities was substantial and was probably dominant below $10\,m$ and certainly dominant below $20\,m$ in Knight Inlet. I observed the largest variations in salinity and temperature above $10\,m$ at the sill with comparatively little variations below that point. Despite the statement made by Gregg (1975) pertaining to well-mixed regions that I mentioned earlier, I would conclude that the water below $10\,m$ in the region of the sill is well-mixed in light of the investigations done by Farmer and Smith (1980a, 1980b) and Smith and Farmer (1980).

The concentration of large fluctuations in the thermocline/halocline region along the inlet

did not surprise me since regions of strong gradients are common areas for finestructural features to be found (Coachman and Charnell, 1977). Entrainment induced by breaking internal waves, causes mixing of cooler, saltier water with surface water, and the finestructure I observed in the area of the interface could be attributed to entrainment.

The deeper water contained several large minima/maxima in temperature (especially in 1987), and I observed many sharp changes of temperature that resembled step-like structure. Patches of fluctuating temperature and salinity occurred throughout the deeper water which had thicknesses of several meters, sometimes as much as $10\,m$.

The microprofiler, FLY, revealed that large variations in temperature occurred in the deeper water of Knight Inlet in 1987. These variations were not so obvious in the CTD record. Although the CTD provides fine resolution of temperature and conductivity for studying finestructure, difficulties in despiking and processing perhaps makes the instrument most useful as only a qualitative indicator of where features are located. Also, it is important to determine the noise level of the instrument in order to more accurately conduct an analysis such as mine. A more specialized free-falling instrument, such as the FLY, equipped with a fast thermistor and a velocity sensor is probably best to use if a quantitative analysis of micro-/finestructure is wanted. The advantage of using a CTD is that most oceanographic institutions already own CTD's, and the more specialized instruments are not as readily available and are probably more costly to buy and maintain.

Bibliography

Baker Jr., D. J., 1981. Ocean instruments and experiment design. In: *Evolution of Physical Oceanography.* H. M. Stommel, C. Wunsch, and B. A. Warren, eds., MIT Press, Boston, 396-433.

Canada, Department of Fisheries and Oceans, Canadian Hydrographic Service. *Canadian Tide and Current Tables, 1986 (1987), Vol. 5 (Vol. 6), Juan de Fuca and Georgia Straits.*

Coachman, L.K. and R. L. Charnell, 1977. Finestructure in outer Bristol Bay, Alaska. *Deep-Sea Research*, **24(10)**, 869-889.

Cordes, R. E., S. Pond, B. R. de Lange Boom, P. H. LeBlond, 1980. Estimates of entrainment in the Fraser River plume, British Columbia. *Atmosphere-Ocean*, **18(1)**, 15-26.

Defant, A., 1961. *Physical Oceanography, Volume 1*, Pergamon Press, New York, 729 pp.

Dyer, K. R., 1973. *Estuaries: A Physical Introduction*, John Wiley and Sons, Toronto, 140 pp.

Farmer, D. M. and H. J. Freeland, 1983. The physical oceanography of fjords. *Progress in Oceanography*, **12(2)**, 147-220.

Farmer, D. M. and J. D. Smith, 1978. Nonlinear internal waves in a fjord. In: *Hydrodynamics of Estuaries and Fjords*, J. Nihoul, ed., Elsevier Oceanography Series, No. 23, 465-494.

Farmer, D. M. and J. D. Smith, 1980a. Tidal interaction of stratified flow with a sill in Knight Inlet. *Deep-Sea Research*, **27A**, 239-254.

Farmer, D. M. and J. D. Smith, 1980b. Generation of lee waves over the sill in Knight Inlet. In: *Fjord Oceanography*, D. M. Farmer, H. J. Freeland, and C. D. Levings, eds., Plenum Press, New York, 259-269.

Fofonoff, N. P., S. P. Hayes, and R. C. Millard, 1974. WHOI/Brown CTD microprofiler: methods of calibration and data handling. *Woods Hole Oceanographic Institution Tech. Rep.*, WHOI, 74-89.

Fozdar, F. M., G. J. Parker, and J. Imberger, 1985. Matching temperature and conductivity sensor response characteristics. *J. Phys. Oceanogr.*, **15(11)**, 1557-1569.

Freeland, H. J., and D. M. Farmer, 1980. Circulation and energetics of a deep, strongly stratified inlet. *Can. J. Fish. and Aquatic Sci.*, **37(9)**, 1398-1410.

Freeland, H. J., D. M. Farmer, and C. D. Levings, 1980. *Fjord Oceanography*, Plenum Press, New York, 715 pp.

Gade, H. E., and A. Edwards, 1980. Deep water renewal in Fjords. In: *Fjord Oceanography*, D. M. Farmer, H. J. Freeland, and C. D. Levings, eds., Plenum Press, New York, 453-489.

Gade, H. E., and E. Svendsen, 1978. Properties of the Robert R. Long model of estuarine circulation in fjords. In: *Hydrodynamics of Estuaries and Fjords*, J. Nihoul, ed., Elsevier Oceanography Series, No. 23, 423-437.

Gaul, R. D., 1968. Performance analysis of a salinity-temperature depth system. *IEEE Trans. of Geosci. Electron.*, **GE-6**, 185-189.

Georgi, D. T., R. C. Millard Jr., and R. W. Schmitt, 1983. Conductivity microstructure measurements with a CTD. In: *Proceedings, Third Working Symposium on Oceanographic Data Systems, Woods Hole, MA, 2-4 October 1983*, C. D. Tollios, M. K. McElroy, and J. Syck, eds., IEEE Comp. Soc. and WHOI, 5-14.

Gregg, M. C., 1975. Microstructure and intrusion in the California Current. *J. Phys. Oceangra.*, **5(2)**, 253-278 pp.

Gregg, M. C., and T. B. Meagher, 1980. The dynamic response of glass rod thermisters. *J. Geophys. Res.*, **85(C5)**, 2779-2786.

Gregg, M. C., J. C. Schedvin, W. C. Hess, and T. B. Meagher, 1982. Dynamic response calilbration of the Neil Brown conductivity cell. *J. Phys. Oceanogr.*, **12(7)**, 720-742.

Guildline Instruments. *Model 8705 Digital CTD Probe and Model 87102 Control Unit, Tech. Man., Vol. 1.*

Horne, E. P. W., and J. M. Toole, 1980. Sensor response mismatches and lag correction techniques for temperature-salinity profilers. *J. Phys. Oceangra.*, **10(7)**, 1122-1130.

Imberger, J., 1985. The diurnal mixed layer. *Limno. and Oceanogra.*, **30(4)**, 737-770.

Long, R. R., 1975. Circulation and density distribution in a deep, strongly stratified, two-layer estuary. *J. Fluid Mech.*, **71**, 529-540.

Long, R. R., 1980. The fluid mechanical problem of fjord circulations. In: *Fjord Oceanography*, D. M. Farmer, H. J. Freeland, and C. D. Levings, eds., Plenum Press, New York, 67-116.

Lueck, R. G., O. Hertzman, and T. R. Osborn, 1977. The spectral response of thermisters. *Deep-Sea Research*, **24(10)**, 951-970.

Mack, S. A., 1985. Two-dimensional measurements of ocean microstructure: the role of double diffusion. *J. Phys. Oceangra.*, **15(11)** 1581-1604.

McAlister, W. B., M. Rattray Jr., and C. A. Barnes, 1959. The dynamics of a fjord estuary: Silver Bay, Alaska. *Dept. of Oceanogra. Tech. Rep. 62* Univ. of Washington, Seattle, 70 pp.

Neumann, G., and W. J. Pierson Jr., 1966. *Principles of Physical Oceanography.* Prentice-Hall, Inc., Englewood Cliffs, New Jersey, 545 pp.

Osborn, T. R., and C. S. Cox, 1972. Oceanic finestructure. *Geophys. Fluid Dyn.*, **3**, 321-345.

Pearson, C. E., and D. F. Winter, 1978. Two-layer analysis of steady circulation in stratified fjords. In: *Hydrodynamics of Estuaries and Fjords*, J. Nihoul, ed., Elsevier Oceanography Series, No. 23, 495-514.

Pedersen, Fl. Bo, 1978. A brief review of present theories of fjord dynamics. In: *Hydrodynamics of Estuaries and Fjords*, J. Nihoul, ed., Elsevier Oceanography Series, No. 23, 407-422.

Phillips, O.M., 1966. *The Dynamics of the Upper Ocean*, Cambridge Univ. Press, Cambridge, 261 pp.

Pickard, G. L., 1961. Oceanography of British Columbia mainland inlets. *J. Fish. Res. Bd. Canada*, **18(6)**, 907-999.

Pickard, G. L., and W. J. Emery, 1982. *Descriptive Physical Oceangraphy*, Pergamon Press, Oxford, 249 pp.

Pickard, G. L., and K. Rodgers, 1959. Current measurements in Knight Inlet, British Columbia. *J. Fish. Res. Bd. Canada*, **16(5)**, 635-678.

Pickard, G. L., and B. R. Stanton, 1980. Pacific fjords-a review of their water characteristics. In: *Fjord Oceanography*, D. M. Farmer, H. J. Freeland, and C. D. Levings, eds., Plenum Press, New York, 1-51.

Pingree, R. D., 1969. Small-scale structure of temperature and salinity near station Cavall. *Deep-Sea Research*, **16(3)**, 275-295.

Pond, G. S., and G. L. Pickard, 1983. *Introductory Dynamical Oceanography*, Pergamon Press, Oxford, 329 pp.

Rattray Jr., M., 1967. Some aspects of the dynamics of circulation in fjords. In: *Estuaries*, G. H. Lauff, ed., Amer. Assoc. for the Adv. of Sci., Washington, D. C., 52-62 pp.

Schmitt, R. W., R. G. Lueck, and T. M. Joyce, 1986. Fine- and microstructure at the edge of a warm-core ring. *Deep-Sea Research*, **33(11/12)**, 1665-1689.

Smith, J. D., and D. M. Farmer, 1980. Mixing induced by internal hydraulic disturbances in the vicinity of sills. In: *Fjord Oceanography*, D. M. Farmer, H. J. Freeland, and C. D. Levings, eds., Plenum Press, New York, 251-257.

Thomson, R. E., 1981. *Oceanography of the British Columbia Coast*, Canadian Special Publication of Fisheries and Aquatic Sciences 56, Department of Fisheries and Oceans, Canada, 291 pp.

University of British Columbia, 1987. *Department of Oceanography, Data Report 55: British Columbia Inlet Cruises, 1986*, University of British Columbia, Vancouver, 53 pp.

von Arx, W. S., 1962 *An Introduction to Physical Oceanography*, Addison-Wesley, Reading, Massachusetts, 422 pp.

Webb, A. J., 1985. The propagation of the internal tide around a bend in Knight Inlet, B. C., Ph. D. thesis, University of British Columbia, 160 pp.

Wetton, B., 1981. Dynamics of the surface layer: Knight Inlet, British Columbia. unpublished report of Physics Co-op Work Project, University of Victoria, 68 pp.